

T.R.
GEBZE TECHNICAL UNIVERSITY
GRADUATE SCHOOL OF NATURAL AND APPLIED SCIENCES

**THE EFFECT OF AIR FLOW MALDISTRIBUTION ON
EVAPORATOR HEAT TRANSFER RATE AND FROSTING**

ERGIN BAYRAK
**A THESIS SUBMITTED FOR THE DEGREE OF
MASTER OF SCIENCE**
DEPARTMENT OF MECHANICAL ENGINEERING

GEBZE
2016

T.R.
GEBZE TECHNICAL UNIVERSITY
GRADUATE SCHOOL OF NATURAL AND APPLIED SCIENCES

**THE EFFECT OF AIR FLOW
MALDISTRIBUTION ON EVAPORATOR
HEAT TRANSFER RATE AND FROSTING**

ERGİN BAYRAK

**A THESIS SUBMITTED FOR THE DEGREE OF
MASTER OF SCIENCE
DEPARTMENT OF MECHANICAL ENGINEERING**

THESIS SUPERVISOR
PROF. DR. ALP ER ŞEVKİ KONUKMAN

GEBZE
2016

**T.C.
GEBZE TEKNİK ÜNİVERSİTESİ
FEN BİLİMLERİ ENSTİTÜSÜ**

**HAVA AKIŞININ DENGESİZ
DAĞILIMININ EVAPORATÖR ISI
TRANSFER HIZI VE BUZLANMA
ÜZERİNDEKİ ETKİSİ**

**ERGİN BAYRAK
YÜKSEK LİSANS TEZİ
MAKİNE MÜHENDİSLİĞİ ANABİLİM DALI**

**DANIŞMANI
PROF. DR. ALP ER ŞEVKİ KONUKMAN**

**GEBZE
2016**



YÜKSEK LİSANS JÜRİ ONAY FORMU

GTÜ Fen Bilimleri Enstitüsü Yönetim Kurulu'nun 15/06/2016 tarih ve 2016/37 sayılı kararıyla oluşturulan jüri tarafından 27/06/2016 tarihinde tez savunma sınavı yapılan Ergin Bayrak'ın tez çalışması Makine Mühendisliği Anabilim Dalında YÜKSEK LİSANS tezi olarak kabul edilmiştir.

JÜRİ

ÜYE

(TEZ DANIŞMANI) : Prof. Dr. Alp Er Şevki KONUKMAN

ÜYE

: Doç. Dr. İlyas KANDEMİR

ÜYE

: Prof. Dr. Feridun ÖZGÜÇ

ONAY

Gebze Teknik Üniversitesi Fen Bilimleri Enstitüsü Yönetim Kurulu'nun

...../...../..... tarih ve/..... sayılı kararı.

İMZA/MÜHÜR

SUMMARY

Evaporators which are used at various conditions have some problems such as refrigerant side maldistribution, air side maldistribution, frost growth at low temperature on surface of fin and tube. In this study, it was investigated considering only air flow distribution problems which may be encountered at practical usage of unit cooler. Accordingly, an evaporator was designed and determined airflow distribution and also air maldistribution degree (AMD), occurring both at each circuit and entire face, by using a 3 mm anemometer. However, depending on the measurements, heat transfer rate of each circuits was calculated by considering the mean velocities of each circuit via FrtCoils Software for non-uniform case and presented the difference with uniform case as well. In order to verification, the product was tested at Friterm Incorporation calorimetric room at first and then tested at conditioning room ensured same and more uniform airflow. Consequently, it was detected whether the deviation of heat transfer rate between experimental result and FrtCoils result was close and also understood whether determined maldistribution degrees had significant impact on heat transfer rate. On the other hand, the same evaporator was investigated under frosting condition in order to observe the effects of different AMD on frosting such as changes of heat transfer rate versus time, the total frost thicknesses, blockage ratios, frost patterns throughout evaporator surface, starting time of required defrost process via digital camera, thermal camera and Matlab Program. As a result, the impact of airflow maldistribution on frosting was able to be revealed in detail.

Key Words: Air maldistribution degree (AMD), total heat transfer rate, frosting, experimental study, FrtCoils Software.

ÖZET

Evaporatörler, buhar sıkıştırırmalı sistemlerde değişik işletme şartları altında kullanılabilen iç akışkan ve hava tarafı dengesiz dağılımı, düşük sıcaklıklarda kanat ve boru yüzeyinde buzlanma büyümesi gibi problemler içerebilen soğutma elemanlarıdır. Bu çalışmada bir endüstriyel soğutucunun pratik uygulamasında karşılaşılabilecek problemlerden yalnızca hava tarafı dağılım problemleri incelenecektir. Bu kapsamda bir evaporator dizayn edilip 3 mm hot bulb prop yardımıyla hem her bir devre üzerinde hem de tüm yüzeyde oluşan hava dengesizlik oranı (AMD) belirlenecektir. Bununla birlikte, alınan ölçümlere bağlı olarak, her bir devre için FrtCoils programında ortalama hava debilerine karşılık gelen kapasiteler hesaplanmış, non-uniform durum toplam kapasitesi belirlenmiş ve uniform durumdaki kapasite ile fark ortaya konmuştur. Bu durumu deneysel olarak doğrulamak amacıyla öncelikle Friterm Test Laboratuvarının kalorimetrik oda kısmında, daha sonra aynı hava debisinin sağlandığı ve daha uniform akışın olduğu iklimlendirme odasında test işlemi gerçekleştirilmiştir. Sonuç olarak, deneysel sonuç ile FrtCoils arasındaki sapmanın yakın olup olmadığı tespit edilebilecek ve ayrıca belirlenen dengesizlik oranlarının ürün kapasitesi üzerinde önemli bir etkiye sahip olmadığı anlaşılacaktır. Diğer yandan farklı dengesiz dağılım oranının zamanla kapasite değişimi, toplam buz kalınlığı, blokaj oranları, yüzey boyunca oluşan buz desenleri ve gerekli defrost işlemi başlama zamanı üzerindeki etkilerini görebilmek amacıyla buzlanma şartlarında test edilen aynı evaporator, dijital kamera, termal kamera ve Matlab görüntü işleme programı yardımıyla incelenmiştir. Sonuç olarak hava dengesiz dağılımının buzlanma üzerindeki etkisi detaylı bir şekilde ortaya çıkartılmıştır.

Anahtar Kelimeler: Hava dengesiz dağılım oranı (AMD), toplam ısı transfer kapasitesi, buzlanma, deneysel çalışma, FrtCoils Programı.

ACKNOWLEDGEMENTS

I wish to express my sincere gratitude to my supervisor, Prof. Dr. Alp Er Şevki KONUKMAN for his supports, recommendations and encouragement in scope of this experimental study.

I would like to firstly appreciated to Friterm Inc. General Manager Naci ŞAHİN for financial supports and confidence and latter to R&D Manager Dr. Hüseyin ONBAŞIOĞLU. Not only for academical support but also the sharing his experiences about cooling system and life and finally my laboratory technicians Yüksel ALTUNKIRAN and Aydın KARABABA for great helping during experiments.

In addition, I express my deepest gratitude to Prof. Dr. Feridun ÖZGÜÇ who is from Istanbul Technical University, for supports at each stage of my thesis.

TABLE of CONTENTS

	<u>Page</u>
SUMMARY	v
ÖZET	vi
ACKNOWLEDMENTS	vii
TABLE of CONTENTS	viii
LIST of ABBREVIATIONS and ACRONYMS	x
LIST of FIGURES	xii
LIST of TABLES	xv
1. INTRODUCTION	1
2. LITERATURE REVIEW	6
2.1. Summary of literature	15
3. EXPERIMENTAL METHOD	16
3.1. Experimental Apparatus	16
3.1.1. Description of Heat Exchanger	16
3.1.2. Description of Anemometer	18
3.1.3. Description of Thermal and Digital Camera	20
3.2. Experimental Procedure	21
3.2.1. Principle of Control	23
3.3. Experimental Conditions	25
4. THE EFFECTS OF AIR FLOW MALDISTRIBUTION UNDER DRY CONDITION	26
4.1. The Measurement of AMD	26
4.2. The Measurement of Performance of Heat Exchangers	30
4.3. The Measurement of Performance via FrtCoils Software	31
4.4. Results	34
5. THE EFFECTS OF AIR FLOW MALDISTRIBUTION UNDER FROSTING CONDITION	35
5.1. Fundamental frost models	35
5.2. Preparation of Test Operations	38
5.3. The test operations and outcomes	41

5.3.1. The measurement of performance	42
5.3.2. The Analysis of thermal and digital images	45
5.3.2.1. The calorimetric room images	45
5.3.2.2. The conditioning room images	58
5.4. The General Evaluation of Test Operations Considering Visual Results	64
5.4.1. Fan Curves	65
5.4.2. Air side pressure drop curves during the test operation	66
5.4.3. Air Flow Maldistribution Degrees	68
5.4.4. The change of heat transfer rates	70
6. CONCLUSION	81
7. RECOMMENDATIONS	83
REFERENCES	84
BIOGRAPHY	88
APPENDICES	89

LIST of ABBREVIATIONS and ACRONYMS

<u>Abbreviations</u>	<u>Explanations</u>
<u>and Acronyms</u>	
δ	: Frost Thickness (mm)
η_{fin}	: Fin efficiency
σ	: Standard Deviation
a	: Air
AMD	: Air Flow Maldistribution Degree
Avg	: Average
BR	: Blockage Ratio (%)
CFD	: Computational Fluid Dynamic
COP	: Coefficient of Performance
c_p	: Moist air specific heat at constant pressure (J/kg C)
D_o	: Tube Outside Diameter [mm]
DBG	: Densification and Bulk Growth
DDC	: Digital Direct Controller
DWC	: Drop Wise Condensation
e	: Evaporation
EXV	: Electronic Expansion Valve
f	: Fin
FP	: Fin Pitch (mm)
FT	: Fin Thickness (mm)
h_a	: Air Side Heat Transfer Coefficient (W.m-2K-1)
h_m	: Air Side Mass Transfer Coefficient (kg/m ² s)
ISHED	: Intelligent System for Heat Exchanger Design
i	: Inlet
i_{fg}	: Enthalpy of Vaporization (J/kg)
k	: Thermal Conductivity (W/m C)
Le	: Lewis Number
m	: Minute (m)
m_c	: Mass Transfer Rate (kg/s)
N	: Row Number

o	:	Outlet
P	:	Pressure
PID	:	Proportional–Integral–Derivative Controller
PIV	:	Particle Image Velocimetry
PLC	:	Programmable Logic Controller
Q	:	Heat Transfer Rate
r	:	Refrigerant
Re	:	Reynolds Number
RH	:	Relative Humidity (%)
s	:	Surface
STG	:	Solidification and Tip-Growth
t	:	Tube
T	:	Temperature (°C)
TXV	:	Thermostatic Expansion Valve
w	:	Humidity Ratio of Saturated Air (kg/kg _a)
X _L	:	Longitudinal Tube pitch (mm)
X _t	:	Transverse Tube pitch (mm)

LIST of FIGURES

<u>Sekil No:</u>	<u>Sayfa</u>
1.1: Different type of heat exchangers a) annular finned tube b) square finned tube.	2
1.2: a) and b) Illustration of fin and tube heat exchanger.	3
1.3: The principle of cooling cycle including an evaporator.	3
3.1: Description of Heat Exchanger.	16
3.2: Z.Abegg FN050-VDK.4I.V7P1 axial fan.	17
3.3: The schematic view of heat exchanger in detail.	18
3.4: The schematic view of heat exchanger circuits.	18
3.5: Hot bulb anemometer used for air flow measurements.	19
3.6: The manual traverse mechanism.	19
3.7: a) Thermal Camera and b) Digital Camera.	20
3.8: Schematic of the experimental set-up a) conditioning room b) calorimetric room.	21
3.9: The real pictures corresponding related test facilities room a) conditioning room b) calorimetric room.	22
3.10: The schematic of water installation line.	22
3.11: Superheat Control.	23
3.12: Measurement System Diagram.	23
3.13: The principle of control.	24
3.14: PID diagram of experimental set-up.	25
4.1: The view of each circuit measured temperature and air velocity.	27
4.2: Airflow distribution maps a) calorimetric room b) conditioning room.	28
4.3: Average air velocities for each test process.	28
4.4: The measurement of air flow rate of unit cooler at dry condition.	29
4.5: The measurement of air flow rate of unit cooler at frost condition.	29
4.6: The test results for each room.	30
4.7: The refrigerant outlet temperature values measured via thermocouple.	31
4.8: The interface of FrtCoils Version 4.0.5.0.	32
4.9: The percentage of capacity deterioration.	34

5.1:	Frost formation of evaporator surface.	36
5.2:	The illustration of frost growth (a through c).	37
5.3:	Water droplet distribution at each stage.	37
5.4:	The evaporator under frosting test at calorimetric room.	39
5.5:	The location of pressure measurement points.	39
5.6:	Temperature and humidity measurement box.	40
5.7:	The evaporator under frosting test at conditioning room.	41
5.8:	The location of pressure measurement points.	41
5.9:	The entire parameters belonging to calorimetric room during test time.	42
5.10:	The entire parameters belonging to conditioning room during test time.	43
5.11:	The air inlet temperature during the test process.	43
5.12:	The relative humidity during the test process.	44
5.13:	The evaporation pressure during the test process.	44
5.14:	a) The digital and b) thermal images at 70 minutes.	46
5.15:	The digital (left) and post images (right) at 70 minutes.	47
5.16:	a) The digital and b) thermal images at 140 minutes.	48
5.17:	The digital (left) and post images (right) at 140 minutes.	49
5.18:	a) The digital and b) thermal images at 208 minutes.	50
5.19:	The digital (left) and post images (right) at 208 minutes.	51
5.20:	a) The digital and b) thermal images at 267 minutes.	52
5.21:	The digital (left) and post images (right) at 267 minutes.	53
5.22:	a) The digital and b) thermal images at 329 minutes.	54
5.23:	The digital (left) and post images (right) at 329 minutes.	55
5.24:	The post images of circuit 2 and measurements.	57
5.25:	a) The digital and b) thermal images at 80 minutes for each circuit.	58
5.26:	The digital (left) and post images (right) at 80 minutes.	59
5.27:	a) The digital and b) thermal images at 145 minute.	60
5.28:	The digital (left) and post images (right) at 145 minutes.	61
5.29:	a) The digital and b) thermal images at 255 minute.	62
5.30:	The digital (left) and post images (right) at 255 minutes.	63
5.31:	The fan curves used at the test operation.	65
5.32:	a) stall condition at axial fan (Test 3) b) surge condition at centrifugal fan (Test 4).	66

5.33: The fan stall and surge conditions.	66
5.34: The air pressure drop versus time during test operation.	67
5.35: The changing of air flow rate versus time during test operation.	68
5.36: Calorimetric room air speed distribution.	69
5.37: Conditioning room air speed distribution.	69
5.38: The improvement of air flow rate with increasing time in middle of test unit located in calorimetric room.	71
5.39: The thermocouple values at outlet of each circuits (Test 3).	72
5.40: The thermocouple values at outlet of each circuits (Test 4).	72
5.41: The changing of cooling capacity versus minutes during test operation.	73
5.42: System Performance Figure with Different Levels of Airside Maldistribution, EXV.	76
5.43: a) the frost pattern at conditioning room b) the frost pattern at calorimetric room.	76
5.44: The air velocities measured at each circuits.	77
5.45: The relationship between heat transfer coefficient and mass transfer rate.	78
5.46: The capacity changing during the related frosting test.	78
5.47: The superheat changing during the related frosting test.	79
5.48: The changing of superheat temperature versus minutes during test operation.	79

LIST of TABLES

<u>Table No:</u>	<u>Page</u>
3.1: Geometric parameters.	17
3.2: The operation conditions.	25
4.1: The value of AMD occurring at each circuits and entire coil.	27
4.2: The average value of test parameters.	30
4.3: FrtCoils results according to measurement of conditioning room.	33
4.4: FrtCoils capacity results according to measurement of calorimetric room.	33
4.5: The comparison of FrtCoils and experimental results.	33
5.1: The operation condition of frosting test.	42
5.2: The average operation conditions.	44
5.3: The summary of measured fin thickness, tube thickness and total BR of calorimetric room for each circuit.	57
5.4: The summary of measured fin thickness, tube thickness and total BR of conditioning room for each circuit.	64
5.5: The general view of study outcomes.	64
5.6: The mean velocities and standard deviations (AMD) for each circuit.	68
5.7: The evaluation of frosting test results considering FrtCoils.	73
5.8: The comparison of measured parameters among two test.	80
A.1: Measurement uncertainties.	89

1. INTRODUCTION

Significant capacity lost might be occur from air maldistribution due to air-side fouling, improper design and installation of evaporators or fan characteristic or refrigerant side maldistribution due to uneven circuit flow resistance, uneven separation of liquid and vapor refrigerant within the refrigerant distributor or uneven air-inlet temperature distribution caused by air recirculation or air side economizers. These situations may result in different superheat at outlet of evaporator. Thereby, the expansion of valve reduces and its openness in order to ensure desired outlet refrigerant temperature, hence the capacity of evaporator decreases.

The refrigerant side maldistribution is prevented readily by using proper distributor, but the prevention maldistribution caused by air side is very difficult. This phenomenon directly affects the internal temperatures of refrigerant and this matter have more detrimental effects as the evaporator enlarges. When the literature was reviewed, it was observed at most of studies that the air side maldistribution was examined by forming various air side distribution via blockage.

Scope of this project, it was only investigated the effects of air flow maldistribution that occurring in front of evaporator, on heat exchanger performance and frosting by considering as the product with its fan integrated, which is entitled as unit cooler at real practical implementation. However, the impacts were investigated for both dry and frosting test conditions.

Heat exchanger is defined as equipment that transfers the energy from a hot fluid to a cold fluid. In heat exchangers, the temperature of each fluid changes as it passes through the exchangers. The fluids are generally separated by a solid wall to prevent mixing or they may be in direct contact. They are widely used in space heating, refrigeration, air conditioning, electronic components, power stations, chemical plants, petrochemical plants, petroleum refineries, natural-gas processing and the sewage treatment.

In the scope of this study, we used tube and fin heat exchanger, which is used gas and fluid, the heat transfer coefficient on the liquid side is generally higher than that on the gas side. Hence, to have balanced thermal conductance on both sides for a minimum-size heat exchanger, fins are used on the gas side to increase surface area.

This is similar to the case of a condensing or evaporating fluid stream on one side and gas on the other.

Depending on the fin type, the tube-fin exchangers are categorized as shown in Figure 1.1: number of 1 and 2 depicts that annular finned tube heat exchanger and square finned tube exchanger. However, it was dealt with second type of heat exchanger in scope of this study. The fins can be plain, corrugated or louver etc, but it is designed as plain fin because of the fact that the usage of this type fin ensures ease of measurements during the frosting test processes.

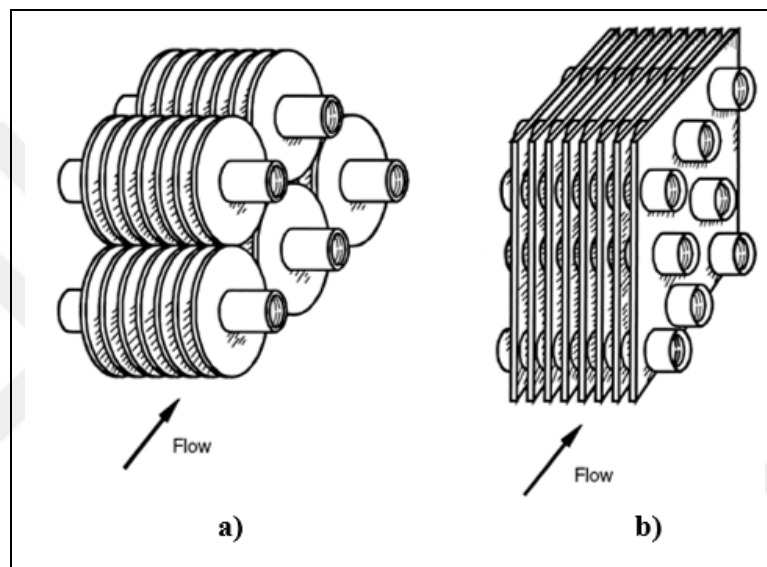


Figure 1.1: Different type of heat exchangers a) annular finned tube b) square finned tube.

Principle of operation is very simple. However, carrying out performance analysis is hard due to plenty of parameters affecting heat transfer rate. Heat exchange occurs as perpendicular among the two fluids, but when carried out mathematical solution. Nevertheless, it is admitted that two fluids flow in opposite direction.

When it is looked at design of finned tube heat exchanger in detail, a fin and tube heat exchanger consists tubes, fins, inlet and outlet manifolds, distributor as illustrated in Figure 1.2. The tubes extend throughout heat exchanger and the fins are placed over these pipes firmly. Furthermore, the distribution and collecting of refrigerant are ensured by the means of distributor and outlet manifold, respectively.

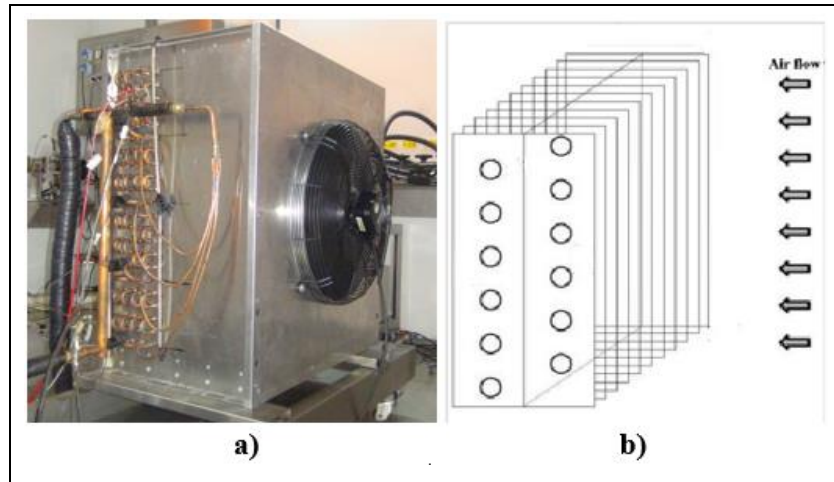


Figure 1.2: a) and b) Illustration of fin and tube heat exchanger.

If it is about the general cooling cycle briefly, the cooling system has to include four essential sections which are as illustrated in Figure 1.3. First of all, a compressor pumps the refrigerant gas coming from evaporator up to a high pressure and temperature. Then, the gas loses heat energy to the outside, cools, and condenses into its liquid phase via condenser and the pressure of liquid phase of refrigerant is decreased and regulated the refrigerant liquid to flow at the proper rate by expansion valve. Finally, the liquid refrigerant evaporates by absorbing energy from room, it exits from evaporator as vapor, returns to compressor and repeats the cycle again and again.

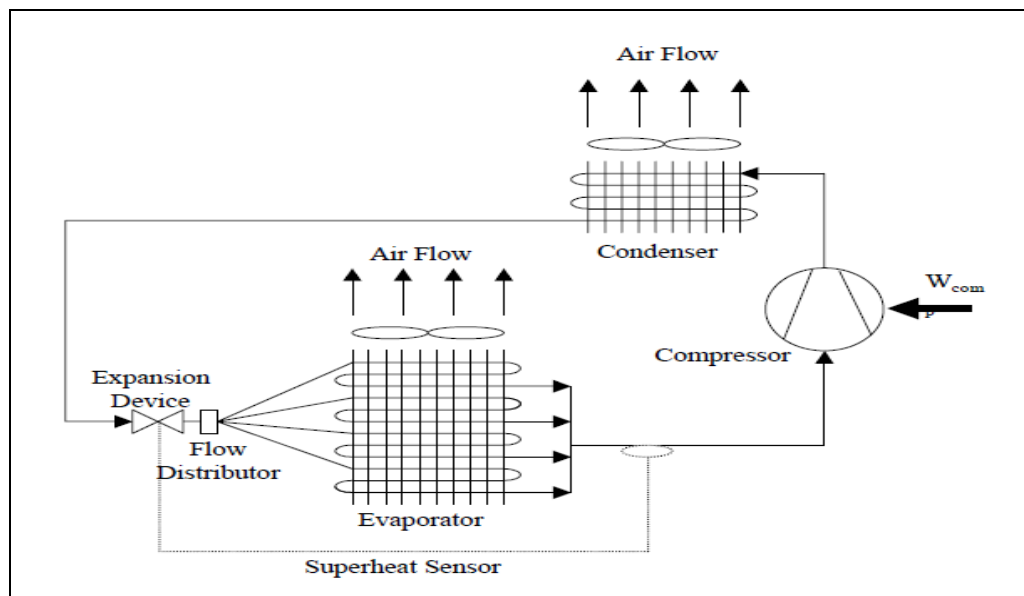


Figure 1.3: The principle of cooling cycle including an evaporator.

Evaporators have a lot of problems such as unsuitable design, air side velocity, temperature and humidity maldistribution and flow side maldistribution, and the usage place ext. Scope of this study, it is going to be examined a rather considerable design problem, that is air side maldistribution. When reviewed the literature, it was noticed that as many researchers investigated the effects of refrigerant side maldistribution on the heat exchanger performance and solution of this negative impact, a little number of researchers dealt with the problem of air side maldistribution, particularly velocity maldistribution having the most important impact on evaporator and the temperature maldistribution as well.

Air side maldistribution might be resulted from following reasons;

- Uneven fouling occurring external surface of evaporator
- Non-uniform formation of frost
- The limits of evaporator

Accordingly, it is going to be selected an evaporator prevented the refrigerant side maldistribution by the using of the distributor type belonging to Sporlan-Parker Company design and taken a large number of air side measurements inlet of heat exchanger via hot bulb anemometer, which has 3 mm probe, so this probe does not lead to significant pressure drop. Then created the graphics showing the air side velocity distribution and determined standard deviation of each circuits as shown below. Each circuit is going to be considered as separate evaporator and the total capacity of evaporator will be acquired summing four circuits, after that these capacities is going to be solved by means of FrtCoils software by considering refrigerant outlet temperatures and average velocities correspond to each circuit.

Then, the test process is going to be performed for in order to identify the performance deviation between the uniform and non-uniform airside conditions at conditioning and calorimetric room respectively. After that process the test results are going to be compared by using the outcomes of the FrtCoils program.

The second part of this study is about frosting investigation at the same unit cooler. The test process is going to be carried out at calorimetric and conditioning room, separately. In this context, frost growths are going to be followed up

depending on the time. Within this time, it is going to discuss the distributions of frost in front of unit cooler, frost thicknesses and blockage ratios at the end of the test, the changing of air pressure drops and heat transfer rates which depending on the frost growth, the effects of type of fan and AMD (Air flow maldistribution degree) considering mass transfer phenomenon.



2. LITERATURE REVIEW

Yaici et al. (2014) performed a numerical work using 3D CFD (Computational Fluid Dynamic) in order to predict to influence of seven different inlet air velocity profiles and different combination of the Reynolds number simulating inlet flow maldistribution on the thermo-hydraulic performance of heat exchangers. Their aim of this process is to collect data for realizing optimum design of header and distributor configurations of heat exchangers to minimize the maldistribution. The numerical results show that the inlet air flow distribution is the considerable impact on the fluid flow, thereby on performance of heat exchanger due to the non-uniform distribution, namely, CFD results indicate that up to 50% improvement or deterioration in the Colburn j and friction f factors are found compared to the baseline case of a heat exchanger with a uniform inlet velocity profile. In addition to this, it was detected that the variation in thermal performance is more pronounced at low Re and this situation tends to decrease at high Re .

In practical application such as automotive cooling systems, the large number of materials may cause in blockage in front of evaporator, which is taken inlet air flow, thereby this issue may induce decreasing the air flow rate or non-uniform air flow maldistribution. In this context, some researchers [Datta et al.,2014] created by placing different upstream screen so as to realize the different blockage type and blockage ratio for each type of blockage variations and examine these situation's effects on the overall performance of the system. As a result of performing of the 52 experiments, depending on severity of air maldistribution, cooling capacity decreased by 8.16% for an area blockage of 50% compared with the normal operating condition. Besides, it is detected that which blockage's effect which is more severe and which blockage have minimum detrimental impact.

In most cases, there may be exist an obliquity, namely non-uniform air flow distribution, between the directions of frontal air flow and normal of coil tubes, which could be based on restricted installation or tortuous air-flow paths. Another study [Chen et al., 2005] which is about in this context about air flow non-uniform distribution that depending on oblique angel of inlet air velocity and influences of this situation on heat exchanger performance, pressure drop and the frosting is investigated. They have presented a set of equations, which can be used to predict the

performance parameters of an evaporator, when there is an oblique angle between the inlet air velocity and frontal face of the evaporator. It was concluded that oblique velocity causes the decrease of evaporator capacity, but this capacity decreasing is not only depending on oblique angle of inlet air, but also this study shows that the oblique angle has some impacts on the evaporator parameters such as the refrigerating capacity, frost weight and the air side pressure drop to different extents.

Another study [Jianying et al., 2008] claimed that the refrigerant system performance data such as suction pressure, evaporation temperature, discharge pressure, refrigerant outlet temperature, etc. may be affected of some extent depending on AMD. In the course of the experimental analysis, the air velocities were measured at 56 points at the inlet of evaporator and that is determined three different air flow distributions. These degrees are according to relative standard deviation formula and then each AMD were entitled as uniform, non-uniform and seriously non-uniform at 18%, 49% and 93%, respectively. Depending on this experiments that performed for each AMD, they concluded that air flow maldistribution was the dominant factor leading to hunting of the thermostatic expansion of valve and lead to non-uniform distribution of the refrigerant circuits, so that superheat temperatures for each circuits were difference. Besides, with air flow maldistribution degree (AMD) increasing, the difference of superheat temperatures increased, frost occurred earlier, the frost layer grew faster, which contributes to diminish the length of refrigeration system the stable working time, the operating characteristics is became lower and the performance of the data aforementioned were degraded more dramatically. This frosting comments are going to be considered again in scope of frosting test operations.

A study [Domanski and Lee, 1997], which is considered the effects of air side and refrigerant side maldistribution on the coil capacity, designed three evaporators which had identical design specifications but different refrigerant circuitry and air distribution. For these cases, the experimental results showed a much greater sensitivity to air maldistribution than refrigerant distribution. Also, they detected that maldistributed air is affected refrigerant distribution, which is caused further coil capacity degradation.

In another study [Payne and Domanski, 2003] initially the maldistributed refrigerant tests was performed with uniform air flow and it was observed that capacity degradation can be as much as 30%, even when the overall evaporator

superheat is kept at a target temperature. Latter the study is the non-uniform air flow test according to constant air flow rate and reduced air flow rate separately. At the constant volumetric air flow rate, the capacity differences between the superheat that depending on the blockage and it is adjusted to constant temperature for different air velocity ratios, which were obtained by adjusting fan speed, obstruction that could be as much as 6%, in the same way, the capacity degradation due to reduced air flow rate, which is decreased with air flow obstruction, was more negative than constant air flow rate tests, hence the drop in capacity was as much as 8.7%. In addition to these results, they have where added that when circuits are not well balanced, the target overall superheat is a result of mixing a highly superheated refrigerant and the two-phase refrigerant leaving different circuits. This causes the significant degradation in the evaporator capacity because of the circuit with superheated refrigerant transfers less than the heat. Also, this issue may occur even though the overall superheat is maintained.

Another related study [Domanski et al., 2004] showed that nearly all of the capacity reduction due to non-uniformities in the velocity profile can be recuperated by simply redesigning the tube-to-tube connection sequence by means of a simulation package.

It was performed that the study [Yashar and Cho, 2007] which aims to measure and determine the velocity distribution of air via PIV method and as a two dimensional for selected 3 typical finned-tube heat exchanger configurations and that used these air data so as to develop a CFD models of these installations and thereby design is more efficient finned-tube heat exchangers. At the end of this study, they were observed that the velocity distribution is strongly influenced by the features within the duct and the orientation of the heat exchanger and therefore it is generally not uniform at all. Besides, the cause of reducing the heat exchanger performance which is each tube of heat exchanger could have different amount of air flow, even no air flow. So that they specified that finned and the tube heat exchanger can be thought as a network of a single tube cross flow heat exchanger and each tube should be performed differently. The another study [Yashar and Domanski, 2007] was application of an evolution program, which is referred as ISHED (Intelligent System for Heat Exchanger Design) and it optimizes refrigerant circuitry by considering air flow distribution.

The study [Domanski et al., 2011] was handled to provide information for predicting the inlet air flow distribution and understand source and magnitude of air side maldistribution at louvered-fin heat exchanger installed vertically in a horizontal duct by using the PIV (Particle Image Velocimetry) and CFD model. They illustrated that the CFD results matched well with the PIV measurements and it stated that this study was the first step so as to be understood that more complex air flow distribution.

The effects of different included angles between the air cooled condenser (V Type) performance was investigated by Lee et al., (2010). Their study attempted to reduce the maldistribution of the airflow through the condenser face, thereby to improve the heat transfer performance. In this context a number of studies used same fan, they were performed as numerical and experimental, they detect that changing the angles of coils has considerable effects on airflow distribution, therefore the heat transfer performance, namely 7.85% and 5.29% respectively. As the similar with my study, the coil face was subdivided by different region and average air velocity was calculated for each region. After that, according to each velocity, the heat transfer coefficient and heat transfer rate were calculated for these region. Consequently, total heat transfer rate was determined by summing up each region values.

Several researchers [Aganda et al., 2000] carried out a numerical studies of the effects of maldistributed air flow through the evaporator of a packaged air-conditioning unit. Their studies were demonstrated that altering the airflow distribution could significantly change the overall performance of the system. It also effects of the air maldistribution, which could lead to reduction in the refrigerant mass flow, that caused a loss up to 38% in evaporator has the heat transfer performance.

At the current study [Domanski et al., 2015], they were examined the effect of the optimizing the refrigerant circuitry on the evaporator performance which is carrying out according to the measured air distribution via PIV method of the coil through the surface. They concluded that the measurement has improvement performance was about 2.2% capacity and 2.9% COP increase, when compared with manufacturer's original circuitry. In addition to this outcome, it was specified that local airside velocity is one of the most important parameters because of this situation has profound impact on the overall heat exchanger performance.

Another study [Kim et al.,2008] investigated the using of flow balance valve at the inlet and outlet of evaporator with respect to air flow distribution factor in order to recover of loss cooling capacity and COP resulting from the non-uniform air flow distribution. In this context, the simulation model of predicting cooling capacity and the system performance in cooling mode compared with measured data and used to detect to effects of air and refrigerant flow mal-distribution on capacity and COP. According to this study results, they were founded that while using refrigerant flow of balancing control at the exit of circuit had little benefit due to the increasing of pressure drop, using refrigerant flow balancing the control at the inlet of circuit could ensure significant performance augmentation that depending on the severity of air flow maldistribution.

The other study [Qiao et al., 2010] which is regarding on the compensation of the non-uniform air flow distortion at water coil by optimizing fin density via Genetic Algorithms was carried out scope of this project, it was investigated that the effect of the two different air distribution profile on performance of the coil and that detected as much as 3% capacity degradation for these two conditions. In order to recover this capacity, it was optimized the fin density through the coil. Consequently, although they had negligible capacity which gains but ensured fin material saving by about 10%.

There are a large number of frosting study at literature. Some of them is about the formation of frosting and the others are about the frost thickness and it has effects on the heat exchanger performance which depending on the structural conditions such as fin spacing, tube spacing and the environmental conditions such as evaporating temperature, relative humidity and air flow rate. The scope of this study, it is going to be investigated that the effect of air maldistribution on frosting parameters such as total frost thickness and frost thickness distribution at each circuits, total blockage ratio, the change of the capacity and pressure drop during test etc. Consequently, the real aim is to detect the relationship between air velocity and frost thickness, which is not exactly clear at literature.

An important numerical frosting study [Huang et al., 2008] investigated the effects of frost thickness on heat transfer performance considering different fin pitches and fan types. Their study, which has given as very important information about initial frost surge and the effect of fan types on frosting condition, concluded that the initial surge which is related to the frost thermal conductivity unlike the

surface roughness because surface roughness is only effective at turbulent flow region. Latter, the defrost period should start when the half of flow area is blocked by frost and also the larger fin pitch should be used in case of excessive operation period. Moreover, they recommended that while the using of axial or centrifugal fan are not different for larger fin pitch heat exchanger, the centrifugal fan should be used except the long term operation with thick frost at small fin pitch heat exchanger. On the other hand, they specified that when the airflow is reduced depending on the frost growth, as the centrifugal fan becomes unstable, the axial fan is more stable and the air flow rate decreases faster due to stall in the middle region.

It is performed that the experimental study [Haijie et al.,2014], which was the examined the effects of the fin spacing, fin coating material, relative humidity, evaporating temperature and the air flow rate on the performance of air coolers during frosting process. Air flow rate was controlled by varying the frequency of fan motor of the air cooler and that examined the first occurrence of frost and frost layer thickness for each fan frequency. As a result, increasing the air flow rate could delay the first occurrence of the frosting because of the fin and tube temperatures increase and the increased air velocity could blow away the frost crystal particles, hence the growth rate of frost thickness could be delayed owing to appropriate air flow rate, thereby, defrosting interval can be increased. Also, they specified that the frosting rate is not sensitive to the airflow rate because the test results revealed that the frosting rate is almost same for different frequencies.

The another numerical and experimental studies [Da Silva, 2012] regarding frost formation is aim to observe of the frost formation phenomenon on the evaporator by the taking into account air flow reduction resulting from frost formation and the thermal-hydraulic performance of evaporators operating under frosting conditions. It was concluded that the high degree of difference between surface temperature and dew-point temperature decreases the frost density, as opposite increase the mass transfer rate. Moreover, they recommended that air entrance evaporator region should have smaller fin density and also stated that air flow reduction is the main cause for the cooling capacity reduction.

It is carried out an another experimental study [Kim et al., 2002] under frosting condition so as to investigate heat and mass transfer characteristics of evaporator. Depending on the experimental outcomes found, they identify a correlation that could be used to optimum design an evaporator under frosting conditions. They are

also pointed out that although frosted surface occurring the early stage of frost formation improves the thermal performance and fin efficiency, frost layer acts an insulation layer and causes increasing of pressure drop by the time of progress; thereby this issue results in less air flow rate and reduction of performance. Moreover, uneven frost formation brings that about the higher pressure drop as compared with even frost distribution.

Another frosting study [Yan et al., 2003] investigated experimentally that the effects of various parameters such as relative humidity, fin pitch, row number under frosting conditions but it is going to be dealt with the effect of air flow rate at same condition. In this context, they are carried out test process in order to show the effect of air flow rate on heat transfer and pressure drop characteristic of heat exchanger. As a result of the frost formation is greater for a lower air flow rate because of the surface of heat exchanger is colder, when the exposed lower air flow rate, this situation causes the increment of pressure drop due to the fact that the more frost formation occurs, the more blocking passage occurs. In addition to, increasing of frosting rate which leads to degrade faster the heat transfer rate and the overall heat transfer coefficient.

It was carried out an experimental study [Tashiro and Hamada, 2014] in order to investigate the effects of humidity and the air inlet velocity on frost formation and it deal with understanding what is the dominant factor of the frost formation. If taken into account effects of air velocity in this study, they have concluded that higher inlet velocity reduces the thickness of frost layer because of the fact that high heat transfer rate makes the frost layer denser although as inlet velocity increases, the frost mass also increase as well. Hence, they specified that the inlet velocity have considerable effect on the frost density. In addition to, they added that the effect of inlet air velocity is minor impact in the region of high relative humidity.

In this study [Cui et al., 2011], the performance of fin-and-tube heat exchanger under the frost condition was investigated as a numerical and validated via analytical method. Furthermore, effects of fin pitch, relative humidity, airflow rate and evaporating temperature on frost thickness, heat exchanger coefficient and pressure drop was examined separately as well. As a result, if it is talked about the effects of air flow rate related with our topic, the amount of the frost accumulation increases as the velocity of moist air decreases because of the temperature difference between

moist air and fins are larger. Depending on this situation, the heat exchange coefficient degrades faster and the pressure drop enlarges significantly.

The studies belonging to Kwan-Soo Lee and his colleagues are investigated. Accordingly, the first study regarding frosting is about frost formation on cold flat surface [Lee, 1997]. They developed a formulation of frost layer occurring on cold flat surface. In order to validate present model, it was compared with experimental data. They concluded that frost layer grows rapidly with increasing air velocity due to active mass transfer. Besides, surface temperature of frost increases with increasing air velocity because thermal resistance of frost increases depending on growth of frost layer. In addition to, they stated that if the Reynolds number is over 10000, frost thickness in air flow direction is almost the same.

Same author and his colleagues [Lee et al., 2014] investigated the frost retardation on fin-tube heat exchangers with respect to air velocity directly. The most important claim for authors that they have highlighted that air velocity on the frost growth rate is unclear although there has been a large number of basic study. Accordingly, they investigated dependence of mass transfer rate on the air velocity via experiments and mathematical mode. It was defined a critical air side heat transfer coefficient which is at maximum mass transfer rate and this term was validated. Consequently, they identified that the frost growth was considerable retarded when heat exchanger was operated avoiding the critical air-side heat transfer coefficient.

According to another study performed by same researchers [Lee et al., 2013], they presented a numerical model, carried out considering experimental outcomes and taken into account the airflow reduction depending on the frost formation. Accordingly, it was concluded that the dominant factor on frost density was air temperature and velocity, also these parameters had greater impact when compared with air humidity and surface temperature. Besides, they stated that the porous character of the frost layer was found to be a significant factor in the pressure drop in the heat exchanger and obtained a new approach between the pressure drop and Reynolds number.

Another study [Moallem et al., 2010] was taken into account the effect of air velocity on frosting on microchannel heat exchangers. Scope of this study it was concluded that while water retention and air velocity lead to minor changes the frost

time and frost weight, surface temperature and relative humidity are main factors that affect these parameters.

Another researcher [Padhmanabhan et al., 2011] created a new algorithm considering the air redistribution, occurring that depends on non-uniform frost thickness on the heat exchanger face and its impacts on capacity and frost thickness. They specified that for the high air velocities, the heat transfer coefficient is higher, this case results in higher fin surface temperature and mass transfer coefficient. As the higher fin surface temperature inhibits the frost growth, higher mass transfer coefficient increases the frost deposition. According to their experimental outcomes, frost thickness has decreased at higher velocities. It means that the surface temperature has more significant impact on frost growth than mass transfer coefficient. Although, this study is very good in terms of technical mind, there may be a problem about the air redistribution, that is, the air redistribution has started after the 80% blockage ratio of frost. Normally, the defrost operation should start about 60% blockage ratio of frost, so that the practical application of this condition is not possible.

The validated numerical study [Chen et al., 2003] considered the effects of fan types under frosting conditions as similar with scope of this study. According to this study, changing the fan from axial type to centrifugal type does not have significant impact on performance, blockage ratio and air flow rate.

In contrast to mentioned above regarding air velocity effect on frosting, a current numerical study [Lee et al., 2015] demonstrated that the average frost thickness increased by increasing inlet velocity according to their numerical study and other experimental studies cited. They based on this finding to increasing mass transfer but neglected to increment of surface temperature. Moreover, they developed a numerical model calculating the average frost thickness, average frost density and frost surface temperature.

The final project report [Groll et al., 2011], considering real fan impact, was investigated the effects of air and refrigerant maldistribution by considering thermostatic, electronic and individual circuit refrigerant (hybrid) flow control separately. Study concluded that as the hybrid control is the better solution in terms of extending of runtime of frosting test and capacity recovering against air flow blockage and maldistribution, the thermostatic expansion valve control (TXV) is vice versa. The electronic expansion valve control (EXV) used my thesis ensures more

advantage at frosting test when compared with TXV control because the superheat temperature and evaporation pressure is constant longer time. Furthermore, for blocked-coil tests, they found that the performance decreases with increasing airside maldistribution, and that this degradation of performance decreases for increasing condenser air inlet temperature.

2.1. Summary of Literature

This literature review has identified a number of studies that investigated the change realizing at air flow of heat exchanger and they effect on dry condition and frost condition test, respectively.

In part 1, it is mentioned the effects of air flow maldistribution on the heat transfer rate of the heat exchanger, although the air maldistribution has been smaller effect on heat transfer rate when compared with refrigerant side maldistribution, it has been carried out a large number of study and this problem is able to prevent by redesigning the refrigerant circuits according to air flow rate in general. However, as the product is bigger, the possibility of air flow maldistribution increases, so that this problem could be more important for air cooled condenser used at power plant and dry coolers.

In part2, it is clarified that the effects of airflow rate and non-uniform distribution in front of heat exchanger are still unclear for frosting conditions and need to be focused to this situation at further studies as experimental. However, the interesting point was detected that there was quite limited study considering real fan effect on frosting test operations similar as practical conditions. The previous studies generally deal with the investigations under constant air flow conditions.

3. EXPERIMENTAL METHOD

The test operations were performed at Friterm Inc. Heat Exchanger Test Laboratory. During the test operations, it has been followed a procedure and used some apparatus and this section mentions this details meticulously.

3.1. Experimental Apparatus

In this section, the heat exchanger used in study, hot bulb anemometer used to purpose of measurement of air velocity at windward of heat exchanger, a digital and thermal camera in order to identify the frost thicknesses at specific area and temperature variations among the refrigerant circuits, respectively.

3.1.1. Description of Heat Exchanger

It was used a fin and tube heat exchanger, entitled as unit cooler, in this study, which is specified in Table 1 and illustrated in Figure 3.1. The unit cooler is a fin-and-tube cross-flow heat exchanger which transfers heat from a forced air flow to the refrigerant. It was manufactured by FRITERM Thermal Devices Incorporation. As stated in Table 1, fin type was selected as plain because of better visualization and easy measurement of frost occurring at fin surface.

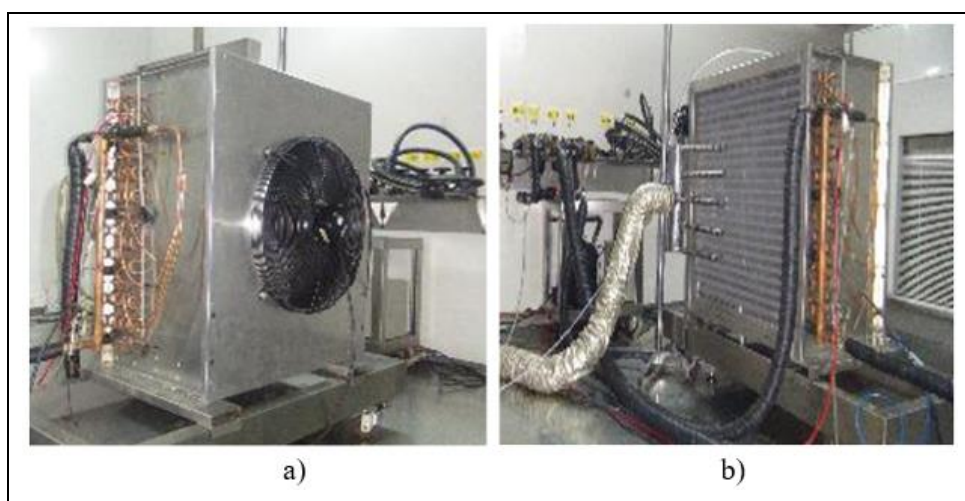


Figure 3.1: Description of Heat Exchanger.

Table 3.1: Geometric parameters.

Geometric parameters	Values
Number of rows	4
Number of tubes per row	22
Transverse tube pitch	35 mm
Longitudinal tube pitch	35 mm
Tube length	745 mm
Tube diameter (inner/outer)	11.86 mm/ 12.5 mm
Fin thickness	0.15 mm
Fin spacing	7 mm
Fin type	Flat
Fin height	770 mm
Tube arrangement	inline

The evaporator is equipped with a 500 mm fan from the German manufacturer Ziehl-Abegg with a maximum capacity of 9500 m³/h that illustrated below in Figure 3.2. Fan diameter was selected as higher because the air flow maldistribution could be more influential for large diameters of fan.

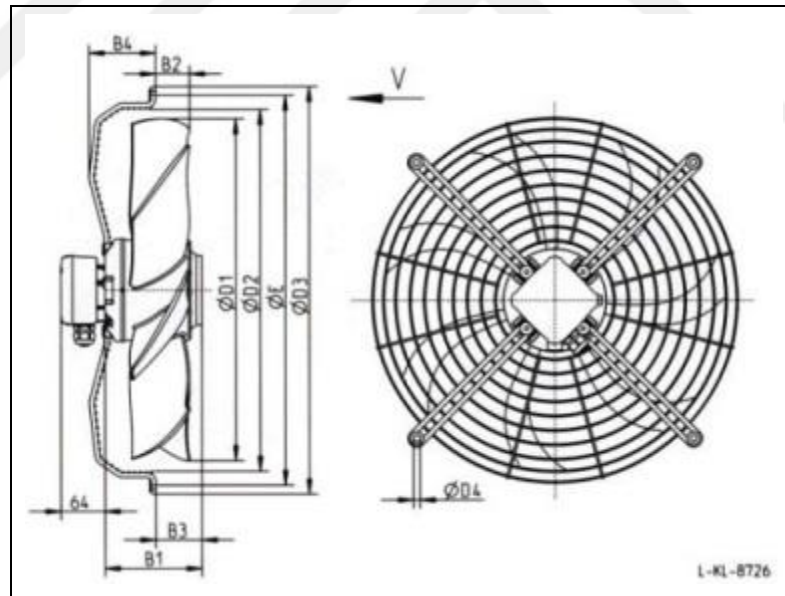


Figure 3.2: Z.Abegg FN050-VDK.4I.V7P1 axial fan.

Figure 3.3 shows the representative view of heat exchanger including tube rows and its location layout entitled staggered grid, evaporator used scope of this study consists of a lot of fin that has four tube rows of 22 tubes in each, yielding a total of 88 tubes.

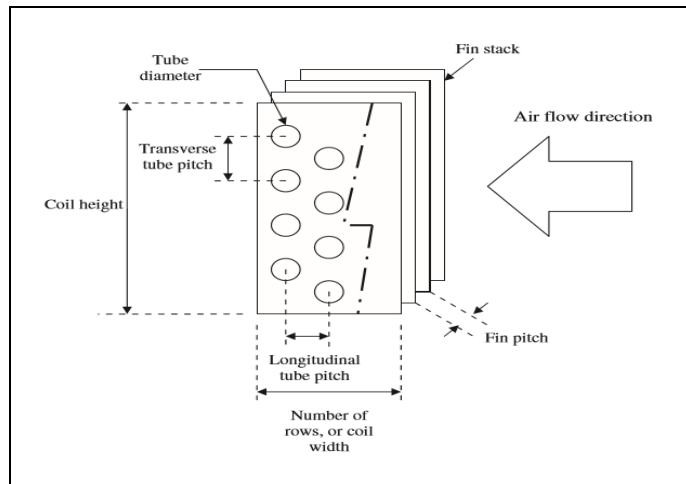


Figure 3.3: The schematic view of heat exchanger in detail.

The evaporator has four circuits and each circuit has equal tube length, feeding almost same refrigerant mass flow rate by means of ideal nozzle type distributor as shown in Figure 3.4.

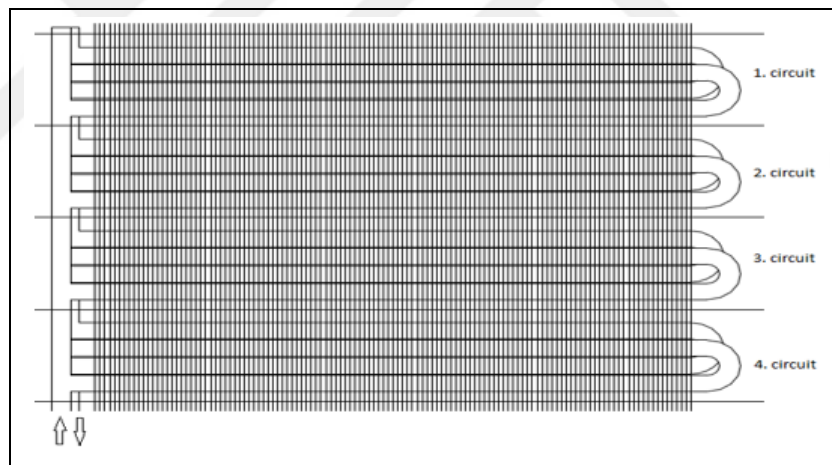


Figure 3.4: The schematic view of heat exchanger circuits.

3.1.2. Description of Anemometer

As illustrated in Figure 3.5, the hot bulb anemometer, which has 3 mm diameter, is used for the purpose of measurement of 3-D air velocity and temperature at inlet of heat exchanger and the cause of using small diameter probe can't disrupt the incoming air flow and that ensure taking measurements at corner points of evaporator. Owing to this device, we could detect the air maldistribution degree as regards both temperature and air flow rate and learn where the distorted areas occur.

Air flow measurement was carried out at 80 points of each circuits via a manual traverse system as shown in Figure 3.6.



Figure 3.5: Hot bulb anemometer used for air flow measurements.



Figure 3.6: The manual traverse mechanism.

During the frosting experiments, it was needed visual images in order to detect frost thicknesses, blockage ratios, the temperature distribution in front of unit cooler. For this purpose, it was used a digital camera and a thermal camera, which are SONY HDR-CX570 and FLIR E6, respectively.

3.1.3. Description of Thermal and Digital Camera

Figure 3.7 shows the external view of thermal and digital camera. In order to be taken more easy and accurate digital image, it was used a mechanism designed by us. This mechanism is placed camera ensures the movement from bottom to up, therefore, the frosting image occurring at each circuit and determined area could be measured easily and quickly. On the other hand, the thermal camera was used in order to detect the thermal distribution with time occurring in front of unit cooler.



Figure 3.7: a) Thermal Camera and b) Digital Camera.

3.2. Experimental Procedure

Figure 3.8 and Figure 3.9 show the experimental setups including calorimetric and conditioning room. The setup of calorimetric room is consisted of five components: a test section, where fin and tube heat exchanger was installed; a calorimetric room to maintain a constant air temperature and humidity, which have air handling unit; a refrigeration section to regulate the temperature and flow rate of the refrigerant for the experiments. The only difference between the conditioning room, as the air flow rate can be adjusted with the aid of wind tunnel located in this room and calculated of air capacity according to outcomes of sensors. It does not matter for calorimetric room, because unit coolers having constant air flow rate which have already been used for test operations and the air capacity for this room is calculated from electrical loads. The heat exchanger has inlet and outlet pipe which are used for charging or discharging of refrigerant respectively, also there are two sensors placed on these pipes, which are used to read inlet and outlet temperature and pressure values for each pipes. Air handling unit, where is inside of calorimetric and conditioning room both, which consist of heat exchanger and used in case of extra cooling for condenser tests but we did not need for evaporator tests, heaters and humidifier, which are run proportional according to air inlet temperature sensor and air inlet humidifier sensor adjusting by us respectively, three centrifugal fans which ensure recirculation of air.

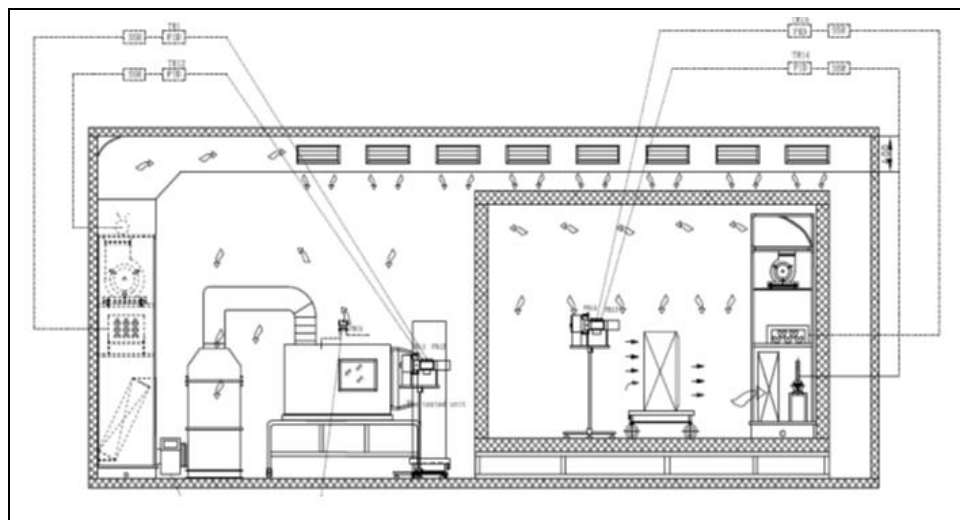


Figure 3.8: Schematic of the experimental set-up (left side: conditioning room, right side: calorimetric room).

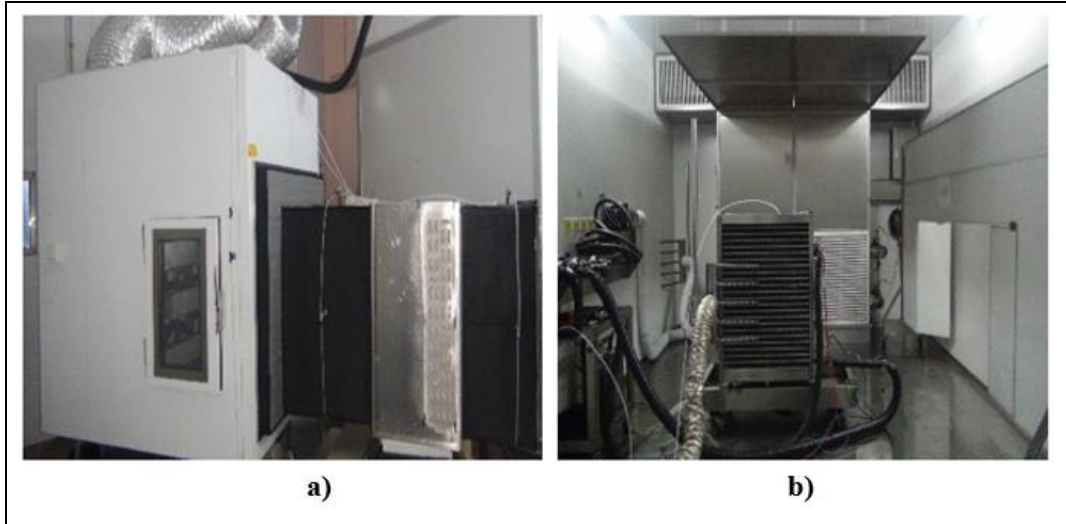


Figure 3.9: The real pictures corresponding related test facilities a) conditioning room b) calorimetric room.

The refrigerant used in these experiments was R404A and refrigerant system has an auxiliary line, which is operated with water, at as shown in Figure 3.10 and used purpose of controlling the refrigerant temperature at some part of installation such as condenser sub cooling temperature. Besides, this refrigerant line has shell and tube condenser used for system's condenser and auxiliary evaporator used in order to adjust evaporation pressure.

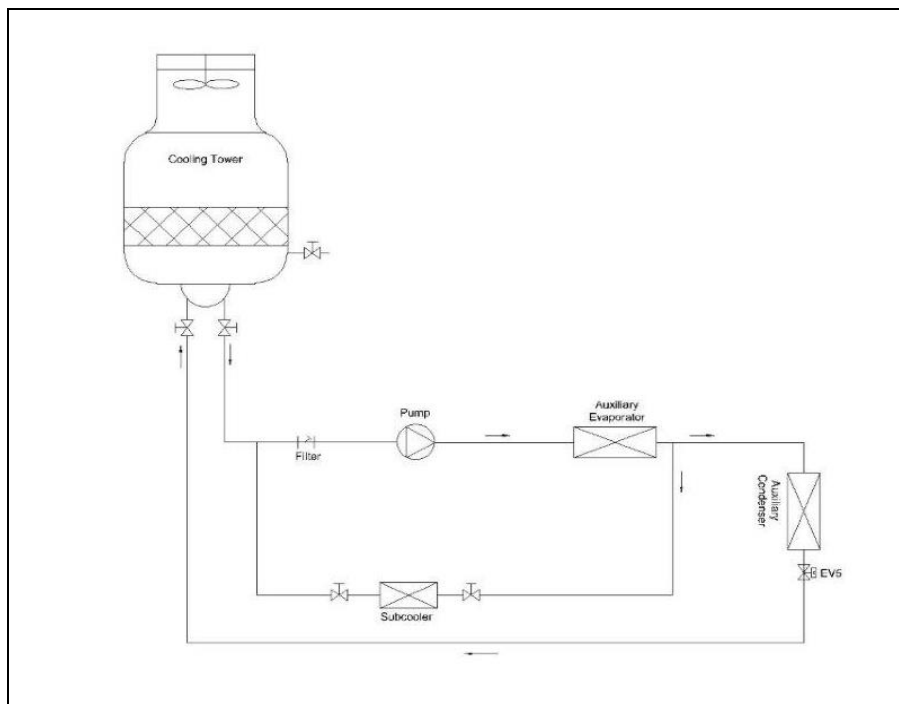


Figure 3.10: The schematic of water installation line.

The type of expansion valve is very important for frosting test because this apparatus affects the characteristic of frosting test significantly. We used the EXV (Electronic Expansion Valve) in scope of this study. A study [Groll et al., 2011] has specified that with an EXV as expansion device, a better control of the superheat than with the TXV (Thermostatic Expansion Valve) and therefore a better usage of the evaporator surface area is possible for steady-state and frost-up tests. Also, the mechanism of superheat control via EXV is illustrated in detail at Figure 3.11.

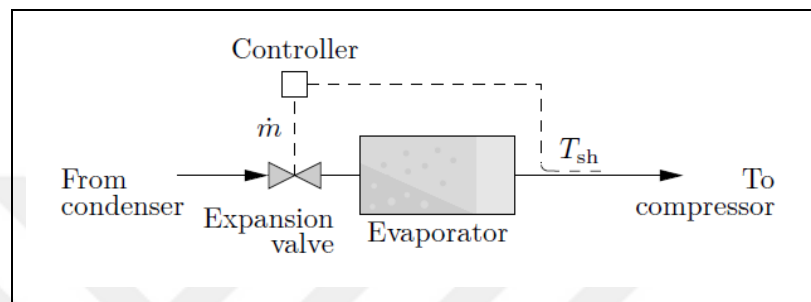


Figure 3.11: Superheat Control.

3.2.1. Principle of Control

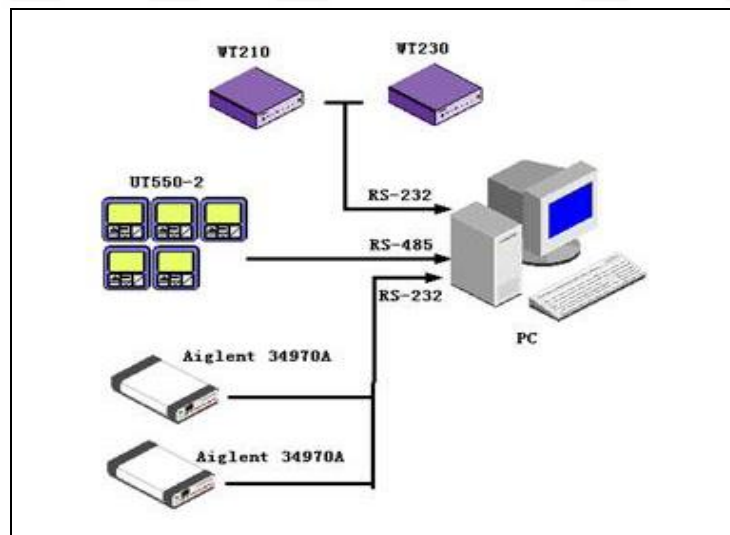


Figure 3.12: Measurement System Diagram.

The measurement system diagram is shown in Figure 3.12. The data is coming from measurement devices and they are collected owing to illustrated instruments and they are communication with high level PC with serial bus. Two Agilent 34970A acquisition units collect most of data from lab and transfer them to PC such as

thermocouple values. Yokogawa digital power meter WT210/230 measures voltage, current, power and electrical energy consumption and the air side heat transfer capacity for the test process carried out at calorimetric room is calculated directly the data coming from this power meter. WT210 and WT230 is a single phase power meter and three phase power meter respectively. While WT210 measures the test unit fan's power, WT230 measures the power input to calorimetric room such as centrifugal fans, heaters, humidifier etc.

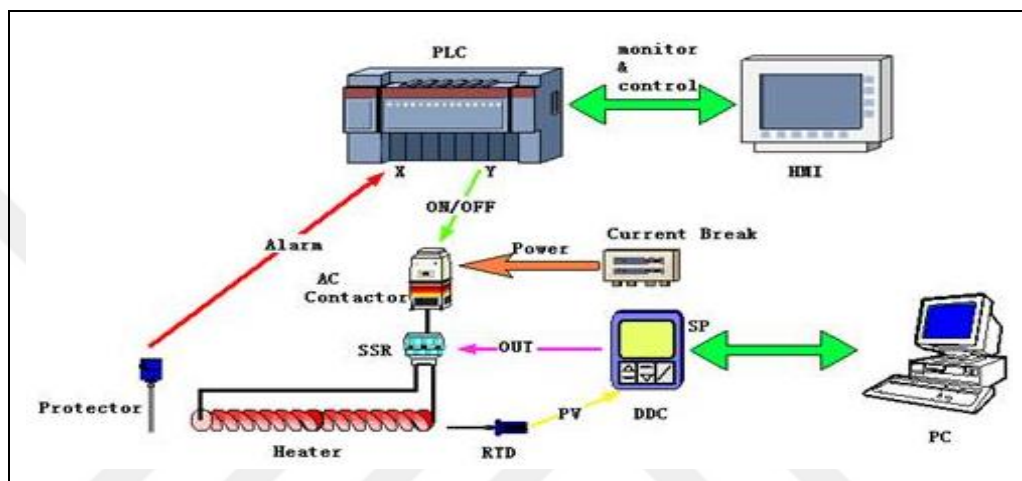


Figure 3.13: The principle of control.

In this laboratory, two level of control provides to equipments as shown in Figure 3.13. First is power supply system, the main power is supply to equipments through current break and AC contactor. This level of control is suitable for all electrical equipments. PLC (Programmable Logic Controller) manages AC contactors status by ON/OFF output signal and if is pushed the icon HMI, the control equipments can be managed status. The secondary control is capacity control, this control method ensures the smooth adjustment such equipments as heater, humidifier, valve, pump and fan. PC or manual setting of set point gives a desire value to DDC (Digital Direct Controller), sensor returns a dynamic process value to DDC during adjusting and DDC sends an analog signal to actuator based on PID (Proportional–Integral–Derivative Controller) algorithm calculation, this signal adjusts the equipment according to percentage of DDC output.

The PID loops was shown in Figure 3.14 and if talk about in detail, PID1 infers that the evaporator outlet temperature is adjusted according to EXV7 electronic expansion valve and the value of flow meter controlling the refrigerant flow rate as

manual during the test process. PID2 infers that the evaporator pressure is adjusted depending on EXV2 electronic expansion valve located on auxiliary line and PID3 infers that the temperature of before expansion valve is adjusted owing to EXV5 electronic expansion valve located on water line.

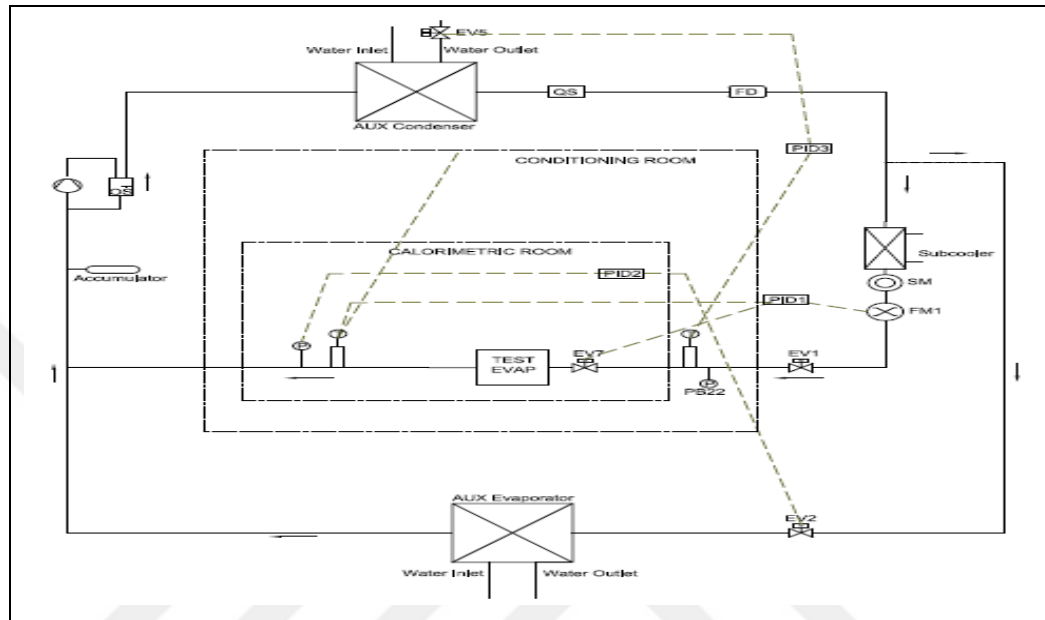


Figure 3.14: PID diagram of experimental set-up.

3.3. Experimental Conditions

The test operations are going to be carried out firstly under dry condition, then under frost condition as specified in Table 3.2.

Table 3.2: The operation conditions.

Test No.	Test Location	Tai [°C]	RH [%]	Te [°C]	Surface Cond.
1	Calorimetric room	10	50	0	Dry
2	Conditioning room	10	50	0	Dry
3	Calorimetric room	3	77	-9	Frost
4	Conditioning room	3	77	-9	Frost

4. THE EFFECTS OF AIR FLOW MALDISTRIBUTION UNDER DRY CONDITION

In this section, effect of inlet air velocity maldistribution on evaporator thermal performance was investigated experimentally. Accordingly, an evaporator, which is consistent with the dimensional limits of laboratory air channel, was designed and identified the distribution and AMD of air velocity passing on each module by using an anemometer. Each circuit of evaporator was considered as an individual module and thermal capacities corresponding to each circuit was calculated by using FrtCoils software considering measurement outcomes. Eventually, non-uniform total capacity was determined and the difference with uniform case was detected. In order to confirm as experimental, the product was tested at calorimetric room at first and then tested at conditioning room ensured same airflow rate but more uniform flow. The capacity difference between experimental and analytical results was compared and validated the effect of airflow maldistribution on performance.

4.1. The Measurement of AMD

The square root of the variance of a sample or population of values. A quantity that represents the spread of values about a mean value. In statistics, the second moment of a distribution. Standard deviation provides an estimation of how much the population is spread about the mean value (NASA uncertainty)

A mathematical method (the ratio of standard deviation to mean velocity) was adopted in order to describe the air flow maldistribution (AMD) similar with the related study [Jianying et al., 2008]. This formula is the following:

$$\sigma = \sqrt{\frac{1}{n-1} \sum_{i=1}^n \left(\frac{v_i - \bar{v}}{\bar{v}}\right)^2} \quad (4.1)$$

Where v_i is the air velocity measured, \bar{v} is the average value of the air velocities measured and n is the number of test points as is illustrated at Figure 4.1.

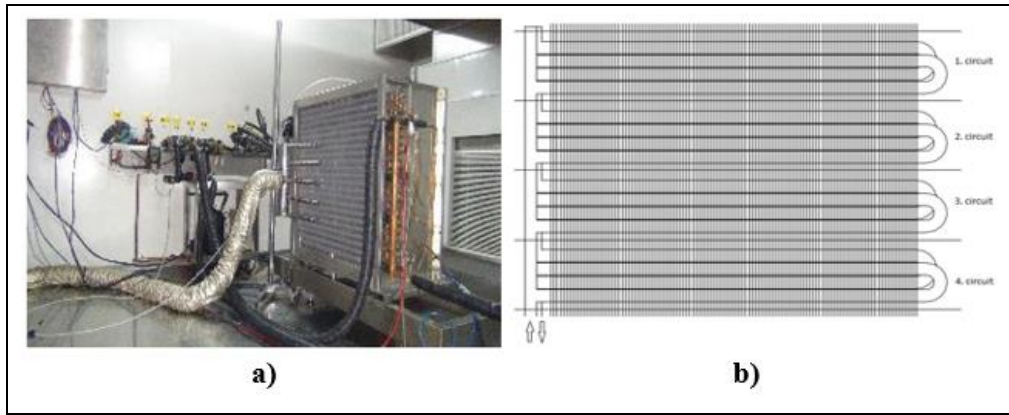


Figure 4.1: The view of each circuit measured temperature and air velocity.

Table 4.1 show that the values of AMD for both each circuit and entire coil. The first set of results belonging to conditioning room were obtained from the wind tunnel measurements which has no contraction part at inlet of air. In order to ensure more uniform flow, a contraction part for wind tunnel was designed and installed in conditioning room, therefore an improvement at outlet temperatures of refrigerant detected. The results without contraction; 6.6°C, 7.8°C, 7.7°C, 6.9 °C and with contraction; 6.6°C, 7.5°C, 7.3°C, 6.5°C. Depending on these results, it was supposed somewhat AMD improvement about by between 2%-5%, that is close to 10%. Determining of this improvement clearly wasn't possible due to difficulties of measurements in contraction part. With reference of this detection, test operations and its outcomes were evaluated with respect to this situation. It was seen a deviation of measured velocities between two tests due to accuracy of probe but these values are in the limits of uncertainty range.

Table 4.1: The value of AMD occurring at each circuits and entire coil.

Air Maldistribution Degrees				
	Calorimetric Room		Conditioning Room	
Circuits	Mean Velocity (m/s)	AMD	Mean Velocity (m/s)	AMD
Circuit 1	4.60	14.75%	3.23	16.93%
Circuit 2	4.28	18.43%	3.81	10.35%
Circuit 3	3.79	17.17%	4.10	12.20%
Circuit 4	4.46	15.95%	3.86	15.02%
The entire coil	4.28	21.6% (±1.87%)	3.75	15.7% (±1.60%)

Figure 4.2 illustrate the air flow distribution in front of evaporator for both of test operation. The evaluation in detail is going to be done at frosting part because of the fact that although determined maldistribution hasn't significant effect on heat transfer mechanism, it may be effective on mass transfer mechanism.

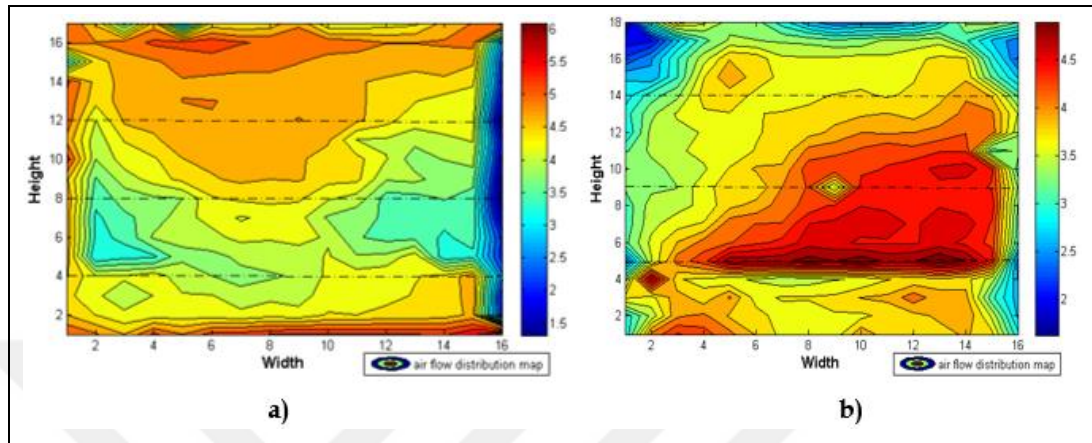


Figure 4.2: Airflow distribution maps a) calorimetric room b) conditioning room.

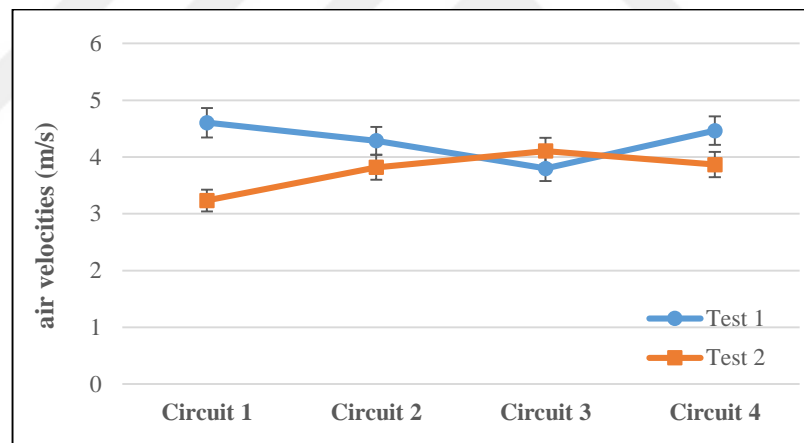



Figure 4.3: Average air velocities for each test process.

If it is investigated the air velocities for each circuits considering uncertainty phenomenon by means of Figure 4.3, it isn't correct commenting regarding as the air velocities differences between each circuits for both conditioning room test and other room because these measurements does not execute at all points of circuits. It is going to clarify this situation under frosting test condition and prepare the air velocity contours occurring on entire surface; thus, the air distribution trend would understand better thanks to these maps.

In order to evaluate the test results reasonable, the air flow rate for each test have to be quite close. In this context, instead of accepting of hot bulb measurement results, the unit cooler's air flow rate was measured at wind tunnel located in conditioning room for both dry and frost test conditions. This process was carried out by adjusting the zero static pressure difference between inlet and outlet of unit cooler as shown in Figure 4.4 and 4.5. Thus, the real air flow rates belonging to conditioning room tests were determined as more sensitive.

FRITERM Termik Cihazlar San. Ve Tic. A.S. 

Heat Exchanging Coil Performance Test Data


Test Time 2015-12-18 9:29:21 Print Time 2015-12-18 12:31:21

Coil type	Heater	Project no		Model name	Friterm
Order no	2014/1609-02	Exchange surface area		Fan model	misket capı 14.65mm
Software capacity		Software dPfluid		Geometry	M5050-15 CS (Paslan)
NTxNRxNC	14x3x7	Length x Fin pitch	750x2.8	TT & FT	0.50x0.12

SC2_ Bare Coil(Ref.evap)		Nozzles 80 110 150 150 189				
Condenser InletTemp.	<input type="text" value="0"/>	°C	Condenser InletTemp.	<input type="text" value="0"/>	°C	
Condenser InletTemp.	<input type="text" value="0"/>	°C	Condenser InletTemp.	<input type="text" value="0"/>	°C	
Condenser InletTemp.	<input type="text" value="0"/>	°C	Condenser InletTemp.	<input type="text" value="0"/>	°C	
Condenser InletTemp.	<input type="text" value="0"/>	°C	Condenser InletTemp.	<input type="text" value="0"/>	°C	

	Unit	1	2	3	4	AVG.
Cond. Room Air Inlet DB	°C	3.00	2.99	2.99	2.99	2.99
Cond. Room Air Inlet DP	°C	-9.11	-9.11	-9.10	-9.10	-9.10
Air side pressure drop	Pa	-0.32	-0.18	0.06	-0.38	-0.21
Nozzle Pressure Diff.	Pa	494.13	494.31	494.80	494.35	494.40
Atmospheric pressure	kPa	100.938	100.940	100.942	100.943	100.941
Air mass flow	kg/h	9750.90	9752.94	9757.98	9753.63	9753.86
Air volumetric flow	m ³ /h	8125.75	8127.45	8131.65	8128.02	8128.22
Temp. Before Nozzles	°C	3.27	3.26	3.25	3.25	3.26
DMP1 Watt	W	15.00	15.00	15.00	15.00	15.00
DMP1 Current	A	0.16	0.16	0.16	0.16	0.16
DMP1 Voltage	V	227.55	228.24	227.37	227.96	227.78

Figure 4.4: The measurement of air flow rate of unit cooler at dry condition.

FRITERM Termik Cihazlar San. Ve Tic. A.S. 

Heat Exchanging Coil Performance Test Data

Test Time 2015-12-18 9:29:21 Print Time 2015-12-18 14:59:35

Coil type	Heater	Project no		Model name	Friterm
Order no	2014/1609-02	Exchange surface area		Fan model	misket capı 14.65mm
Software capacity		Software dPfluid		Geometry	M5050-15 CS (Paslan)
NTxNRxNC	14x3x7	Length x Fin pitch	750x2.8	TT & FT	0.50x0.12

SC2_ Bare Coil(Ref.evap)		Nozzles 80 110 150 150 189				
Condenser InletTemp.	<input type="text" value="0"/>	°C	Condenser InletTemp.	<input type="text" value="0"/>	°C	
Condenser InletTemp.	<input type="text" value="0"/>	°C	Condenser InletTemp.	<input type="text" value="0"/>	°C	
Condenser InletTemp.	<input type="text" value="0"/>	°C	Condenser InletTemp.	<input type="text" value="0"/>	°C	
Condenser InletTemp.	<input type="text" value="0"/>	°C	Condenser InletTemp.	<input type="text" value="0"/>	°C	

	Unit	1	2	3	4	AVG.
Cond. Room Air Inlet DB	°C	3.05	2.98	3.00	3.01	3.01
Cond. Room Air Inlet DP	°C	-0.46	-0.52	-0.49	-0.31	-0.45
Air side pressure drop	Pa	-0.07	-0.10	-0.40	-0.87	-0.36
Nozzle Pressure Diff.	Pa	486.52	487.42	487.20	486.55	486.92
Atmospheric pressure	kPa	100.949	100.948	100.948	100.952	100.949
Air mass flow	kg/h	9670.60	9679.53	9677.50	9670.71	9674.59
Air volumetric flow	m ³ /h	8058.83	8066.27	8064.58	8058.93	8062.16
Temp. Before Nozzles	°C	2.78	2.77	2.77	2.77	2.77
DMP1 Watt	W	15.00	15.00	15.00	15.00	15.00
DMP1 Current	A	0.18	0.19	0.20	0.19	0.19
DMP1 Voltage	V	226.18	226.14	226.31	226.23	226.22
Inlet Relative Humidity	%	77.32	77.29	77.38	78.52	77.63

Figure 4.5: The measurement of air flow rate of unit cooler at frost condition.

4.2. The Measurement of Performance of Heat Exchangers

The test operation of unit cooler was initially carried out at calorimetric room, the unit cooler was tested at conditioning room by removing fan and it is related case in order to change air maldistribution type and degree. During the test process, the most important parameters such as evaporation pressure, air inlet temperature and relative humidity were ensured quite stable as presented in Table 4.2. Also, the obtained heat transfer rates are very close and in the limits of uncertainty range as illustrated in Figure 4.6, that are 7.567 kW and 7.439 kW.

Table 4.2: The average value of test parameters.

Test Room	Coil	AMD (%)	m_r (kg/h)	Pe (MPa)	Tinlet (°C)	RH (%)	Q (kW)
Calorimetric Room	with fan	21.6% ($\mp 1.87\%$)	212.1	0.600	10	36.6	7.567
Conditioning Room	no fan	15.7% ($\mp 1.60\%$)	208.35	0.600	9.99	22.88	7.439

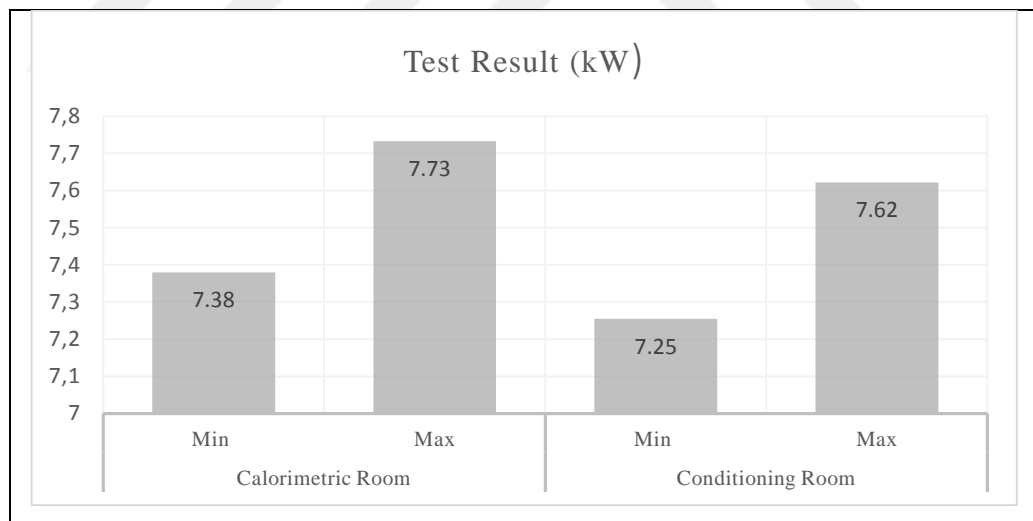


Figure 4.6: The test results for each room.

The most important phenomenon, which should be taken into account, in order to do correct evaluation about air side distribution effects are the convenient design of refrigerant distributor. Accordingly, the thermocouple data taken from each circuit are shown in Figure 4.7. The temperature differences among each circuit are almost less than 1%, in spite of the air side and refrigerant side non-uniformity together.

Sporlan Company has addressed this topic, that is, if all the temperatures are within a few degrees of each other, refrigerant distribution is good [Pate, 2008] Therefore, it could be admitted that the maldistribution resulting from refrigerant is uniform. However, owing to more uniform flow media at conditioning room, the outlet temperatures have approached to desired value, which is 6.5°C.

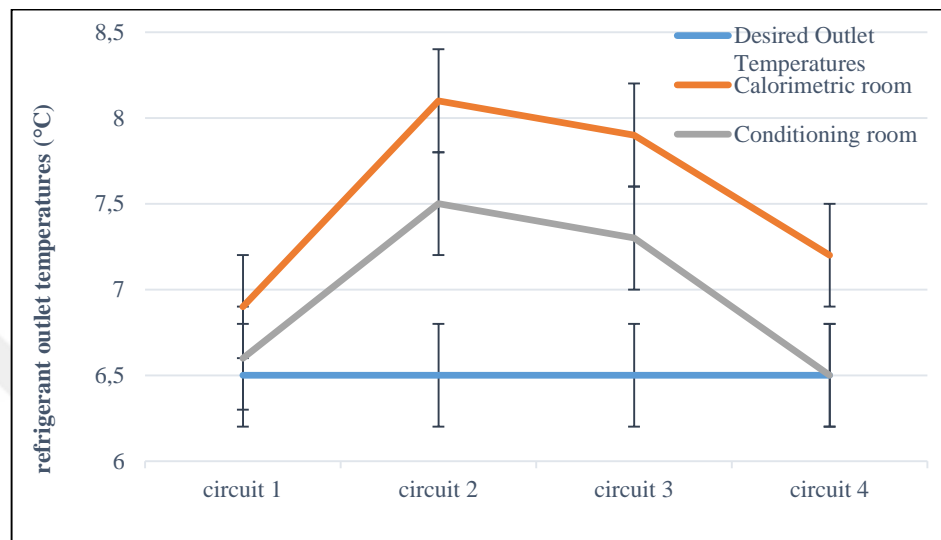


Figure 4.7: The refrigerant outlet temperature values measured via thermocouple.

4.3. The Measurement of Performance via FrtCoils Software

There are many algorithms which use both of the methods to carry out a performance analysis. Heat exchanger design software FrtCoils as shown the interface of program at Figure 4.8 is developed by Friterm Incorporation. This program has the ability of calculation of cooling & heating coils, evaporators and condensers. In scope of this study, this commercial program was used and the following analysis was done via this program for both uniform and non-uniform situations separately considering air velocity measurements.

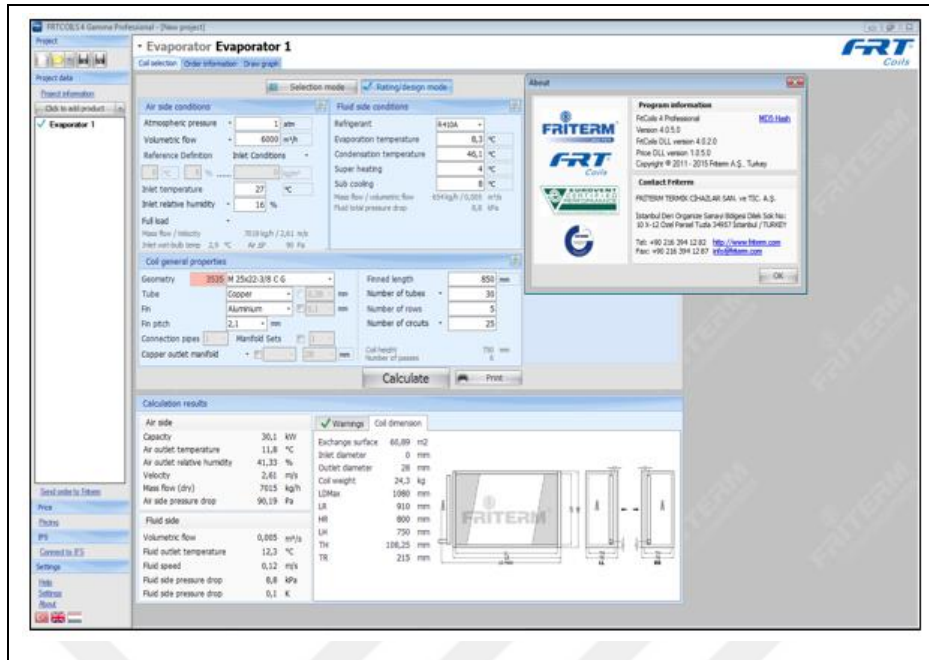


Figure 4.8: The interface of FrtCoils Version 4.0.5.0.

Table 4.3 and 4.4 show the capacity outcomes calculated by means of FrtCoils software for test operations performed at conditioning room and calorimetric room, respectively. The calculations have been carried out considering that each circuit is individual evaporator and eventually, it has been obtained the total capacities for uniform and non-uniform situation considering measurement uncertainties.

Table 4.3: FrtCoils results according to measurement of conditioning room.

Circuits (from up to bottom)	AM D (%)	Measured velocity (m/s)	Uncertainty range (m/s)	Frt result (nonuniform)	Frt result (uniform)
1	16.93	3.235	3.42675	1.781	1.9
			3.04325	1.689	
2	10.35	3.82	4.041	1.856	1.9
			3.599	1.767	
3	12.20	4.104	4.3392	1.931	1.9
			3.8688	1.836	
4	15.06	3.86	4.083	1.925	1.9
			3.637	1.832	
Max.Capacity				7.493	7.6
Min.Capacity				7.124	

Table 4.4: FrtCoils capacity results according to measurement of calorimetric room.

Circuits (from up to bottom)	AMD (%)	Measured velocity (m/s)	Uncertainty range (m/s)	Frt result (nonuniform m)	Frt result (uniform)
1	14.75	4.6035	4.863675	2.059	1.9
			4.343325	1.957	
2	18.43	4.285	4.52925	1.901	1.9
			4.04075	1.833	
3	17.17	3.798	4.0179	1.829	1.9
			3.5781	1.732	
4	15.95	4.464	4.7172	1.955	1.9
			4.2108	2.002	
Max. Capacity				7.744	7.6
Min. Capacity				7.524	

Table 4.5 and Figure 4.9 demonstrate the percentage of capacity deterioration according to FrtCoils design value depending on FrtCoils non-uniform and test non-uniform result separately.

Table 4.5: The comparison of FrtCoils and experimental results.

Test Room		Test result (kW)	Frt result (uniform)	Frt result (nonuniform)	Max. capacity deterioration	
					Frt-Frt	Test-Frt
Calorimetric Room	Min	7.38	7.6	7.524	-1.00%	-2.89%
	Max	7.733		7.744		
Conditioning Room	Min	7.255	7.6	7.124	-6.26%	-4.54%
	Max	7.622		7.493		

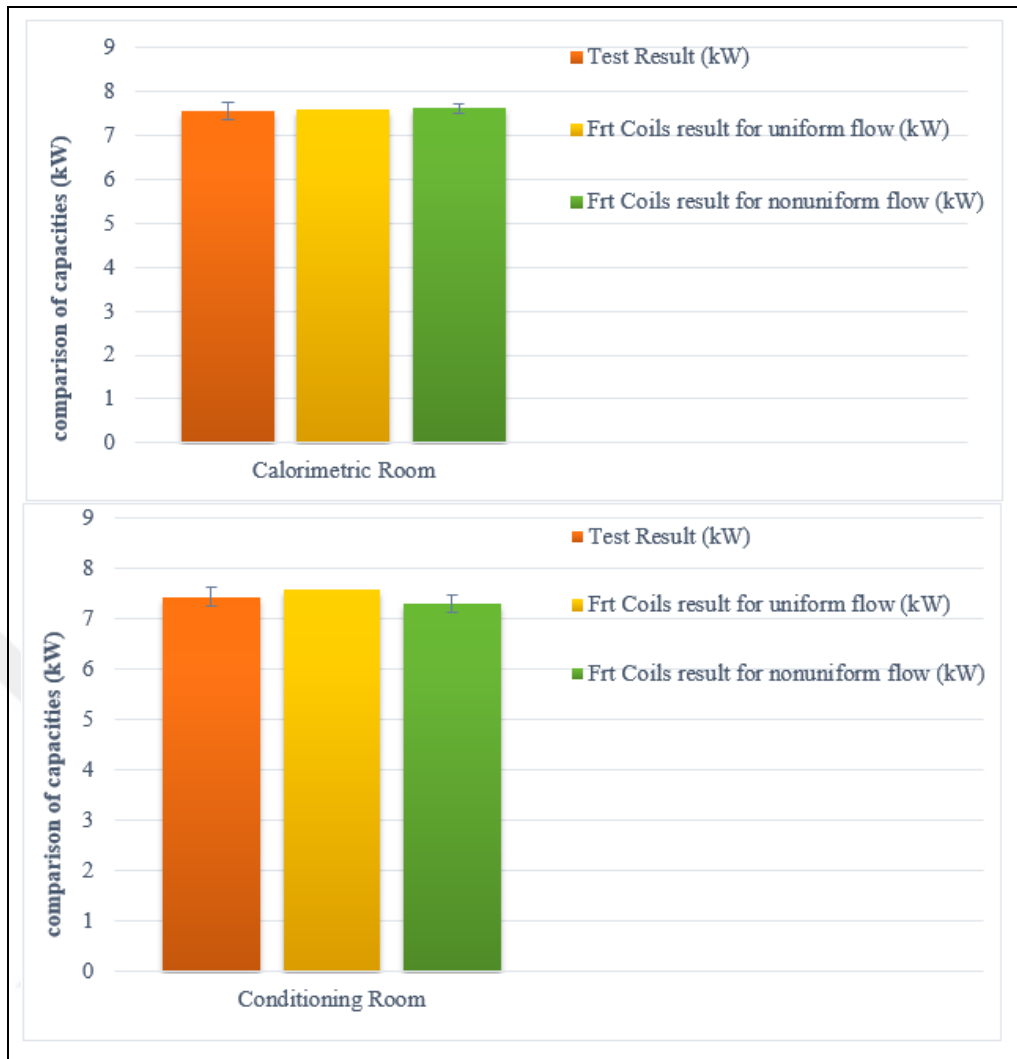


Figure 4.9: The percentage of capacity deterioration.

4.4. Results

In this study, the impact of air flow distribution on evaporator with specific design is investigated. FrtCoils software and experimental results are verified that although it has been ensured a little improvement at outlet of refrigerant circuits by more uniform air flow, no significant change at heat transfer rate was observed. Hence, the AMD up to about 19% doesn't have significant impact on the heat transfer rate, which is consistent with a study [Jianying et al., 2008]. Therefore, unit cooler investigating in this case study can be used easily without considering air flow effects. Furthermore, the heat transfer rate outcomes taken with FrtCoils and experiments are quite close, because of the fact that the AMD identified does not affect the thermal characteristic of internal flow.

5. THE EFFECTS OF AIR FLOW MALDISTRIBUTION UNDER FROSTING CONDITION

In this section, in order to see the effect of AMD when forming the frost at heat exchanger, the test operations were carried out at calorimetric room as integrated fan at first, then at conditioning room as without fan and external case of fan. Thus, it was able to be ensured the case having different AMD and AMD type as well. However, the parameters concerning the test operation such as the changes of air temperature, air relative humidity, surface temperature, air-side pressure drop and refrigerant side capacity etc. were followed in detail for each test operation. Meanwhile, the digital and thermal images were captured in front of heat exchanger; thus, the frost temperature distributions, blockage ratios and frost thicknesses occurring throughout all surfaces were investigated. Consequently, it was revealed the effect of AMD on frosting in detail.

5.1. Fundamental Frost Models

One of the most important parameters affecting the thermal performance of evaporator is frost formation on evaporator's fin and tube both. This phenomenon has two impacts on evaporators. The presence of frost increases air side pressure drop reduces the air flow rate of an evaporator fan; as a result, the refrigeration capacity of the evaporator decreases as frost accumulates during operation. Second, the presence of frost layer creates an additional thermal resistance between the air and the refrigerant; thereby, decreases the evaporator performance. Frost forms on the surface of evaporator when the temperature of evaporator surface is below the dew point temperature of inlet air flow as illustrated in Figure 5.1 and this layer results in thermal and flow resistance between moist air and cooling surface, and although the thermal performance in early frosting stage increases slightly thanks to increment of surface area, degrades the performance of evaporator with the frosting time. Therefore, physical understanding heat and mass transfer under frosting condition is rather important to design heat exchanger having better thermal performance. As mentioned at literature section, optimization of heat exchanger under frosting

conditions such as optimum fin spacing has been investigated and still need to visual data in order to improve performance of heat exchanger at this condition.

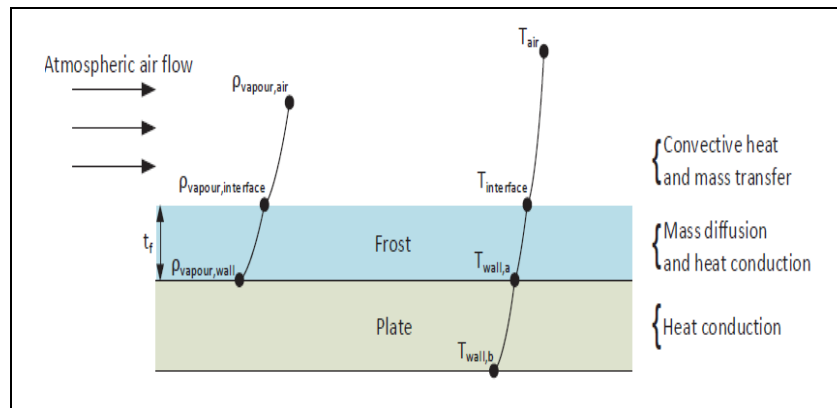


Figure 5.1: Frost formation of evaporator surface.

The study performed by researcher [Mohs, 2013] has specified that frost growth happens in distinct phases: DWC (Drop Wise Condensation), STG (Solidification and Tip-Growth), DBG (Densification and Bulk growth). He defined this terms with following sentences; during the initial DWC period, water droplets condense as a sub-cooled liquid on the cold surface. The droplets form into ice particles after a characteristic time has been reached. The characteristic time is a function of ambient conditions (dry bulb temperature and dew point), cold surface temperature, and surface energy. Once the ice droplets form on the surface, the STG stage begins. The effect of the air movement across the surface is most pronounced during this stage. An increase in the bulk stream velocity causes tip growth to slow, but does not affect the overall properties (density, conductivity, etc) of the layer. Once the DBG stage is reached, the frost layer resembles homogeneous porous medium, with its properties dependent upon ambient and surface conditions.

The frost growth is described by other researchers [J. Cui et al., 2011] by describing into three characteristic periods, which is crystal growth period, frost growth period and fully development period. They defined this terms with following sentences, the crystal growth period is condensation or desublimation of small water vapor on cold surface and these particulars are entitled as icicles as shown in Figure 5.2. New ice crystals grow on these icicles and spread in all directions simultaneously. Moreover, they stated that this initial growth stage has significant influence on the further frost growth process, and also for the frost thickness rises

obviously and frost layer can be seen as roughness visually. The other period is densification of porous layer filling its gaps by small liquid droplets, the ice crystals and the air molecules. While the thickness of frost layer is not remarkable growth, the density of frost layer increases. At the last period entitled as fully developed period starts, when increasing surface temperature resulting from latent heat reaches to the melting point. During this stage, the frost deposited melts partially and seep to porous layer and freezes when contacts with cold surface. This process continues until ensuring the thermal equilibrium. Moreover, this situation results in extra augmentation of the densification and thermal conductivity. Eventually, the frost layer becomes more smooth gradually.

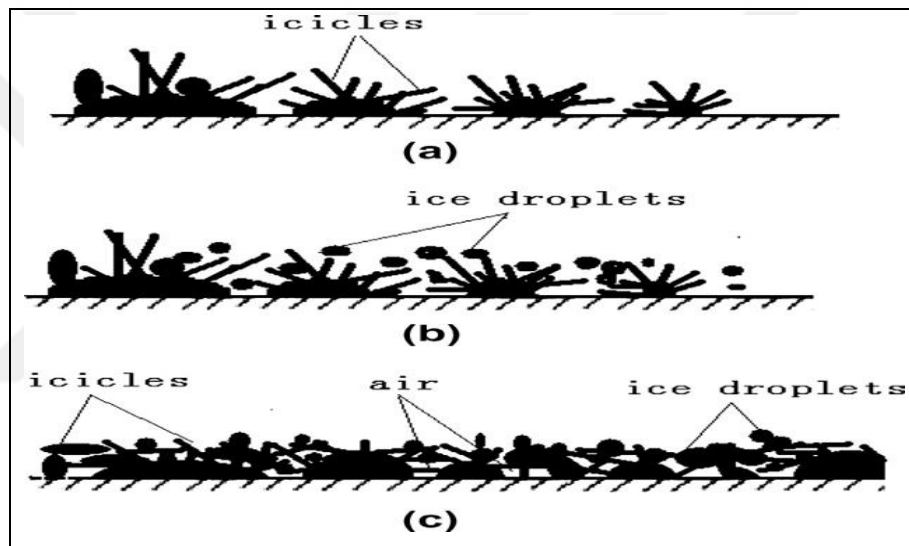


Figure 5.2: The illustration of frost growth (a through c).

Also, it can be seen the water droplet distribution at each stage of frost growth in Figure 5.3. The seed shape is very important because the authors stated that shape of seed has significant effect on further frost growth.

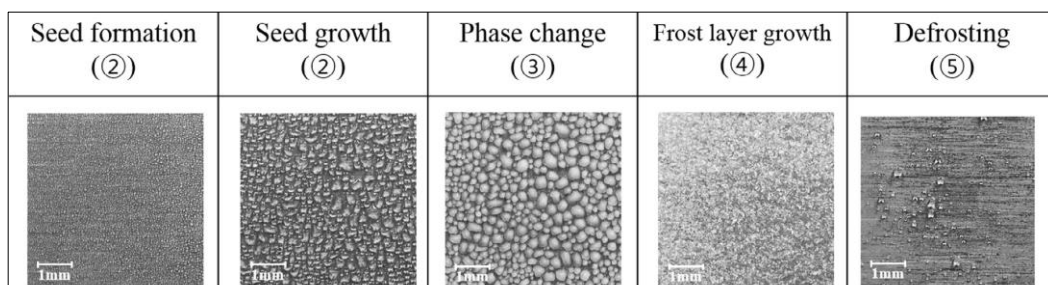


Figure 5.3: Water droplet distribution at each stage.

The increase in airside pressure drop of the heat exchanger, due to a reduction of flow area caused by the growing frost layer, is found to be the most significant parameter in effecting heat exchanger performance. The performance reduction is mainly due to the decrease in airflow rate which caused by the additional backpressure on the fan.

There is also limited discussion on the effect of a frost layer on surface roughness. The presumption [Mohs, 2013] is the frost layer is randomly distributed on the surface, and this should increase surface roughness. The increase in the overall heat transfer coefficient has been shown to be the result of this increased roughness, but as the layer thickens it appears, that have a minimal effect on the heat exchanger performance.

In this research, we experimentally investigated frosting distribution throughout the evaporator with respect to different AMDs. Accordingly, it was firstly used calorimetric room, in order to observe the frost formation at practical conditions, latter same product having equal airflow rate but more uniform airflow was tested at conditioning room in order to observe changes. Besides, it is going to be investigated the effects of air maldistribution as well.

5.2. Preparation of Test Operations

The first preparation was carried out at calorimetric room. The unit cooler, entitled as unit 1, was prepared for frosting test as shown in Figure 5.4. Accordingly, high and low pressure side was admitted as ambient and outlet of evaporator respectively. As illustrated in Figure 5.5, the connections were executed from inlet of air to differential pressure transmitter in order to identify air side pressure drop occurring among inlet and outlet of heat exchanger during the frosting test.

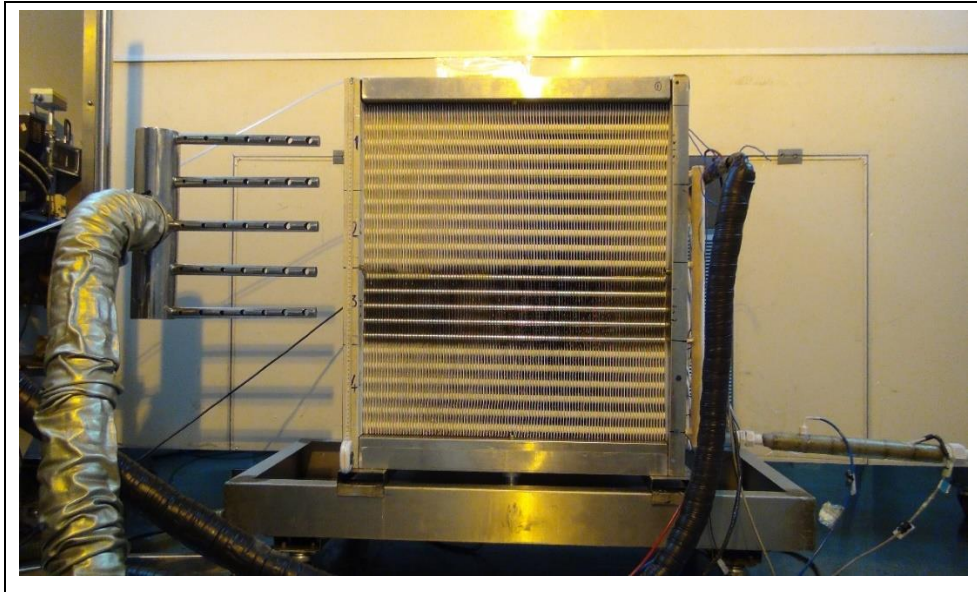


Figure 5.4: The evaporator under frosting test at calorimetric room.



Figure 5.5: The location of pressure measurement points.

Then, it was done refrigerant inlet and outlet pipe connections, placed required sensors on each pipes and taken to vacuum so as to detect to refrigerant leakage, which could occur anywhere of evaporator. Besides, the temperature and humidity measurements of air carried out in front of unit cooler via related sensors located in measurement box as demonstrated in Figure 5.6.

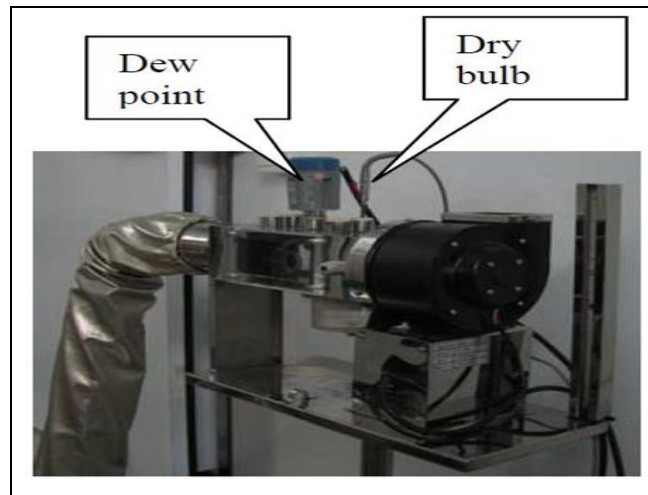


Figure 5.6: Temperature and humidity measurement box.

Eventually, it was started the test operation. Before run the refrigerant compressor, the calorimetric room air inlet temperature and relative humidity was conditioned to desired values by means of conditioning room's evaporator and humidifier situated at air handling unit. When reached to desired values, the refrigerant compressor was started and at this time and the openness of expansion valve was controlled manually during the test operation.

During the test, it was continuously deal with ensuring the relative humidity of room as manual and taken the test result and graphical data at each 1 minutes during the 32 minutes after starting the test operation, then taken per 7.5 minutes. Besides, the digital and thermal images were captured by means of Sony HDR-CX570 and FLIR E6 thermal camera respectively at particular time.

On the other hand, same processes aforementioned above has implied for conditioning room. As different from other room, the evaporator's fan was disassembled and situated to open type wind tunnel as shown in Figure 5.7. However, high and low pressure side was admitted as the inlet and outlet of coil as specified at Figure 5.8. The connections were executed from inlet and outlet of air to differential pressure transmitter in order to identify air side pressure drop during the frosting test.



Figure 5.7: The evaporator under frosting test at conditioning room.

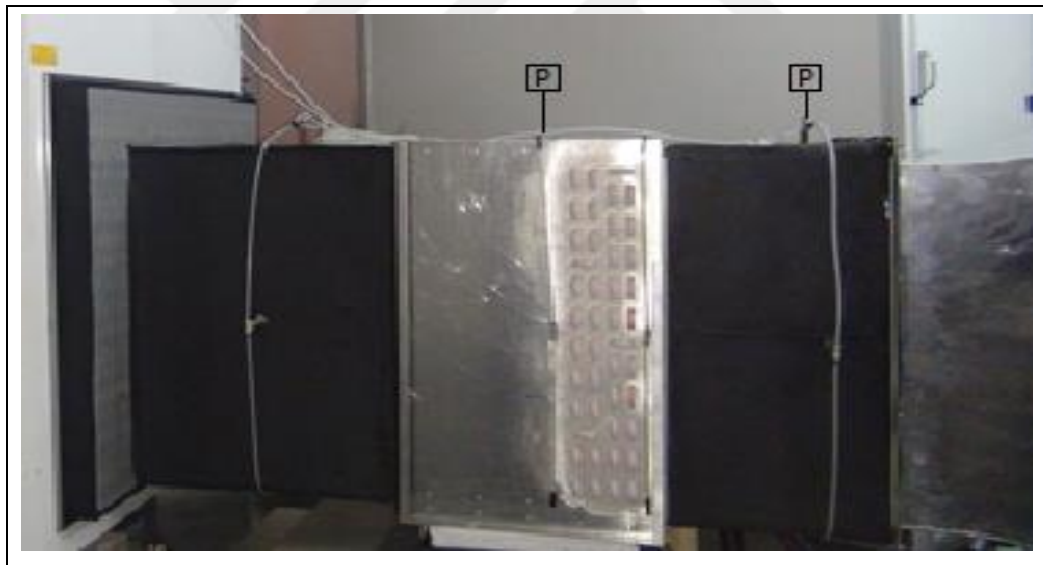


Figure 5.8: The location of pressure measurement points.

5.3. The Test Operations and Outcomes

In this section, it was carried out the thermal tests at specific test conditions as illustrated in Table 5.1 and the analysis of thermal and digital images for each test.

Table 5.1: The operation condition of frosting test.

Test No.	Test Location	Tai [°C]	RH [%]	Te [°C]	Surface Cond.
3	Calorimetric room	3	77	-9	Frost
4	Conditioning room	3	77	-9	Frost

5.3.1. The Measurement of Performance

Figure 5.9 depicts the changing of such critical parameters as refrigerant mass flow, air pressure drop, air inlet temperature and relative humidity etc. belonging to calorimetric test as depend on time. If taken into account in detail, while it isn't seen significant changing at heat transfer rate, air pressure drop characteristic shows some deterioration after a while, which is about 241 minutes.

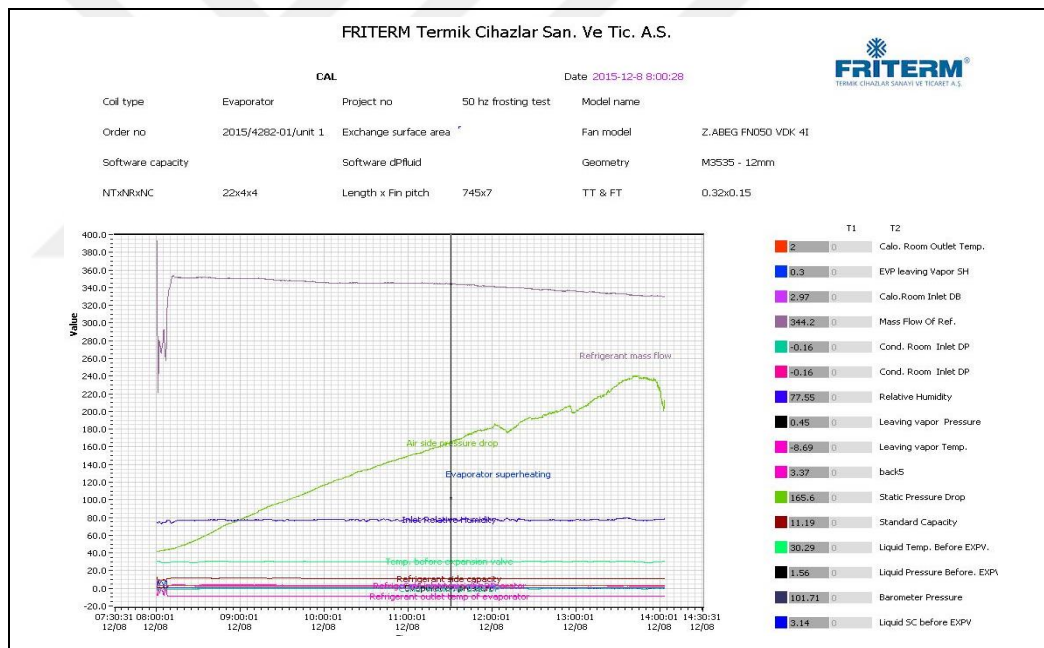


Figure 5.9: The entire parameters belonging to calorimetric room during test time.

The test operation having same operation condition was performed at conditioning room by using centrifugal fan, which is exhaust fan of calorimetric room. According to test results ensured almost constant air inlet temperature and humidity illustrated at Figure 5.10, while decreasing of the refrigerant capacity is bigger than the test operation performed at calorimetric room, in spite of being more air pressure drop than other test due to centrifugal fan characteristic, the deterioration

time of this parameter is about 237 minutes. That is, the test durations for each test carried out same operation condition are almost same.

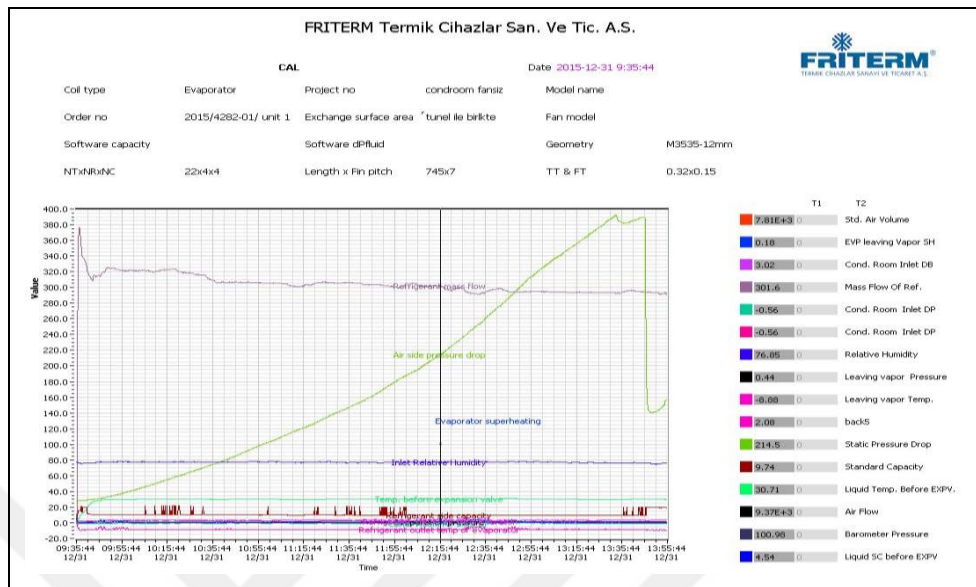


Figure 5.10: The entire parameters belonging to conditioning room during test time.

Figure 5.11, 5.12 and 5.13 show the stability of room during test operation performed both calorimetric and conditioning room. It is clear that the most important parameters, which are air inlet temperature, humidity and evaporation pressure have been approximately held as constant. In this way, comparing of two tests are going to be more easy and right.

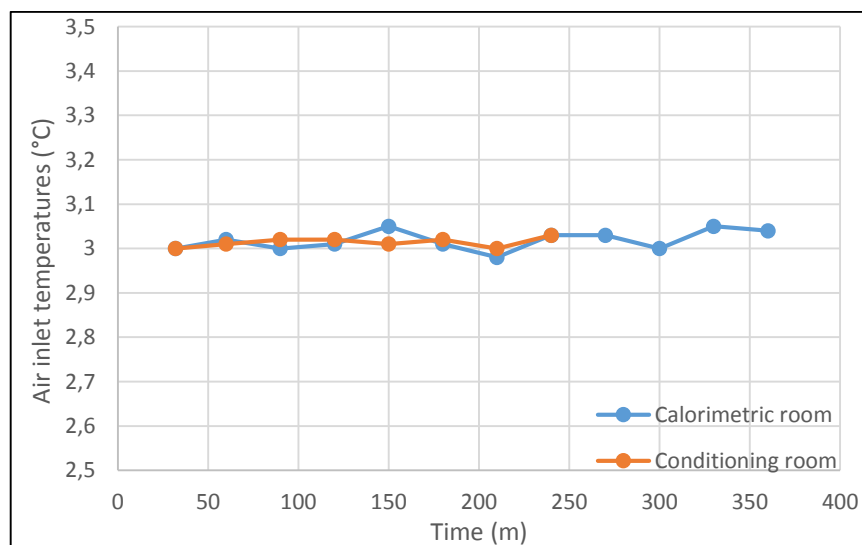


Figure 5.11: The air inlet temperature during the test process.

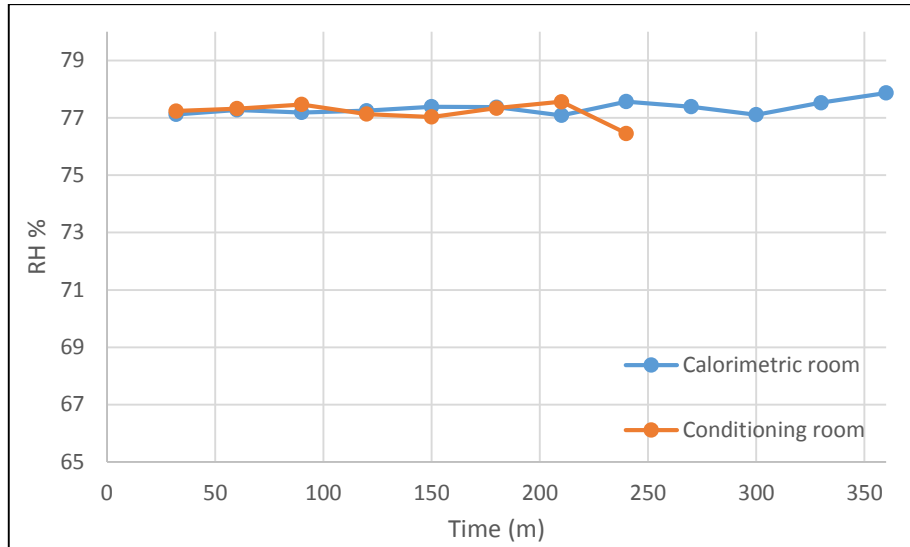


Figure 5.12: The relative humidity during the test process.

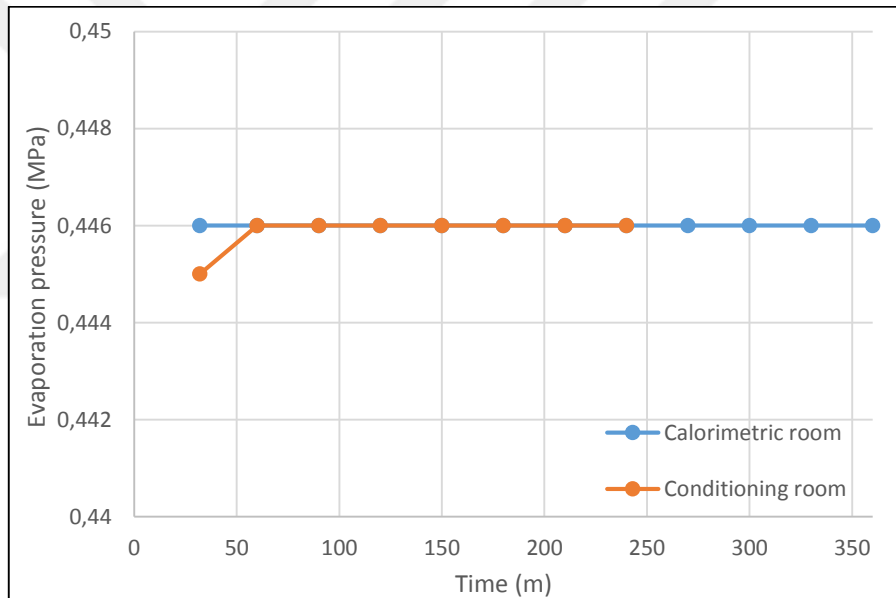


Figure 5.13: The evaporation pressure during the test process.

Also, the average values actualizing through test operation is tabulated at Table 5.2.

Table 5.2: The average operation conditions.

Time	Calorimetric Room			Conditioning Room		
	Ta (°C)	RH (%)	Pe (MPa)	Ta (°C)	RH (%)	Pe (MPa)
Average	3.01	77.34	0.446	3.01	77.19	0.4458

The evaluation and comparing of frosting tests in detail will be done next section after the image process.

5.3.2. The Analysis of Thermal and Digital Images

In scope of this section, it was investigated that the forming of frost patterns, frost thicknesses and blockage ratios during test operations carried out in both rooms. However, in following section, there are digital, thermal images and post-images are captured at specific times. By means of these process, it will be tried understanding the effect of air maldistribution on frost growth.

5.3.2.1. The Calorimetric Room Images

The thermal and digital outcomes obtained at calorimetric room were investigated at 70, 140, 208, 267 and 329 minutes, respectively. However, the digital images were processed in order to determine frost thickness and blockage ratios via Matlab Image Processing Toolbox.

- 70 minutes:

At the end of 70 minutes, the digital and thermal images was captured as shown at Figure 5.14.

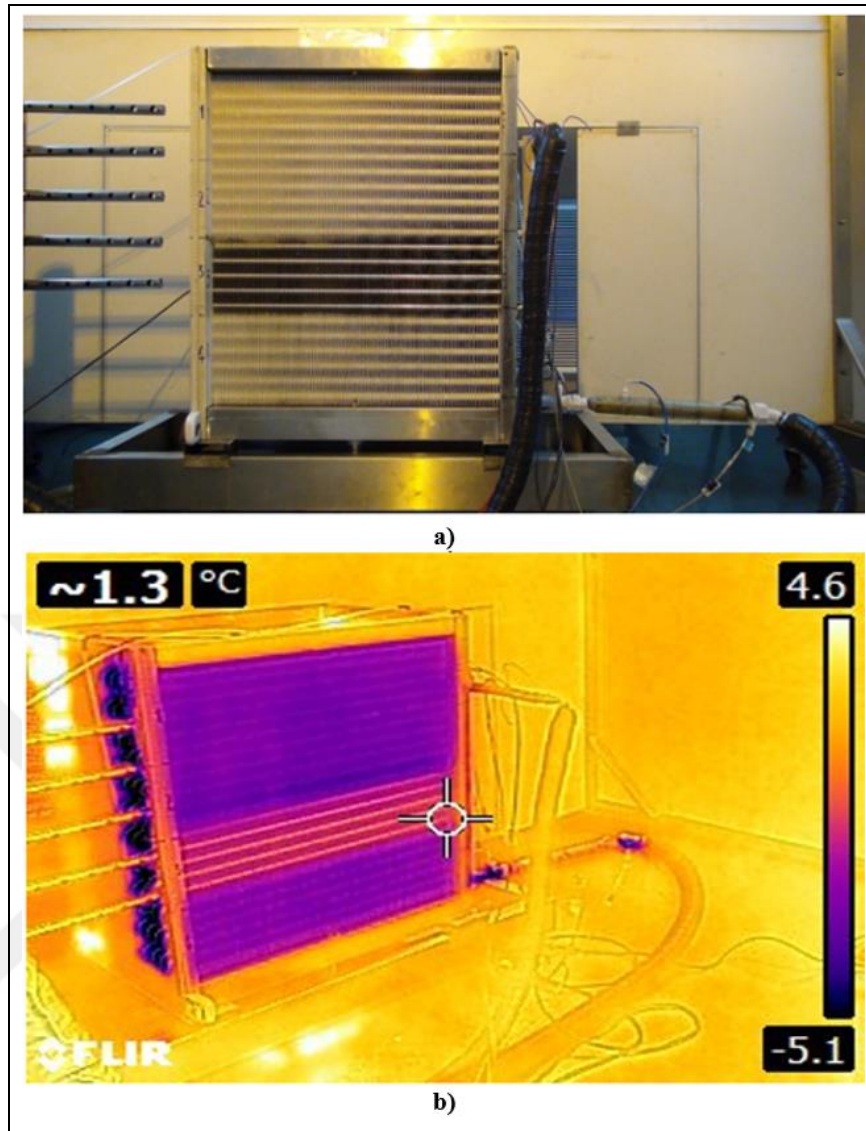


Figure 5.14: a) The digital and b) thermal images at 70 minutes.

It is clear that there is a problem at third circuits. Actually, this issue may result from both refrigerant side and air side. If taken into account to the first test executed at SC1 dry condition, it could be seen obviously that the outlet temperature of refrigerant at each circuits was less about than 1°C , so it can be admitted that the air side maldistribution results in this problem. However, is it mentioned really a problem or what is the negative impacts of this problem on evaporator? It is going to be examined at following section in detail.

Figure 5.15 shows that the post image of specific area of each circuit. By means of image process toolbox, average frost thicknesses occurring through entire surface are determined easily.

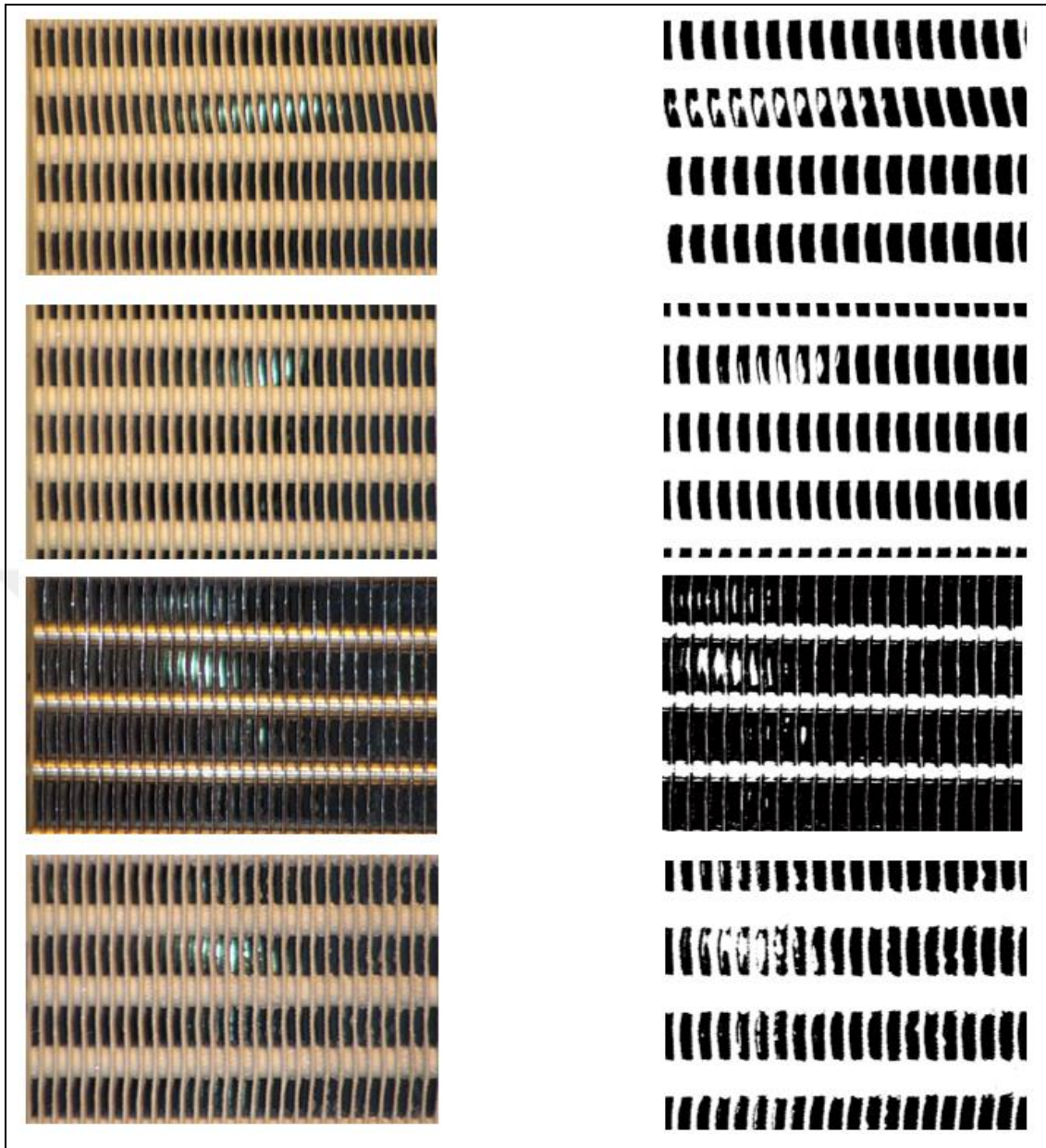


Figure 5.15: The digital (left) and post images (right) at 70 minutes for each circuits.

- 140 Minutes:

The improvement realizing at circuit 3 can be seen clearly at Figure 5.16. This situation is based on characteristic of axial fan. This situation was mentioned by J. M. Huang and his colleagues [2008] as the axial fan will increase the pressure head steadily until starting of stall condition in the middle region of axial fan, which means that the air flow rate in middle region decreases more seriously than first and four circuits. Therefore, this change could result from this impact. This situation is going to be reviewed by considering conditioning room test performed using centrifugal fan.

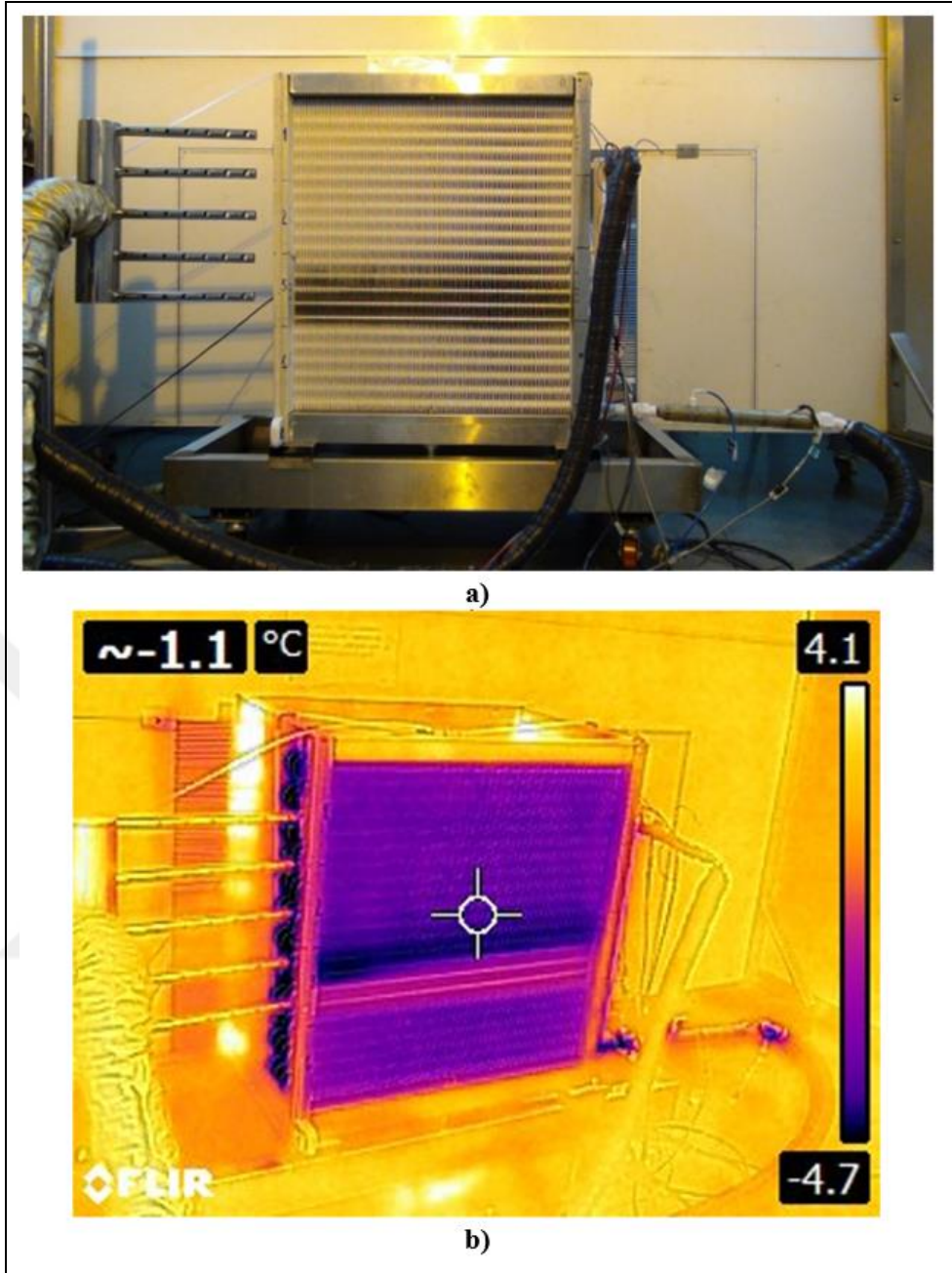


Figure 5.16: a) The digital and b) thermal images at 140 minutes.

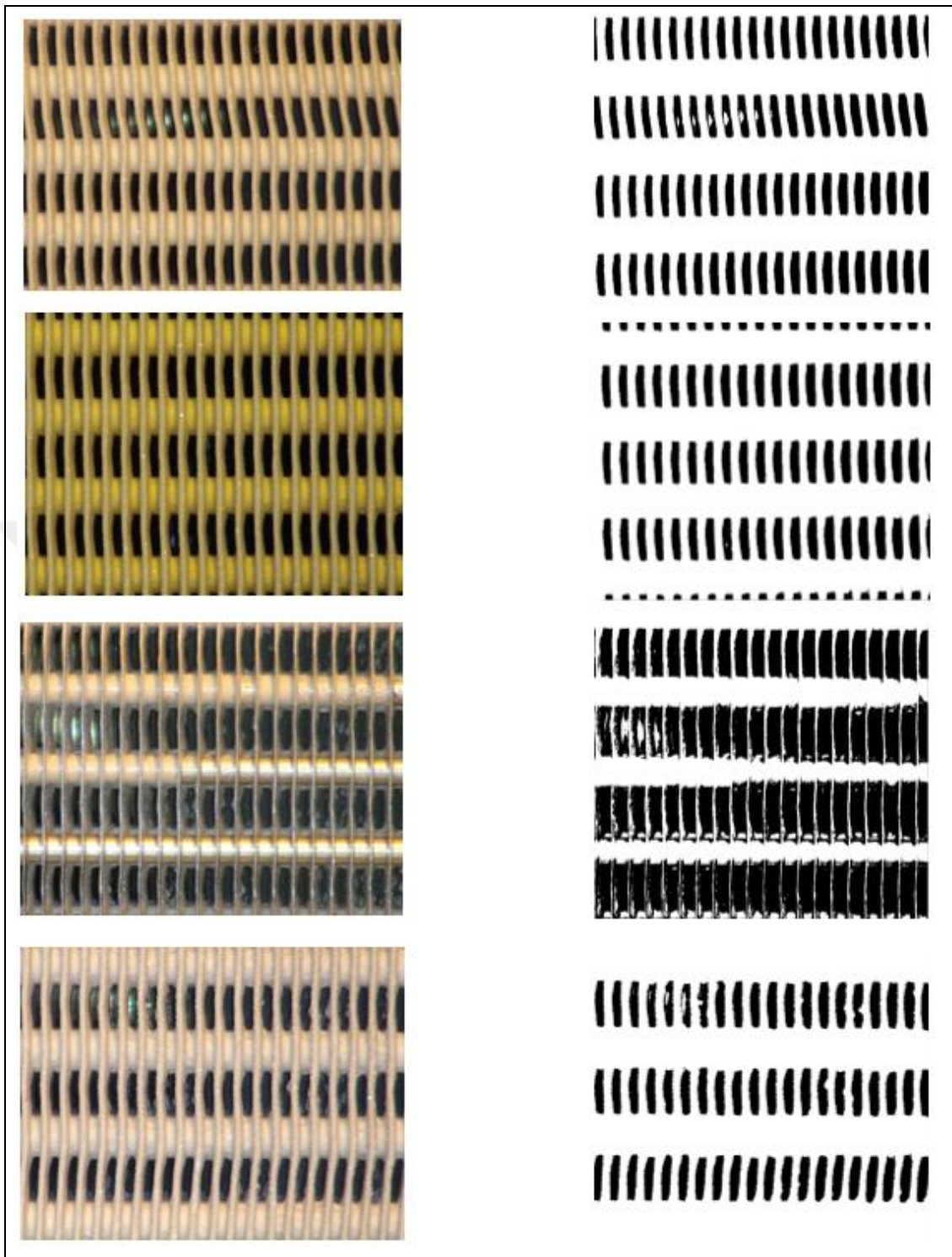


Figure 5.17: The digital (left) and post images (right) at 140 minutes.

- 208 Minutes:

The digital and thermal images can be seen in Figure 5.18, the improvement of the third circuit and growing of frost thickness continues steadily. Figure 5.19 shows the post images at this time.

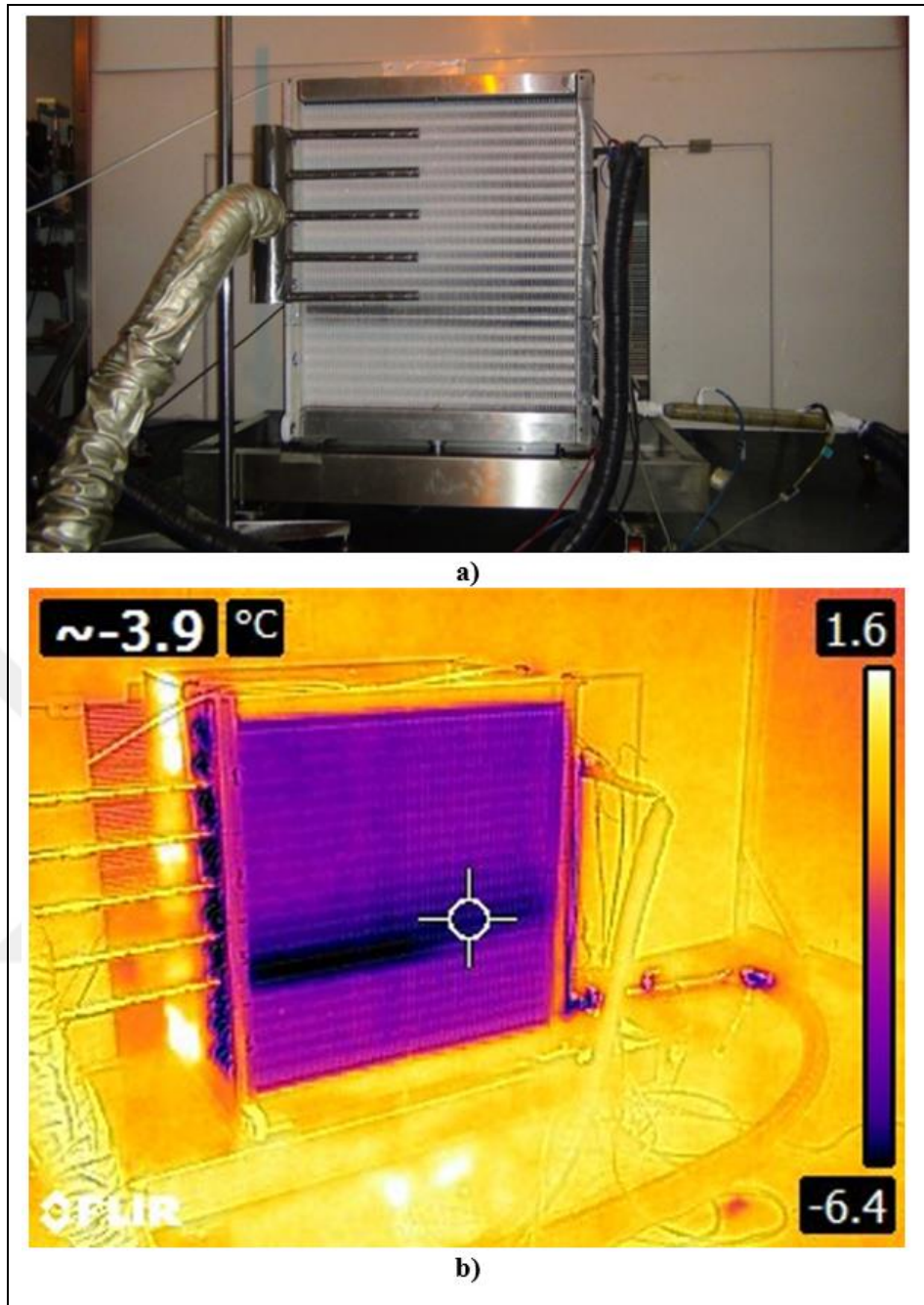


Figure 5.18: a) The digital and b) thermal images at 208 minutes.

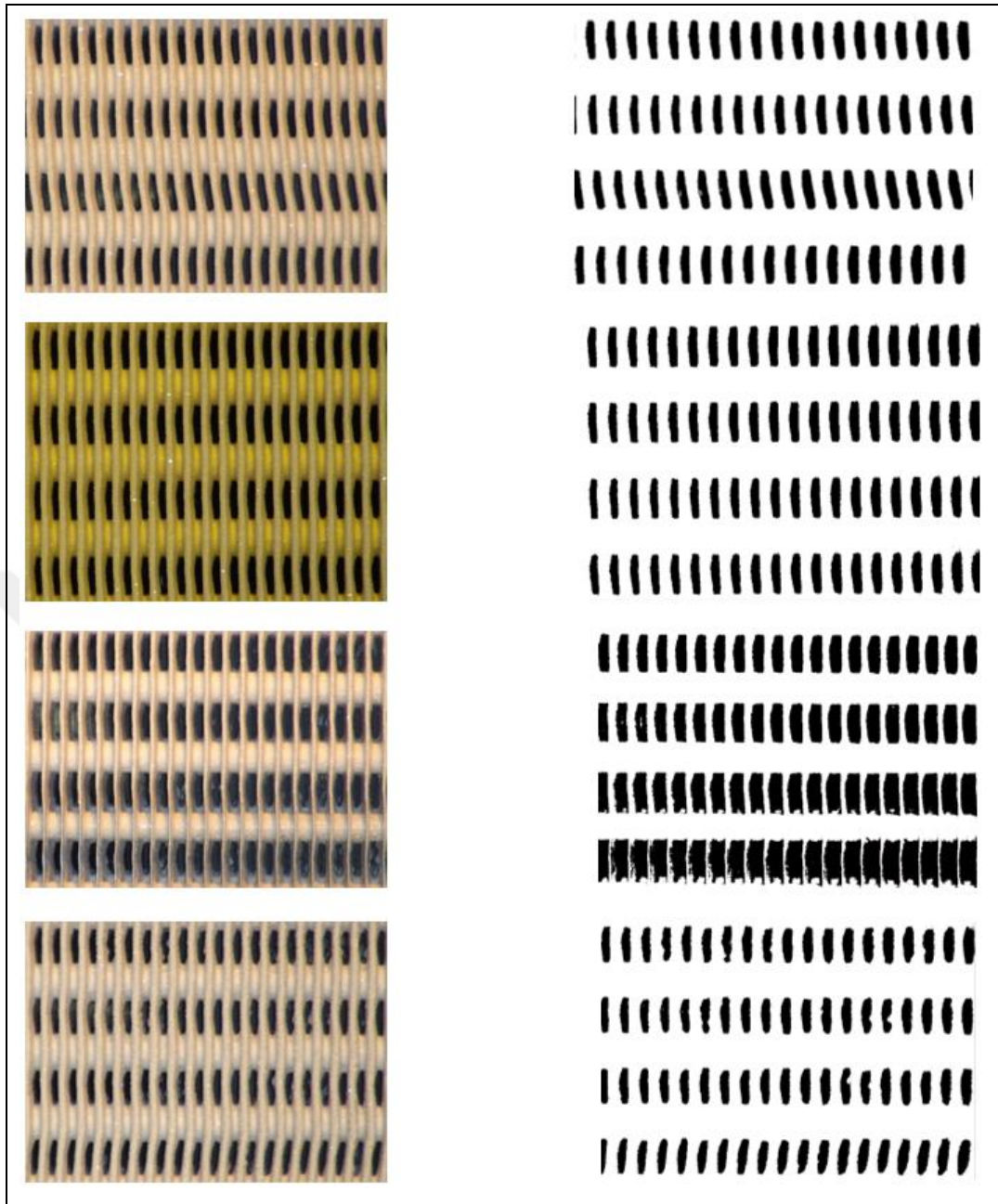


Figure 5.19: The digital (left) and post images (right) at 208 minutes.

- 267 Minutes:

It was repeated the same process like aforementioned sections.

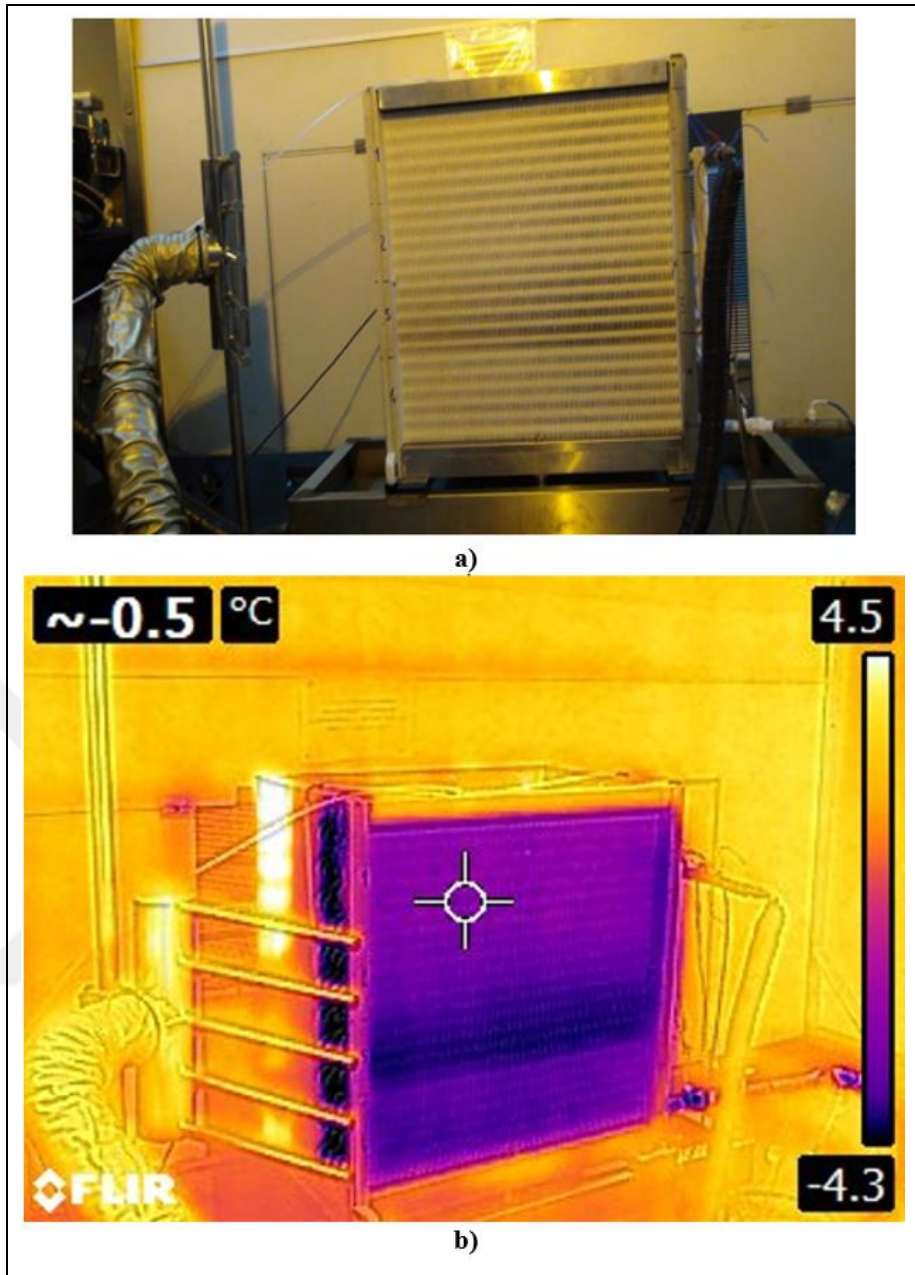


Figure 5.20: a) The digital and b) thermal images at 267 minutes.

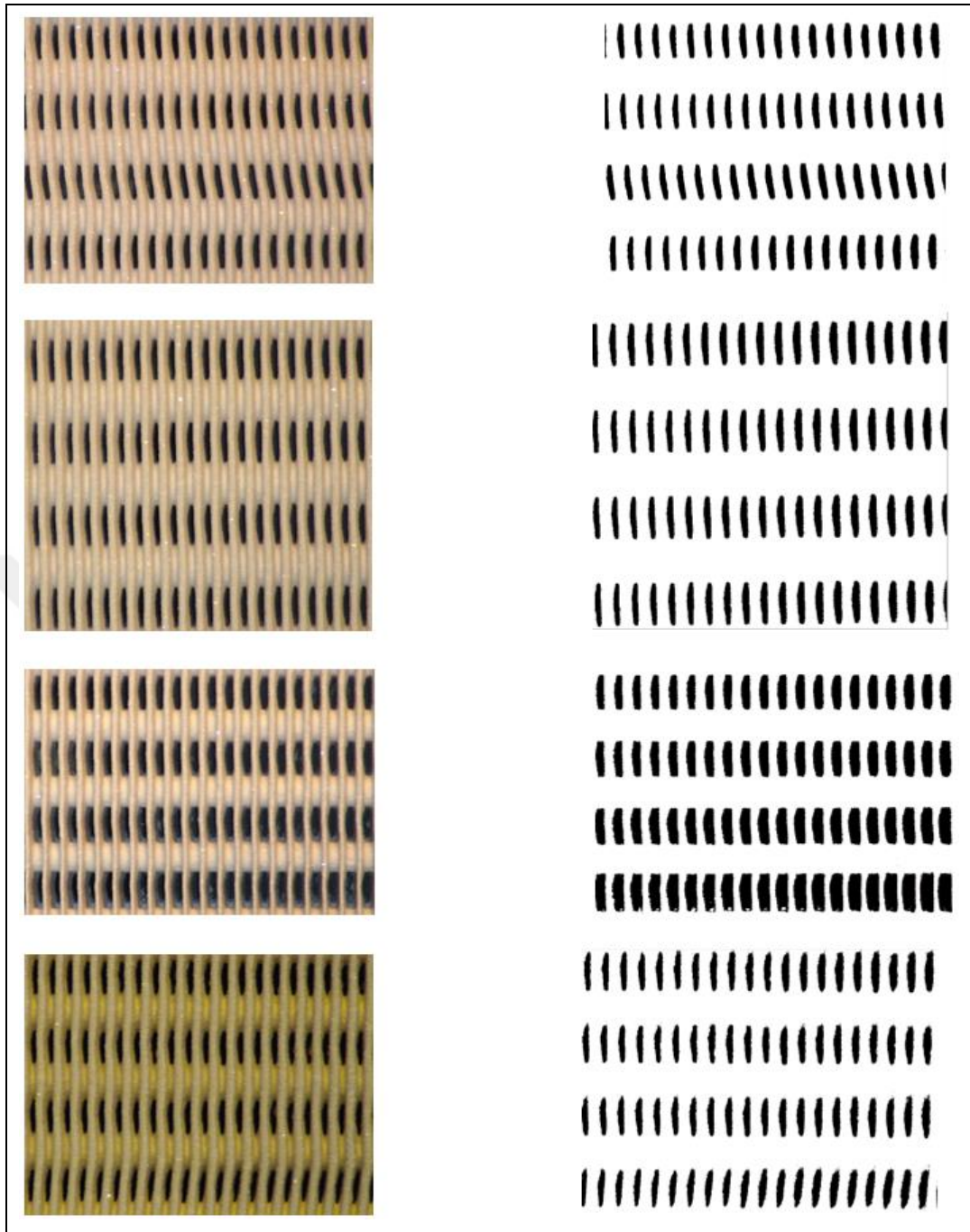


Figure 5.21: The digital (left) and post images (right) at 267 minutes.

- 329 Minutes:

It was repeated the same process like aforementioned sections.

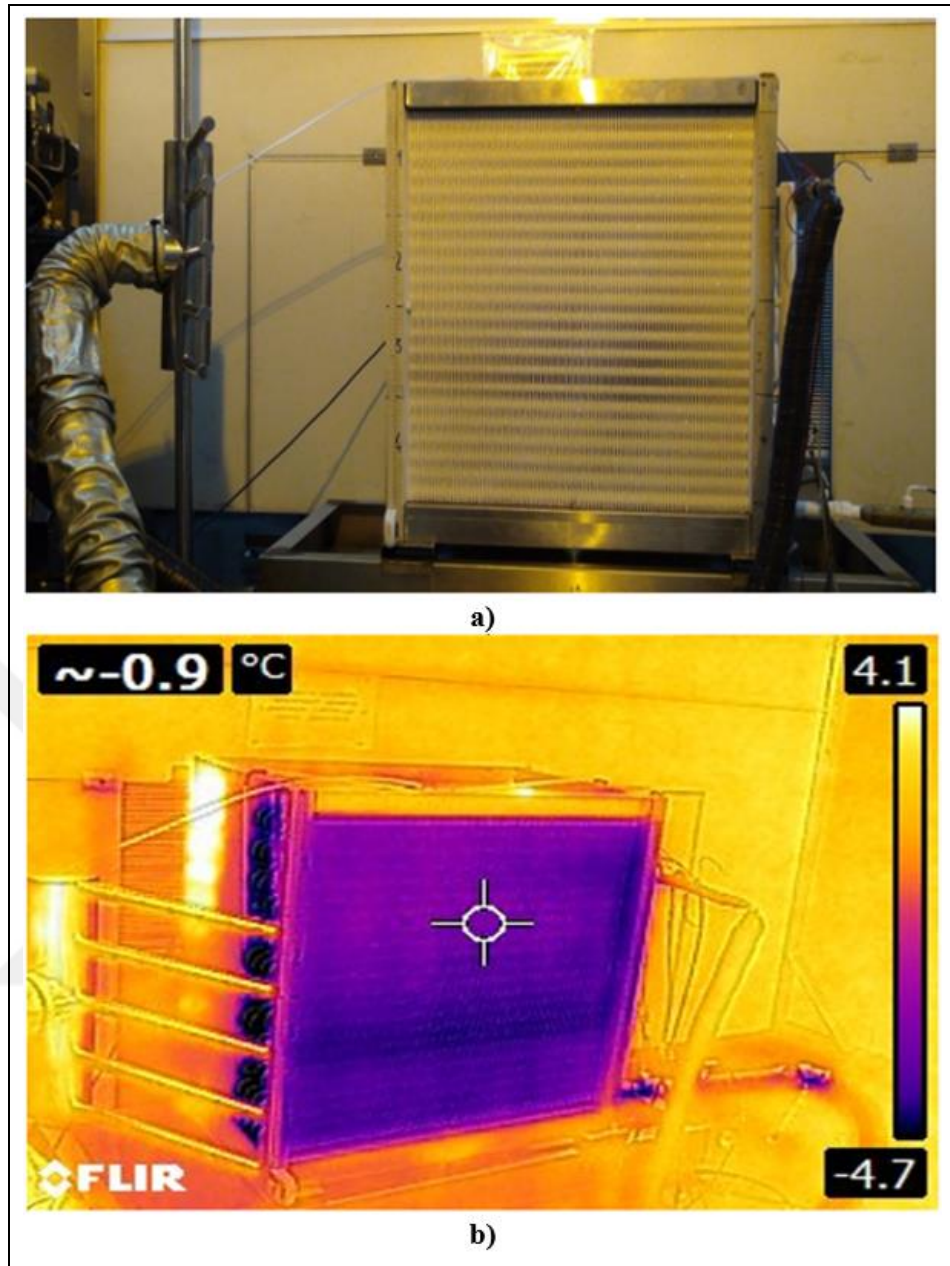


Figure 5.22: a) The digital and b) thermal images at 329 minutes.

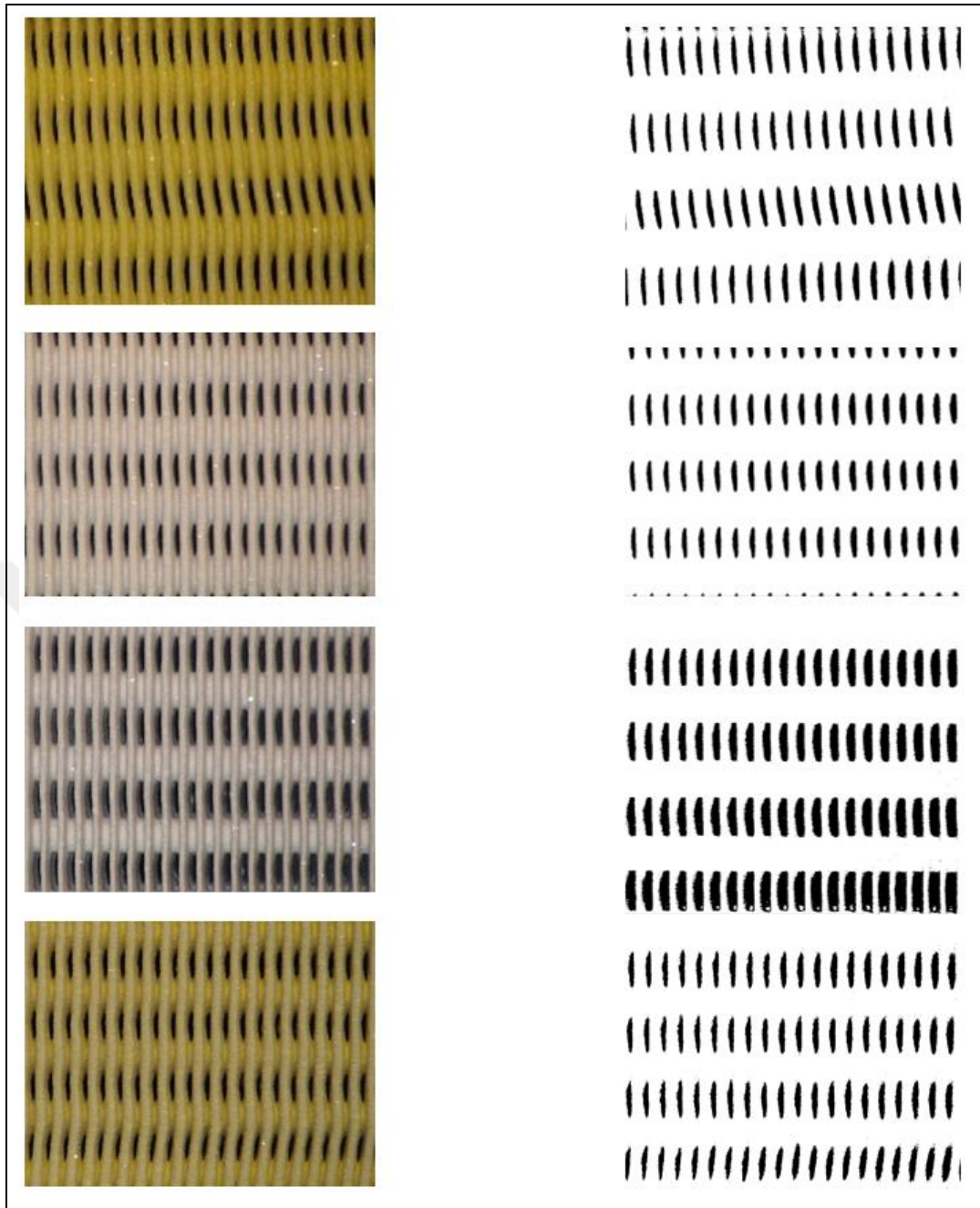


Figure 5.23: The digital (left) and post images (right) at 329 minutes.

The investigation of unit cooler in detail: (according to 267 min, that is after about 24 minutes starting of defrost process)

In order to identify frost thicknesses, tube thicknesses and blockage ratios, it was carried out a large of image processing by using Matlab Image process toolbox. Scope of this study, it was selected a reference dimensions and corresponding pixel measures such as fin pitch or ruler placed near side of evaporator. And then, the other

dimensions belonging to 1 gap were determined with respect to this reference measure and admitted as same for each gap of circuit.

On the other hand, the images were evaluated at a close time to starting of unbalance of fan (it can be seen air pressure drop curve easily). The related equations are specified as following;

- Fin and tubes frost thickness:

$$\delta_f = \left(\frac{(FP - \text{Measured average gap of among two fins}) - FT}{2} \right) \quad (5.1)$$

$$\delta_t = \left(\frac{\text{Measured tube thickness} - \text{Tube diameter}}{2} \right) \quad (5.2)$$

- Blockage ratios:

The space among two fins and two tubes decrease with time because of the frost grows both fins and tubes continuously. So that, the calculation including blockage ratio is identified as following;

$$\text{space area}_{non-frost} = (X_t - D_o). (FP - FT) \quad (5.3)$$

$$\text{space area}_{after frost} = (X_t - D_o - 2\delta_t). (FP - FT - 2\delta_f) \quad (5.4)$$

$$BR = 1 - \frac{\text{space area}_{non-frost}}{\text{space area}_{after frost}} \quad (5.5)$$

Figure 5.24 shows the sample circuit including measured length and reference point. According this measurement, the related parameters were identified for each circuits. The other circuits were done like this sample but related images weren't illustrated.

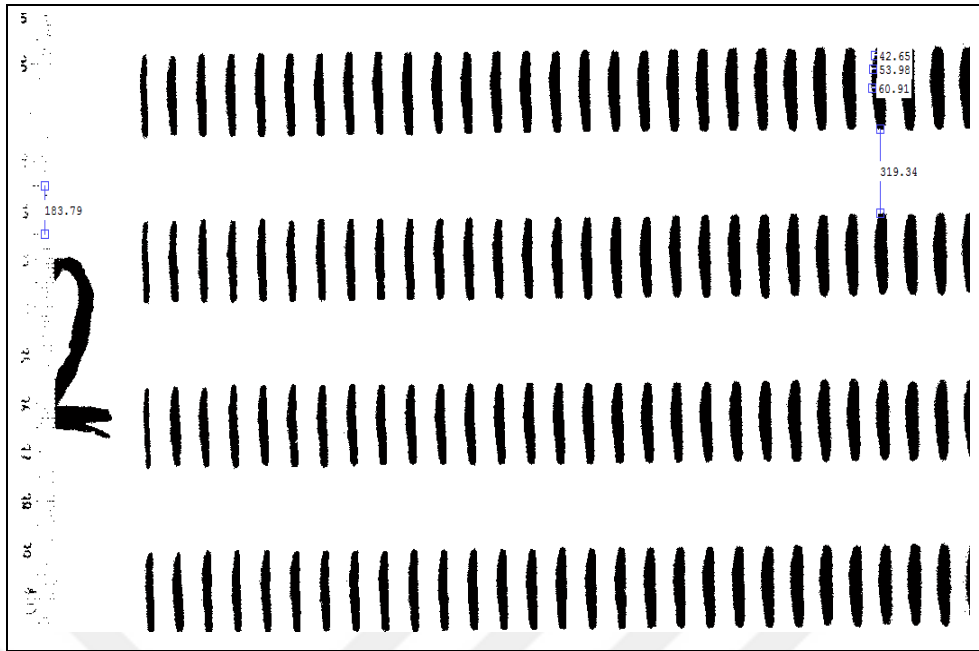


Figure 5.24: The post images of circuit 2 and measurements.

When it is examined that, the thermal and digital images during the calorimetric test operation, it is seen that the circuits of 1, 2 and 4 are almost similar except circuit 3; nevertheless, the entire circuits are going to be checked and taken the average value for each related parameters. According to the equations specified above and measurements, the tube frost thickness, fin thickness and total blockage throughout windward of unit cooler were determined at Table 5.3.

Table 5.3: The summary of measured fin thickness, tube thickness and total BR of calorimetric room for each circuit.

	fin thickness (mm)	tube thickness (mm)	Total BR (%)
Circuit 1	2.1885	2.106	70.66%
Circuit2	1.9963	2.4376	67.33%
Circuit 3	1.5099	1.1798	51.20%
Circuit 4	2.0245	1.6799	62.22%
AVG	1.9298 ±0.208	1.91397 ±0.208	62.85% ±5.22%

As mentioned foregoing sections, the blockage ratios of circuit 1, 2 and 4 are quite close and circuit 3's blockage ratio is smaller than other circuits as expected. However, it is speculated that the blockage ratio at windward of unit cooler is between 50% and 60% because the images have been processed about 25 minutes later after breaking time of air pressure drop curves, which denotes the starting of fan

stall, thereby starting of defrost. This blockage ratio is found consistent with a study [Huang, et al., 2008].

5.3.2.2. The conditioning room images

In this section, it is going to be carried out same process at 80, 145 and 255 minutes as like calorimetric room process. Accordingly, digital and thermal images captured windward of evaporator is going to be evaluated, the post images are illustrated and calculated the related parameters via image processing toolbox.

- 80 minutes:

At the end of 80 minutes, the digital and thermal images was captured as shown at Figure 5.25.

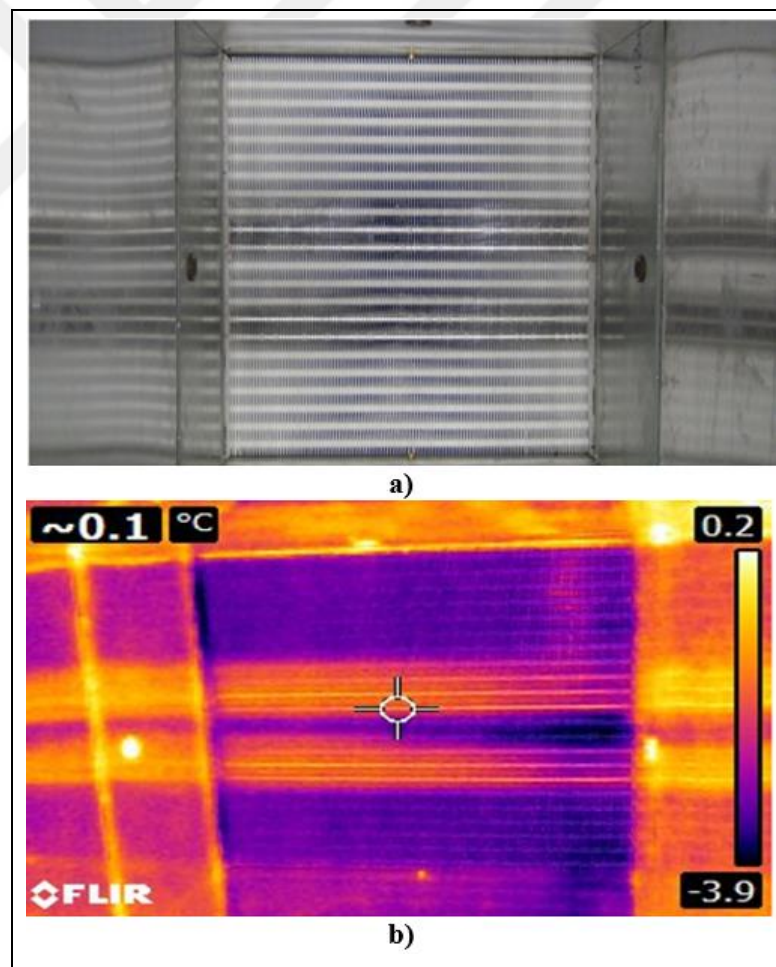


Figure 5.25: a) The digital and b) thermal images at 80 minutes for each circuit.

If taken into account to the circuit 2 and 3, it is realized that the surface temperatures of related circuits are higher than other circuits. It is speculated that this problem could result from the changing internal temperature of fluid as depend on air flow maldistribution and it is going to be discussed at following sections.

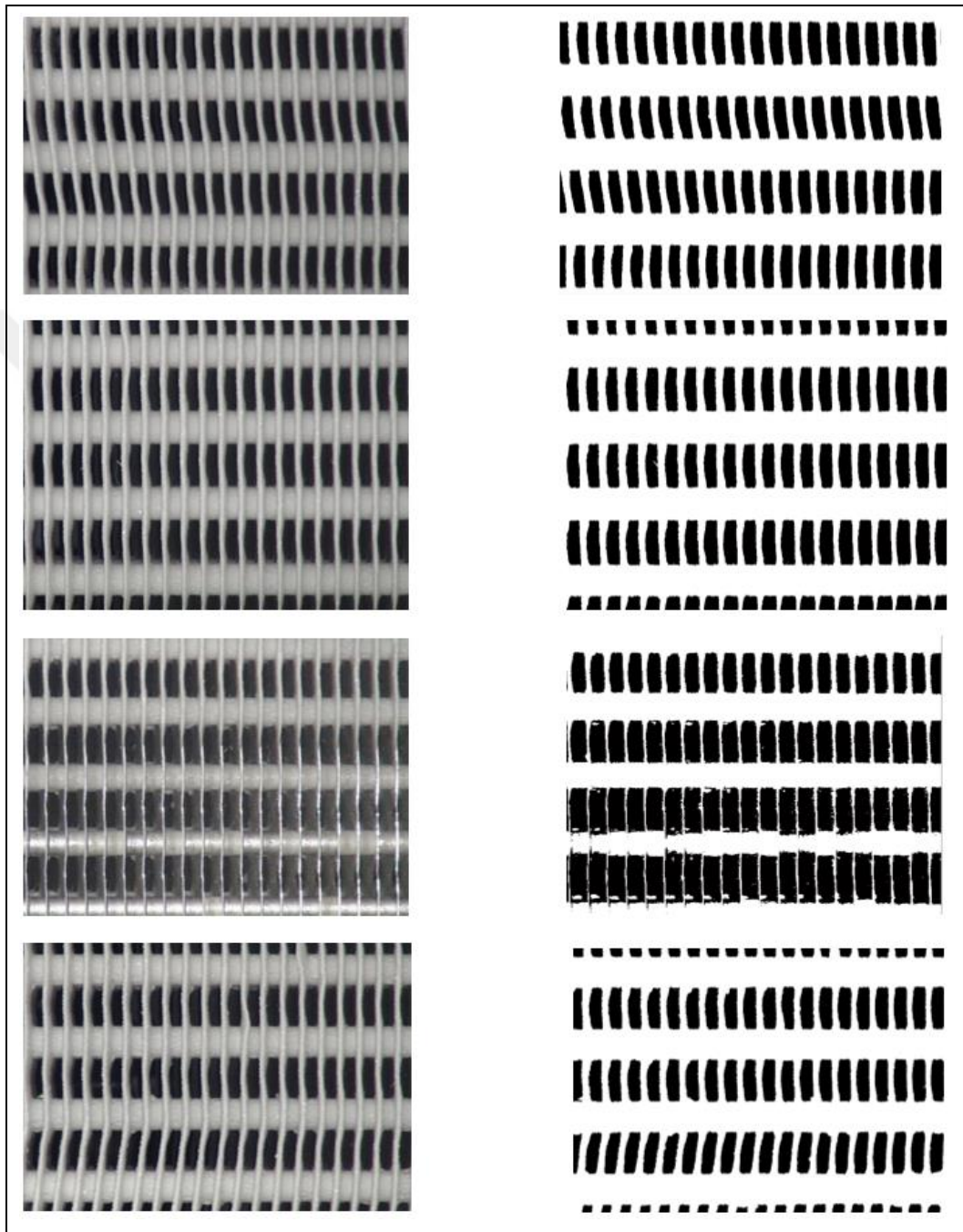


Figure 5.26: The digital (left) and post images (right) at 80 minutes.

- 145 minutes:

It was repeated the same process like aforementioned sections.

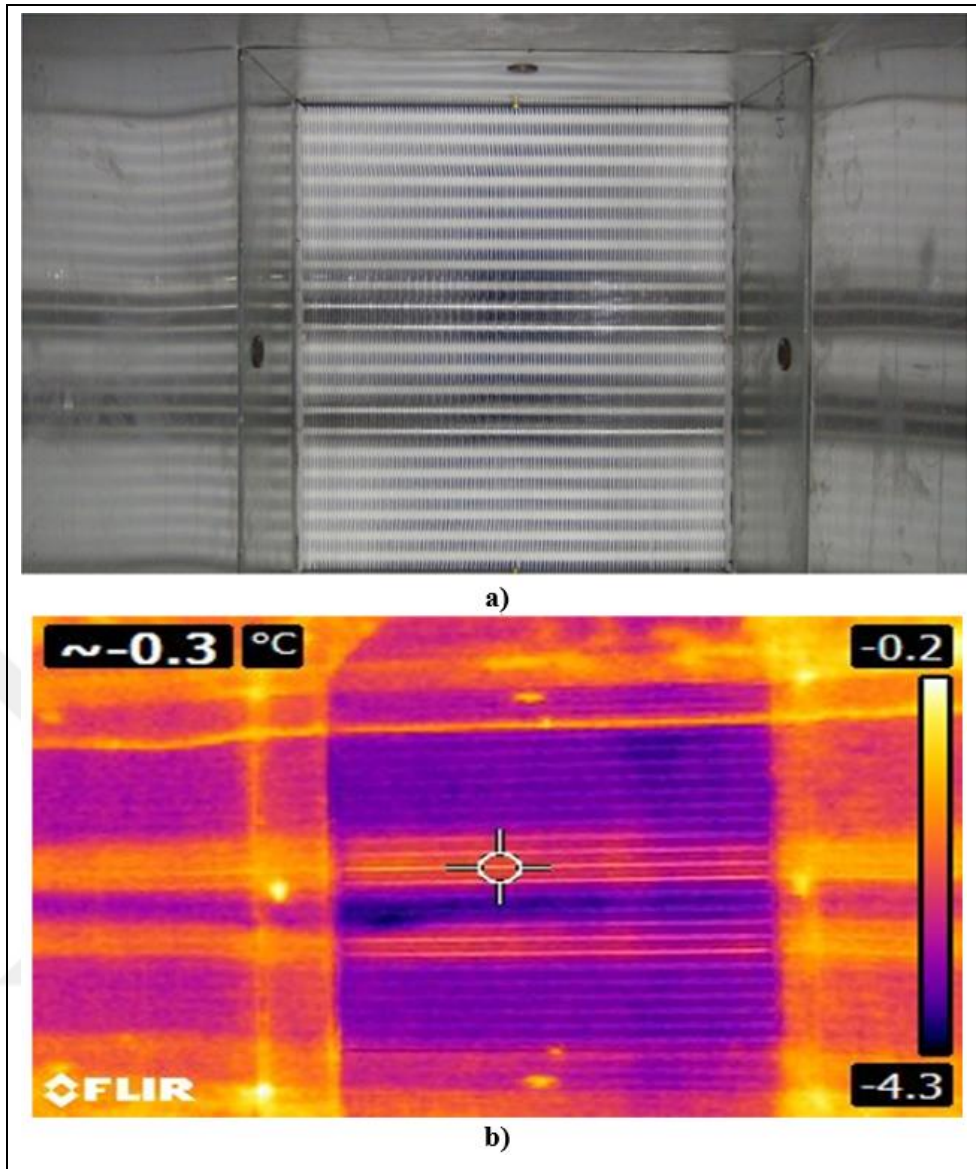


Figure 5.27: a) The digital and b) thermal images at 145 minute.

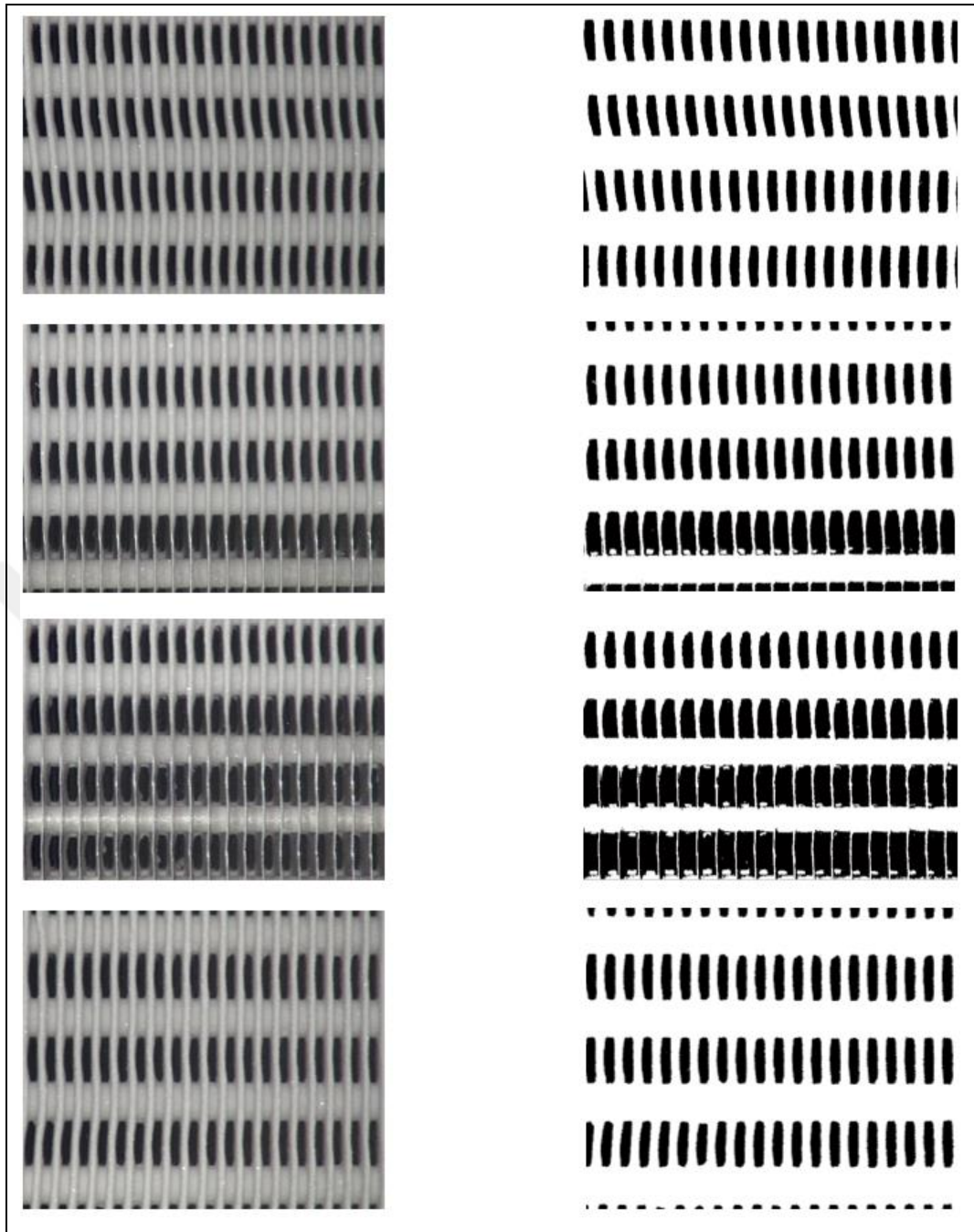


Figure 5.28: The digital (left) and post images (right) at 145 minutes.

- 255 minutes:

It was repeated the same process like aforementioned sections.

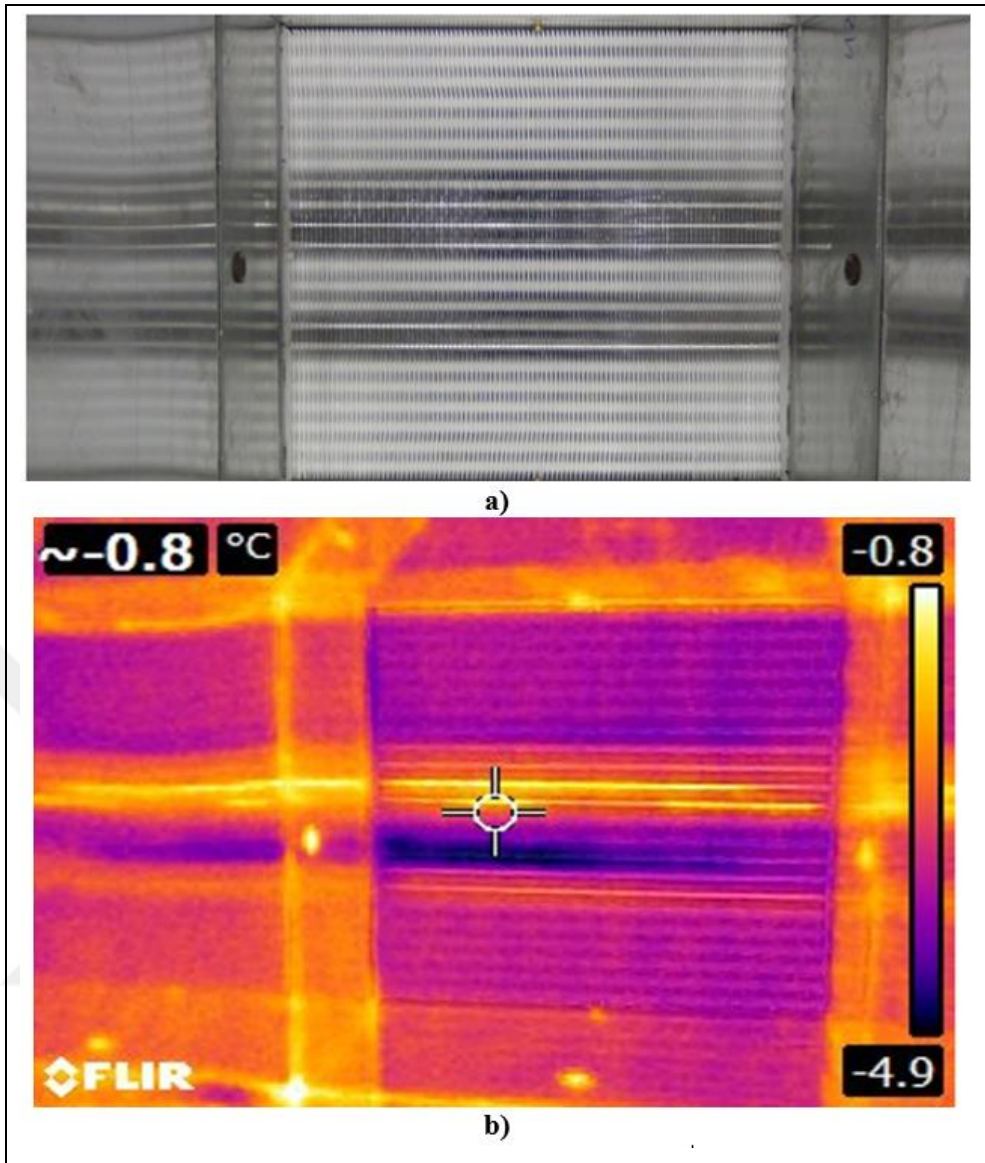


Figure 5.29: a) The digital and b) thermal images at 255 minute.

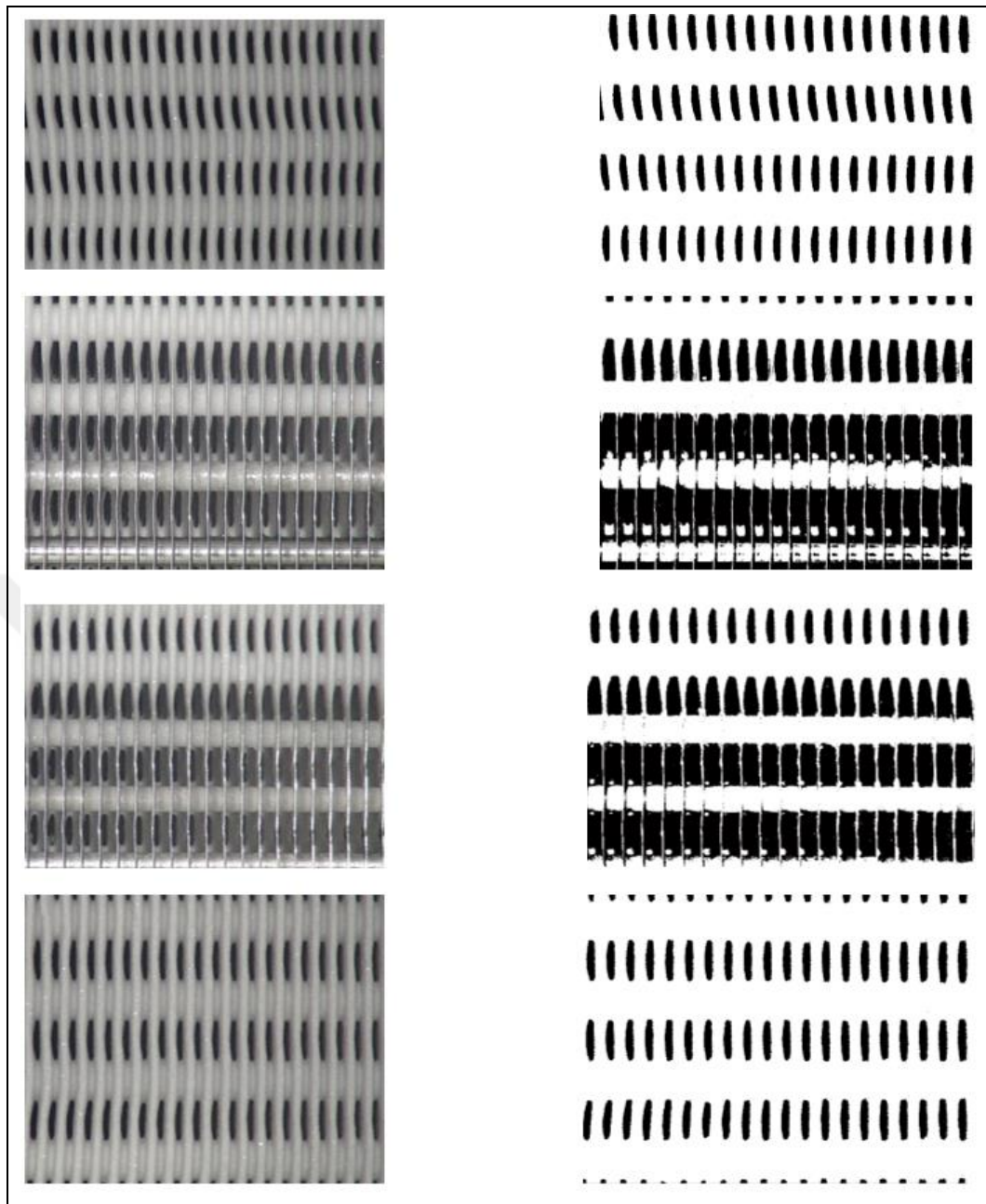


Figure 5.30: The digital (left) and post images (right) at 255 minutes.

Fin and tube thicknesses and total BR of conditioning room for each circuit is calculated with respect to the equations specified in detail at previous section as can be seen in Table 5.4. It should be stated that the calculations have been carried out at 255 minutes because this time is just 15 minutes later after breaking time of centrifugal fan, which denotes the breaking time of air pressure drop sharply. Therefore, it is speculated that the blockage ratio is about 50% at this time, which is admitted starting time of defrost operation, and this values consistent of the study performed by Huang (2008) as similar with calorimetric test operation.

Table 5.4: The summary of measured fin thickness, tube thickness and total BR of conditioning room for each circuit.

	fin thickness (mm)	tube thickness (mm)	Total BR (%)
Circuit 1	2.1101	2.2314	69.23%
Circuit2	0.9607	0.7768	33.02%
Circuit 3	1.185	1.0523	40.72%
Circuit 4	1.9862	2.3046	66.60%
AVG	1.5605 \mp0.208	1.591275 \mp0.208	52.39% \mp5.39%

5.4. The General Evaluation of Test Operations Considering Visual Results

In scope of this part, it is going to be interpreted the differences between two test data, visual images observations during the test operations, considering entire parameters. At following sections consist of a large number of comparison, that are fan curves and the deterioration of axial and centrifugal fan depending on frost growth, the effects of AMD the changes of air side pressure drop and heat transfer rate, respectively. If it is need to remind, these evaluations are very important because of the fact that there are lack of study considering the effects of fan on frosting test operations.

Table 5.5 shows that the most important parameters belonging to frosting tests.

Table 5.5: The general view of study outcomes.

	Conditioning Room (Test 4)	Calorimetric Room (Test 3)
Test Duration Time	3 h 57 min.	4 h 3 min.
Capacity Decreasement	11%	4.3%
Images Time	80 min., 145 min., 195 min.	70 min., 140 min., 208 min., 267 min.
Blockage Ratio	52.39% (\pm 5.39%)	62.85% (\pm 5.22%)
AMD	15.7 % (\pm 1.60%)	21.6 % (\pm 1.87%)
Fin thickness	1.56	1.92
Tube thickness	1.59	1.91
Avg. air inlet temperature	3.01	3.01
Avg. air inlet humidity	77.19 %	77.34 %
Avg. surface temperature	-9 °C	-9 °C
Avg. superheat temperature	0.59 °C	0.87 °C

5.4.1. Fan Curves

Figure 5.31 show that the characteristic curve of pressure drop versus air volumetric flow with respect to fan types, which are centrifugal and axial, respectively. If taken care to these curves, the changes of air volumetric flow at centrifugal fan is quite slower than axial fan. For instance, as the first curve pressure drop is about 375 Pa at 7500 m³/h, the second curve reaches to same air flow rate at about 82 Pa. So that, it has been expected that the forming of frost on evaporator surface would be different although the first air flow rate has been almost same and the air flow maldistribution based on both the fan characteristic and installation of heat exchanger in external limitation could affect this phenomenon and this situation is going to investigated at following sections.

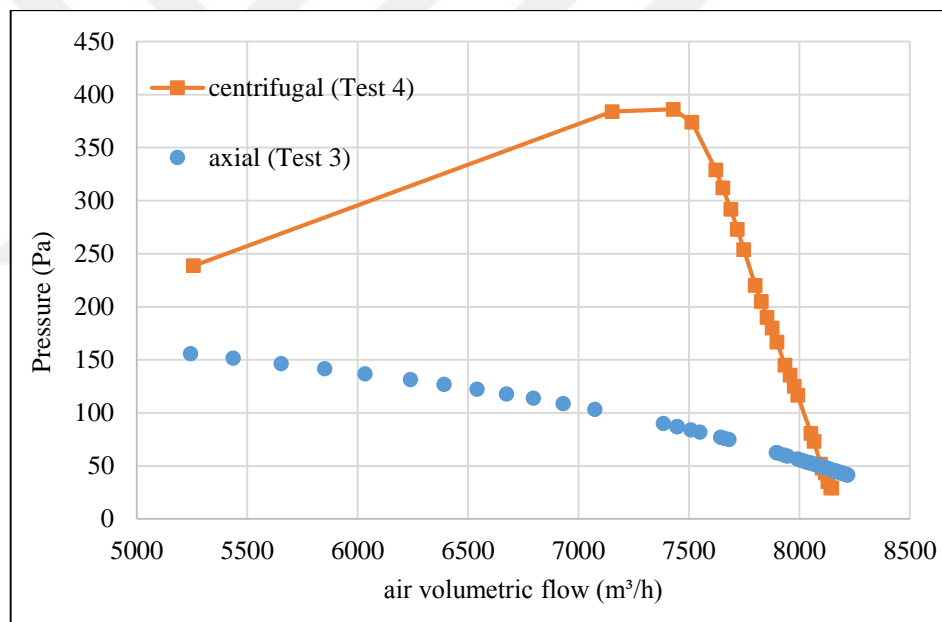


Figure 5.31: The fan curves used at the test operation.

On the other hand, it can be though what is the limitation of pressure drop at fans and exceeding of this limit is whether to result in detrimental effects on fan and its components. When it has been researched this issue, the fan manufacturer Aerovent Company states that this situation can create such problem as increasing of noise and vibration, structural fatigue and damaging of ductwork and other components.

Besides, some researchers specified that if the air volume is highly reduced, the centrifugal fan may surge and the flow becomes unstable whereas the axial fan will increase the pressure head steadily but with a stall in the middle region which will decrease the air volume faster. [Huang, 2008]. The mentioned situations above detected in this study as shown in Figure 5.32 and this table is convenient with Figure 5.33 specified from Aerovent Company. The fan curves given from fan company have already illustrated the permitted pressure drop values, so that this point can be taken as maximum operation condition. Moreover, this point could be considered that the time of starting of defrost process at frosting tests. Also, this time is going to be dealt in terms of blockage ratio considering related articles.

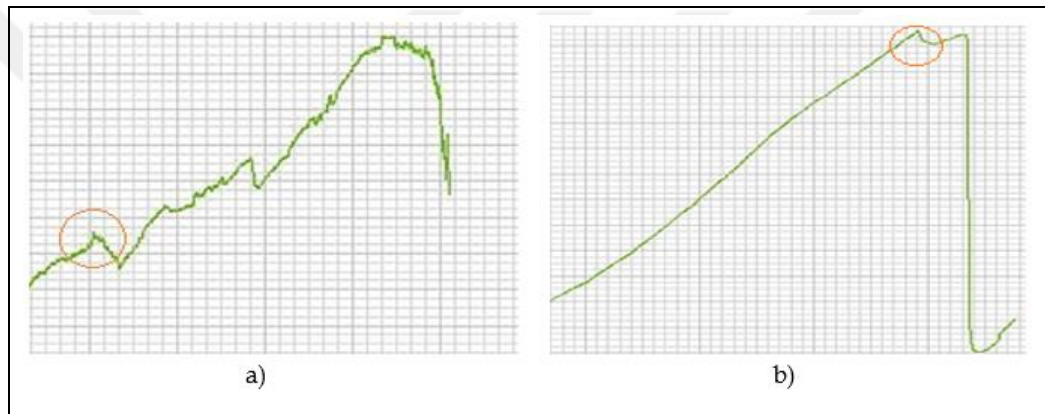


Figure 5.32: a) stall condition at axial fan (Test 3) b) surge condition at centrifugal fan (Test 4).

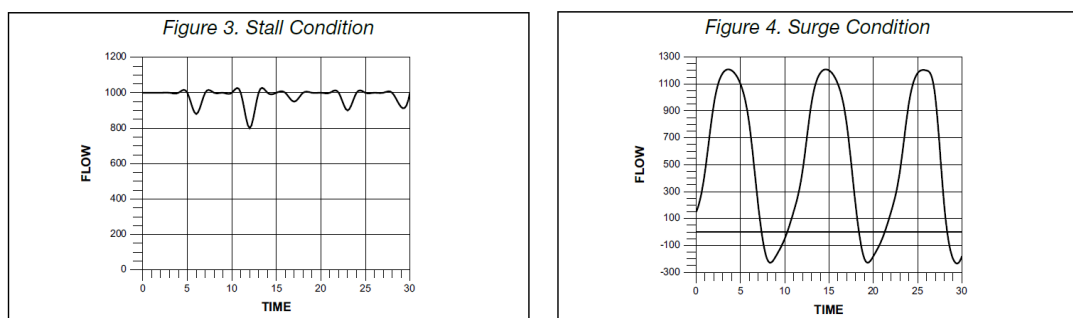


Figure 5.33: The fan stall and surge conditions.

5.4.2. Air side pressure drop curves during the test operation

Frost growth on evaporator's fins and tubes leads to increase the air pressure drop across the heat exchanger; therefore, reduce the air flow rate. Depending on fan

characteristic and air maldistribution degree, the frost blocks more than half of evaporator's fin space after many hours.

The Figure 5.33 and 5.34 demonstrate that the air pressure drop and air flow rate versus time, respectively. The red and blue lines denote centrifugal and axial fan respectively. According to these images, air flow rates are almost same until 40 minutes; therefore, the inclination of each pressure drop curve is similar within this duration. After this time, the inclinations of curves are rather different that depending on fan characteristics.

However, the centrifugal fan pressure drop and air flow rate decrease instantly at about 4 hours. Even if the axial fan seems that the ensuring time is longer than centrifugal fan, the starting time of stall condition is almost same with centrifugal fan, that is about 4 hours and the usage of both fans after this time is incorrect as mentioned previous part. On the other hand, it is speculated that the heat transfer rate belonging to axial fan can be decrease more seriously depending on decreasing of air flow rate sharply. These situations are going to be dealt when evaluated the change of heat transfer rate.

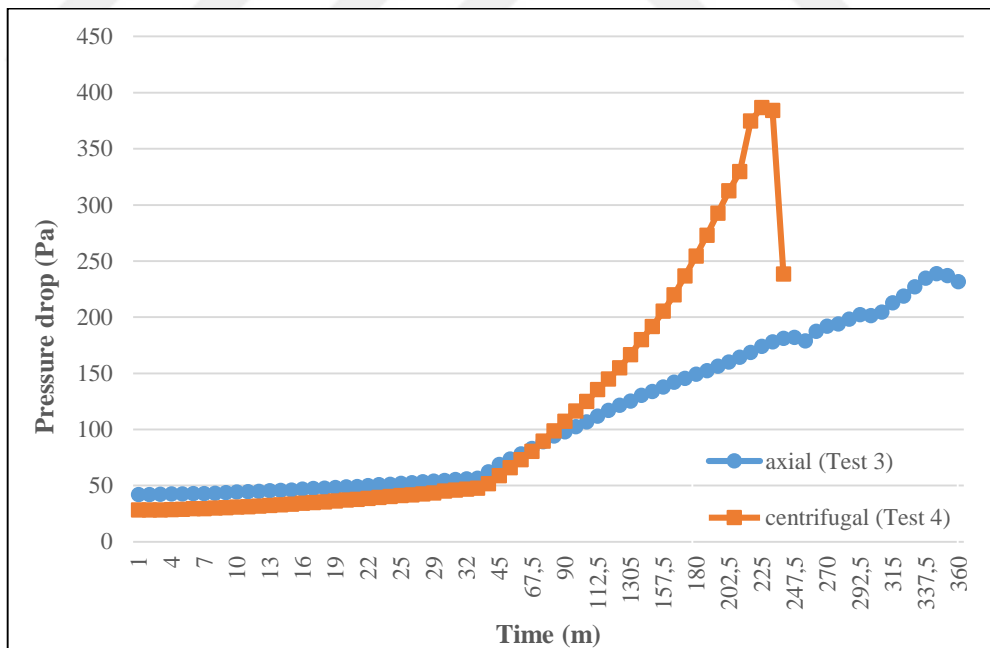


Figure 5.34: The air pressure drop versus time during test operation.

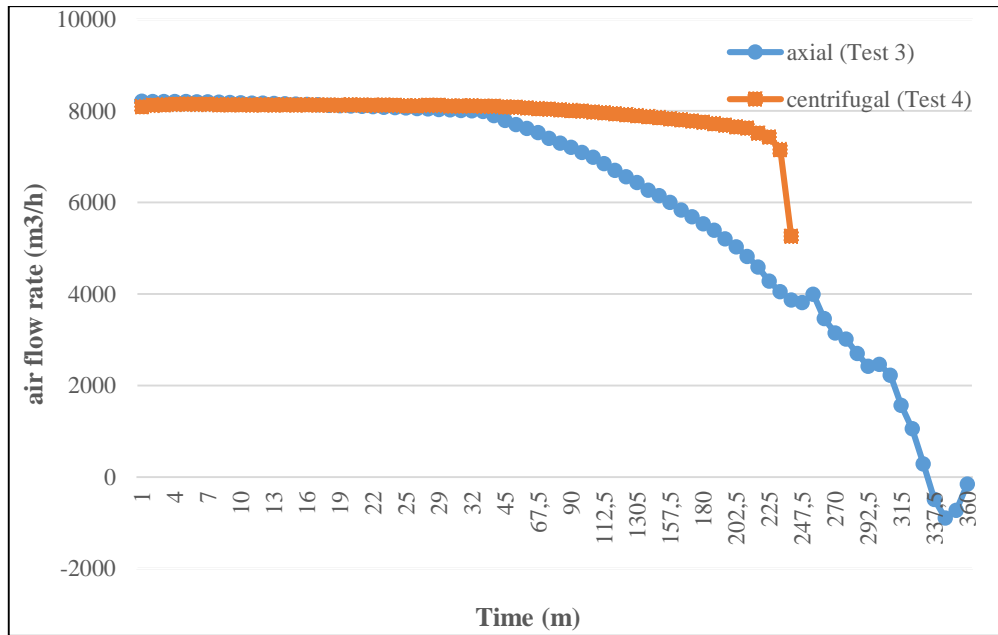


Figure 5.35: The changing of air flow rate versus time during test operation.

5.4.3. Air Flow Maldistribution Degrees:

Table 5.6 demonstrates that standard deviations, defined as AMD, for the test operation carried out at calorimetric room and conditioning room are 21.06% and 17.20%, respectively. It means that the uniformity of flow media of conditioning room is better when compared with calorimetric room's value. If it should be reminded that this difference could not have any detrimental effect on capacity but it may be effective on wet condition test process because even if this maldistribution degree have negligible impact on heat transfer, it could affect the mass transfer characteristic.

Table 5.6: The mean velocities and standard deviations (AMD) for each circuit.

Air Maldistribution Degrees				
Circuits	Calorimetric Room		Conditioning Room	
	Mean Velocity (m/s)	AMD	Mean Velocity (m/s)	AMD
Circuit 1	4.60	14.75%	3.23	16.93%
Circuit 2	4.28	18.43%	3.81	10.35%
Circuit 3	3.79	17.17%	4.10	12.20%
Circuit 4	4.46	15.95%	3.86	15.02%
The entire coil	4.28	21.6% (±1.87%)	3.75	15.7% (±1.60%)

On the other hand, we mentioned at previous section that the interpreting of air velocity data is not correct due to very close values depending on uncertainty of measurement probe and this situation should be considered air velocity contour showing the distribution trend.

In this context, the air velocity contours for each test operation were prepared by means of Matlab Program as demonstrated in Figure 5.36 and 5.37. Accordingly, it can be realized that the type of air maldistribution is rather different alongside AMD. When looked for this situation in literature, it has encountered the study performed by Datta in 2014, which has mentioned that type of air maldistribution has significant effects of on heat transfer rate of heat exchanger used at automotive cooling system.

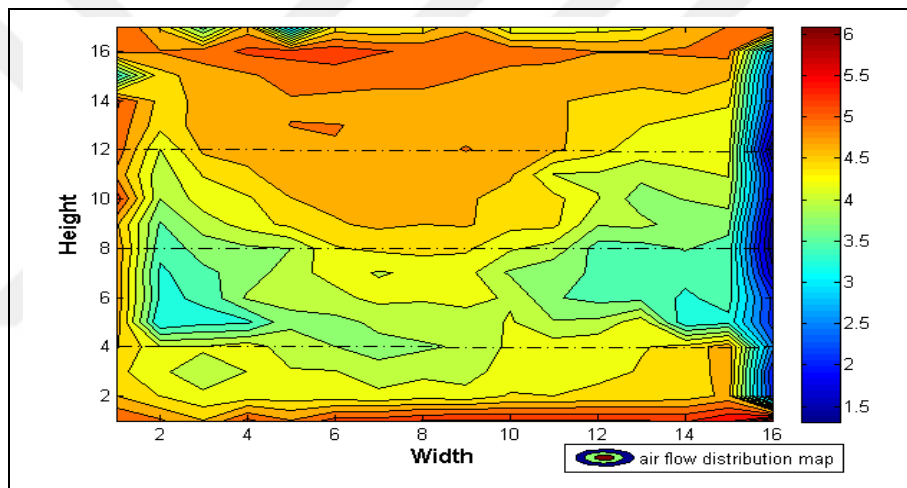


Figure 5.36: Calorimetric Room air speed distribution.

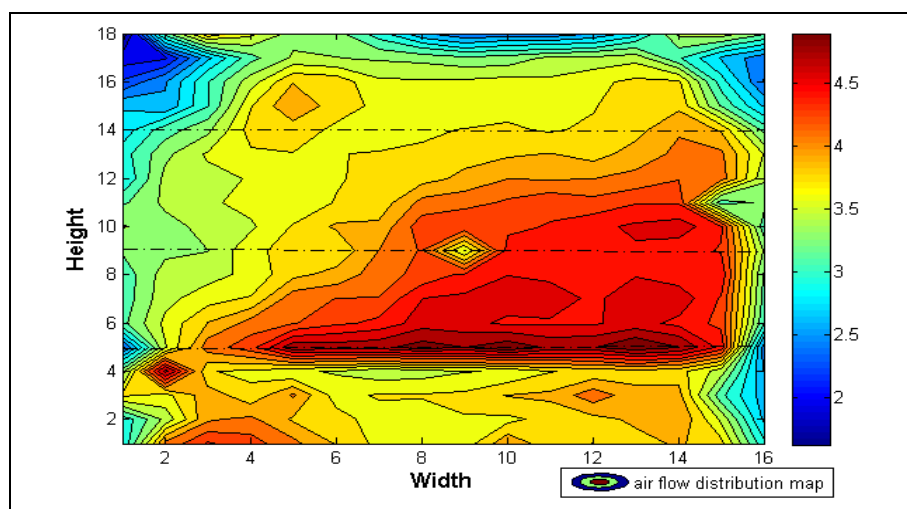


Figure 5.37: Conditioning Room air speed distribution.

5.4.4. The Change of Heat Transfer Rates

The frost layer occurring on the surface leads to increase of thermal resistance between the fin and airflow. Thereby, the cooling capacity of evaporator degrades gradually depending on thermal installation and decreasing of air flow rate. Besides, the air-side heat transfer coefficient increases during initial frosting because of increased surface roughness. However, an increase in the thermal resistance of the frost layer soon offsets the surface roughness effect after a while, and the overall heat transfer coefficient decreases gradually. Besides, the fin efficiency increases initially with the frost growth because a more uniform temperature distribution over the fin. A constant value is then approached.

When investigated the decrement of capacity during the test operation, it is found that these decrements for conditioning and calorimetric room are 11% and 4.3%, respectively. The reason of lower decrement of calorimetric room could be decreasing of air flow rate in middle of the test unit depending on axial fan specification as shown in Figure 5.38. This situation was highlighted by an author [Huang et al., 2008] as like: When the air volume is highly reduced, the centrifugal fan may surge and the flow becomes unstable whereas the axial fan will increase the pressure head steadily but with a stall in the middle region which will decrease the air volume faster. Therefore, it can be speculated that as the uniformity of frost pattern increases, the decrement of heat transfer rate decreases.

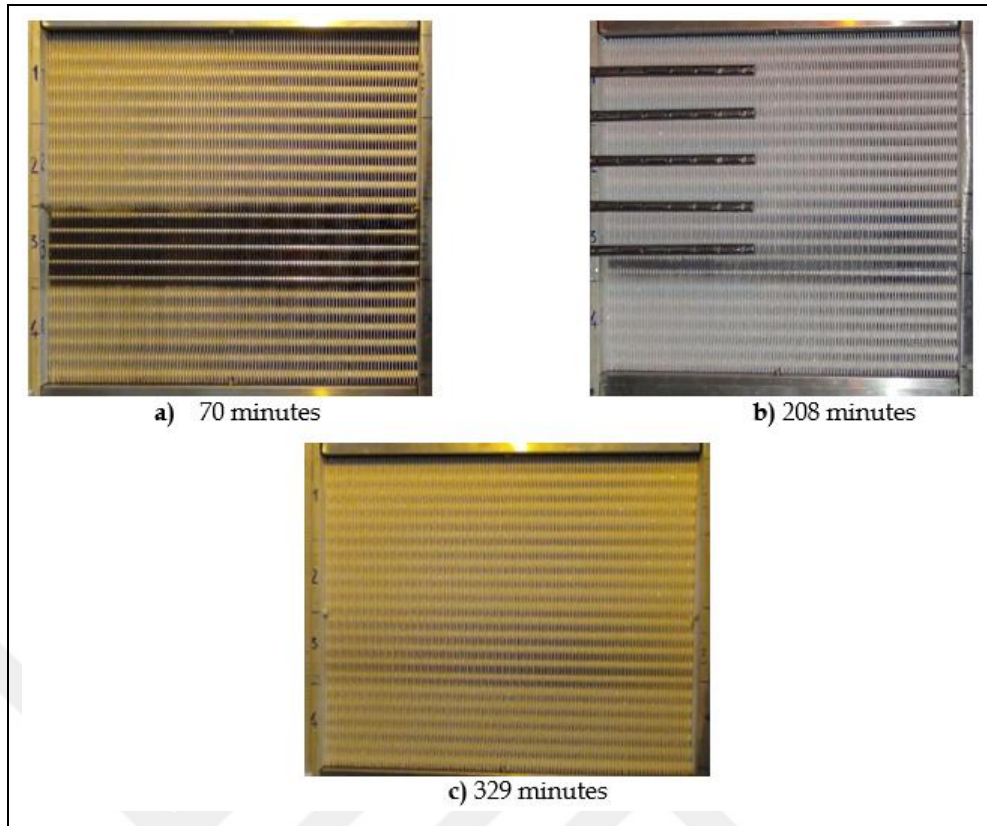


Figure 5.38: The improvement of air flow rate with increasing time in middle of test unit located in calorimetric room.

However, as mentioned previous parts, even if the air flow rate belonging to axial fan decreases more seriously than centrifugal fan, the decrement of heat transfer rate is lower. This situation could be based on that the effect of air flow rate under frosting test is negligible.

In addition to, the improvement at axial fan verifies more clearly by means of the change of circuit outlet temperatures versus time as illustrated at Figure 5.39. Same situation can't be seen for the test process carried out at conditioning room depending on characteristic of centrifugal fan as can be shown at Figure 5.40.

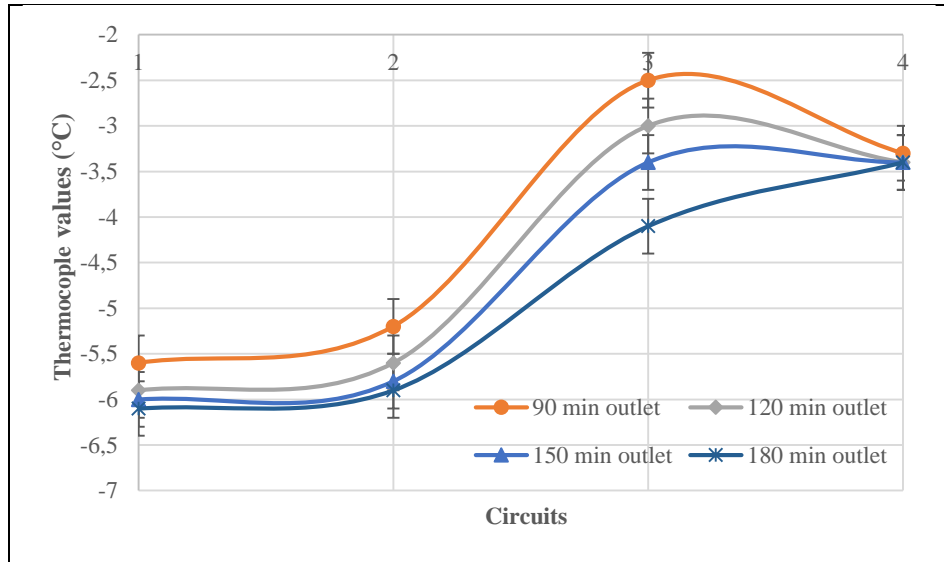


Figure 5.39: The thermocouple values at outlet of each circuits (Test 3).

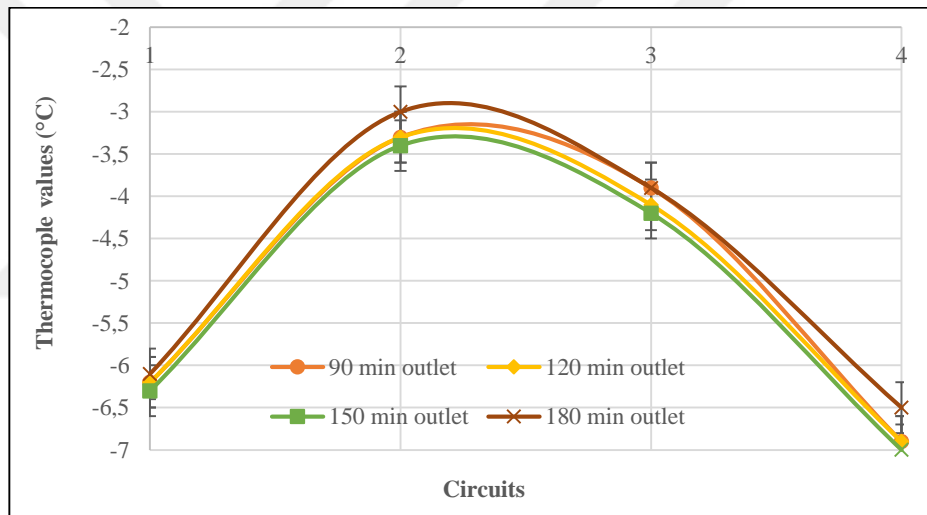


Figure 5.40: The thermocouple values at outlet of each circuits (Test 4).

On the other hand, although the test conditions for each test are almost same except AMD and type of air maldistribution, it has been detected significant capacity difference as illustrated at Figure 5.41. The dry test operations mentioned at Part 1 in detail have proved that the AMD determined is not significant impact on internal heat transfer rate. As different from Part 1, it has to be considered the mass transfer effects scope of this section. If detected the temperature variation among circuits, it is going to be deducted that the AMD affects to internal heat transfer coefficient, thereby, cooling capacity. Furthermore, the cooling capacity could be affected from the effects occurring air side, especially mass transfer coefficient.

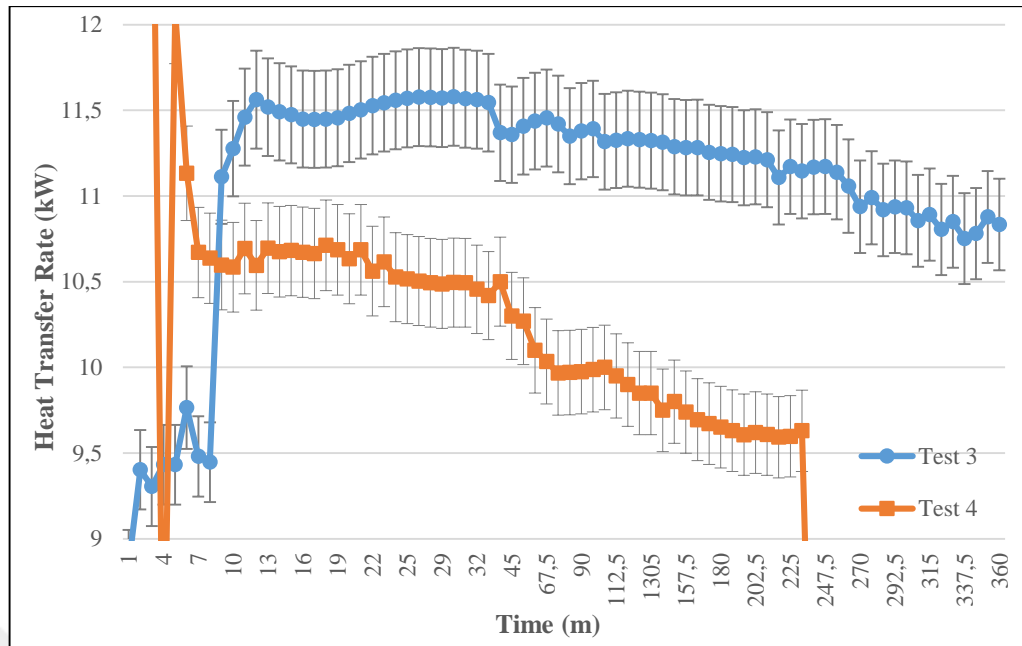


Figure 5.41: The changing of cooling capacity versus minutes during test operation.

When the heat transfer rate results at initial section of test are compared with its design value as shown in Table 5.7, it is found that each test is rather higher than the result of FrtCoils at the beginning of the test operation because of the improvement effects of both mass transfer and fin efficiency at initial period as mentioned. Later stages, this deviation decreases gradually depending on frost growth.

Table 5.7: The evaluation of frosting test results considering FrtCoils.

	FrtCoils Result (kW)	Deviation with FrtCoils
Calorimetric Room	9.9	~14.6 %
Conditioning Room		~6.6 %

According to following equations, at the initial period of frost growth, increasing of air side heat transfer coefficient depending on surface roughness, fin efficiency and a somewhat area enhancement result in increment of mass transfer coefficient as shown at equation 5, thus, it is obtained the increment of capacity owing to new heat transfer coefficient, surface roughness and a somewhat area enhancement as shown at equation 6, so that the desired capacity could be higher according to FrtCoils Software.

$$\dot{Q} = h_a \cdot A_a \cdot (T_a - T_s) + h_m \cdot A_a \cdot (w_a - w_s) \cdot i_{fg} \quad (5.6)$$

$$Le = \frac{h_a}{c_{p,a} \cdot h_m} \quad (5.7)$$

If the Le number is rearranged according to wet condition proposed by Pirompugd [2007];

$$Le = 2,28N^{0,2393} \cdot \left(\frac{FP}{D_o}\right)^{0,2393N+0,4332} \cdot \left(\frac{A_a}{A_t}\right)^{0,0321N+0,747} \cdot Re_{D_o}^{(-0,01833N+0,194 \cdot \frac{F_s}{D_o} - 0,0026 \cdot \frac{X_L}{D_o} - 0,03012 \cdot \frac{X_L}{D_o} + 0,0418)} \quad (5.8)$$

Combining equations (4.6) and (4.7) yield

$$\dot{Q} = h_{wet} \cdot A_a \cdot (T_a - T_s) \quad (5.9)$$

where h_{wet} is the total heat transfer coefficient for wet external surface, given by:

$$h_{wet} = h_a \cdot \left(1 + \frac{i_{fg}}{Le \cdot c_{p,a}} \cdot \frac{w_a - w_s}{T_a - T_s}\right) \quad (5.10)$$

Finally, air side heat transfer rate has determined as follows:

$$\dot{Q} = h_{wet} \cdot \eta_{o,wet} \cdot A_a \cdot (T_a - T_s) \quad (5.11)$$

Where $\eta_{o,wet}$ denotes overall fin efficiency under wet conditions and its equation is determined at following.

$$\eta_{o,wet} = 1 - \frac{A_{fin}}{A_o} \cdot (1 - \eta_{fin}) \quad (5.12)$$

$$\eta_{fin} = \frac{\tanh X}{X} \quad (5.13)$$

$$X = h_{me} \cdot \sqrt{\frac{2 \cdot h_{wet}}{k_{fin} \cdot FT}} \quad (5.14)$$

$$h_{me} = \frac{d_o}{2} \cdot (\rho_{me} - 1) \cdot (1 + 0,35 \cdot \ln(\rho_{me})) \quad (5.15)$$

$$\rho_{me} = 1,25 \cdot \frac{X_t}{d_o} \cdot \sqrt{\frac{X_t}{X_l}} - 0,2 \quad (5.16)$$

On the other hand, the superheat temperature and capacity decrease approximately linearly with time until about 5.5 hours of test. Although it wasn't significant difference at dry condition as mentioned in detail at the first section of this study, the difference heat transfer capacity between two tests at 15 minutes is about 6% in spite of about same air flow rate. It means that the air maldistribution has significant impact on mass transfer. Nevertheless, the interesting point is that the conditioning room cooling capacity is lower although AMD is lower. This situation could result from that the air maldistribution values belonging to each circuit separately is effective on overall heat transfer rate.

The literature about the effect of air maldistribution under frosting conditions is examined. The effect of this phenomena on unit cooler capacity was investigated by using the blockages at specific ratios [Groll et al., 2011]. As a result, according to this study, the blockage formed in front of unit cooler result in capacity drop depending on levels of airside maldistribution as shown at Figure 5.42.

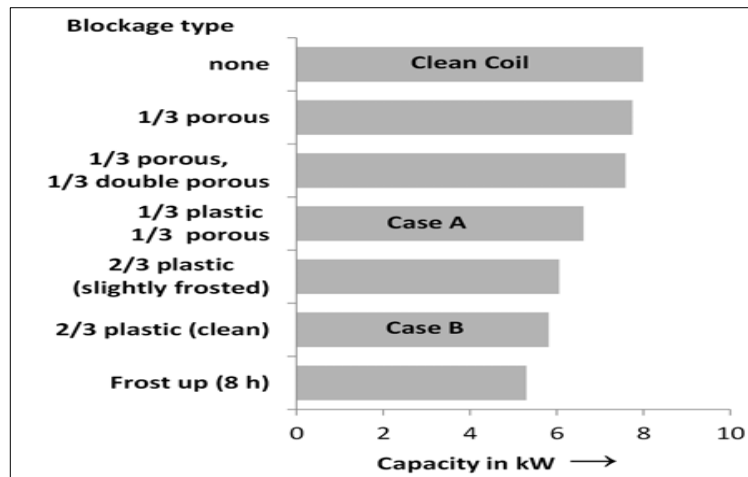


Figure 5.42: System Performance Figure with Different Levels of Airside Maldistribution, EXV.

Another study [Jiaying et al., 2008] investigated the same phenomenon. The authors detected that frost layer formed earlier and the system stability became shorter with AMD increased. In order to verify same condition, it had to be used same fan but different AMDs, so that it isn't possible to determine in scope of this study due to the difference of fan type.

Image 5.43 shows that the frost patterns occurring during test operations. As seen, the patterns forming at circuit 2 and 3 are quite different because of the fact that the air velocities forming related circuits are different as shown at Figure 5.44, therefore, the characteristic of local heat transfer and mass transfer coefficients are different as mentioned at foregoing comments.

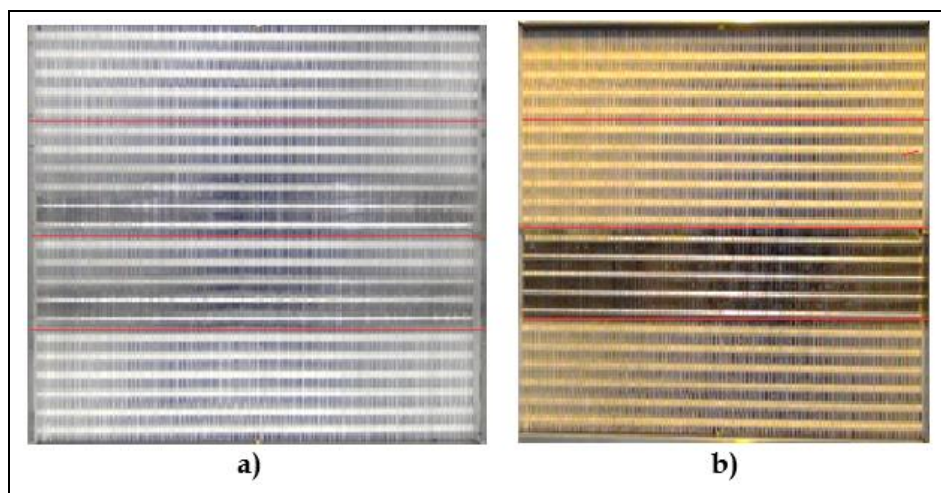


Figure 5.43: a) the frost pattern at conditioning room b) the frost pattern at calorimetric room.

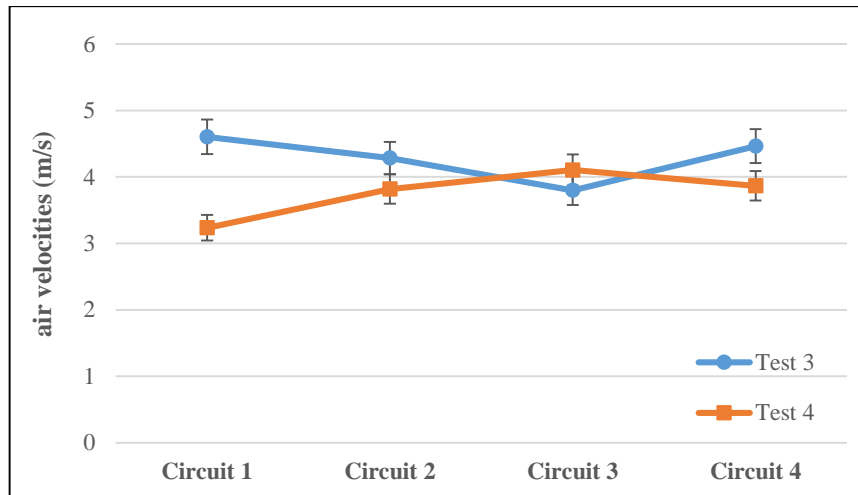


Figure 5.44: The air velocities measured at each circuits.

When examined the literature study dealing with air velocity effects on heat and mass transfer, a study [Padhmanabhan et al., 2011] mentioned that as the lower air velocity results in higher frost thickness, higher air velocity results in higher heat transfer coefficient, therefore higher fin surface temperature. However, higher air velocity ensures higher mass transfer coefficient which tend to increase the total mass deposition. The authors say that the effect of surface temperature has a higher impact on frost growth depending on an equation. The other study is a master thesis [Schmidt and Kristensen, 2014]. The authors emphasized as visual that the lower volumetric flow rate in the bottom section of the evaporator causes the air flow velocity to be lower which leads to a colder air flow which results in thicker frost.

According to another study Bayrak and Konukman (2016), considering real fan effect on frost growth, mentioned an optimum velocity ensuring lower capacity decrement.

In this context, the study [Ye et al., 2014] mentioned a critical air side heat transfer coefficient phenomenon affecting frost growth markedly. This point has entitled as the maximum point of mass transfer rate as can be seen at Figure 5.45. As the relationship between air side heat transfer rate and frost growth is proportional until this point, then vice versa because of the fact that the tendency of the mass transfer rate to increase or decrease with air velocity have been determined by the dominant factor relating the change in the mass transfer coefficient and absolute humidity difference. This situation is formulated in equation 5.17. Therefore, the frost pattern forming our test could be results from the different air velocities through

each circuit. This finding isn't considered in detail because the differences between velocities are rather close and under the uncertainty value.

$$\dot{m}_c = h_m \cdot [w_a - w_s] \cdot A \quad (5.17)$$

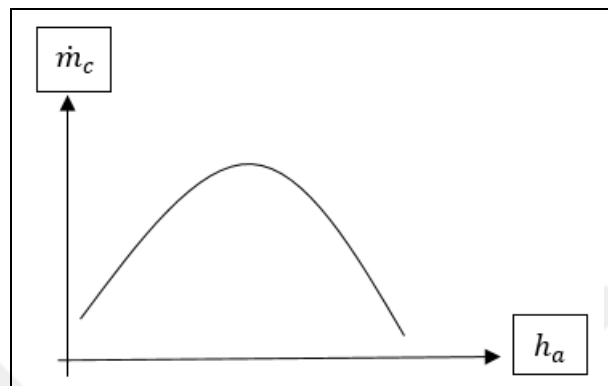


Figure 5.45: The relationship between heat transfer coefficient and mass transfer rate.

If it is evaluated in terms of these tests, the differences among circuits could be based on aforementioned situation. This situation should be investigated in detail further studies.

When researched the literature to be make sure whether the change of capacities found is convenient, it has been encountered the frosting study [Groll et al., 2011] performed with EXV and the decrement of capacity is similar with this study as illustrated at Figure 5.46.

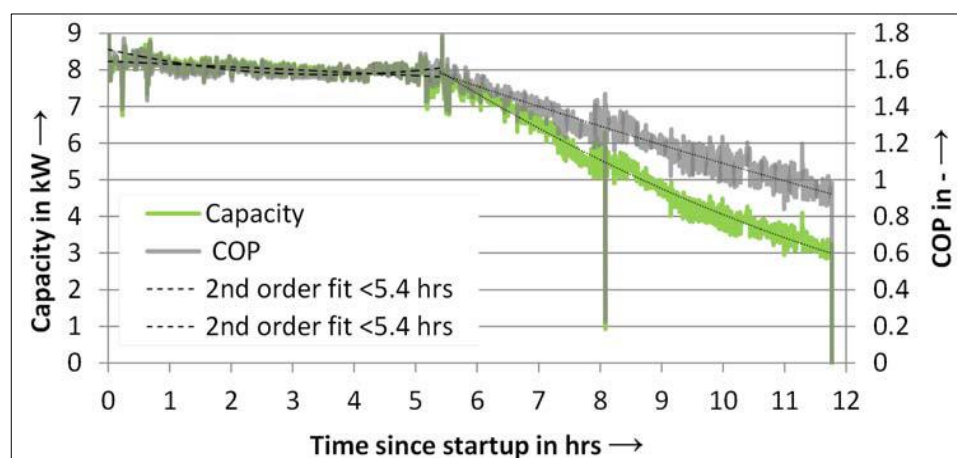


Figure 5.46: The capacity changing during the related frosting test.

On the other hand, the superheat temperatures are similar with same study too as illustrated at Figure 5.47 and 5.48. If it is thought why the superheat temperatures found haven't as much as other test because it has not been continued to test operation due to safety problems.

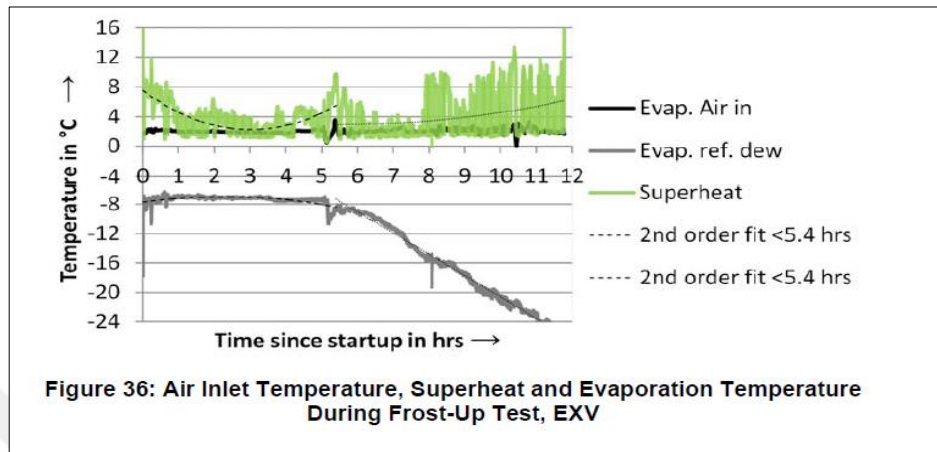


Figure 5.47: The superheat changing during the related frosting test.

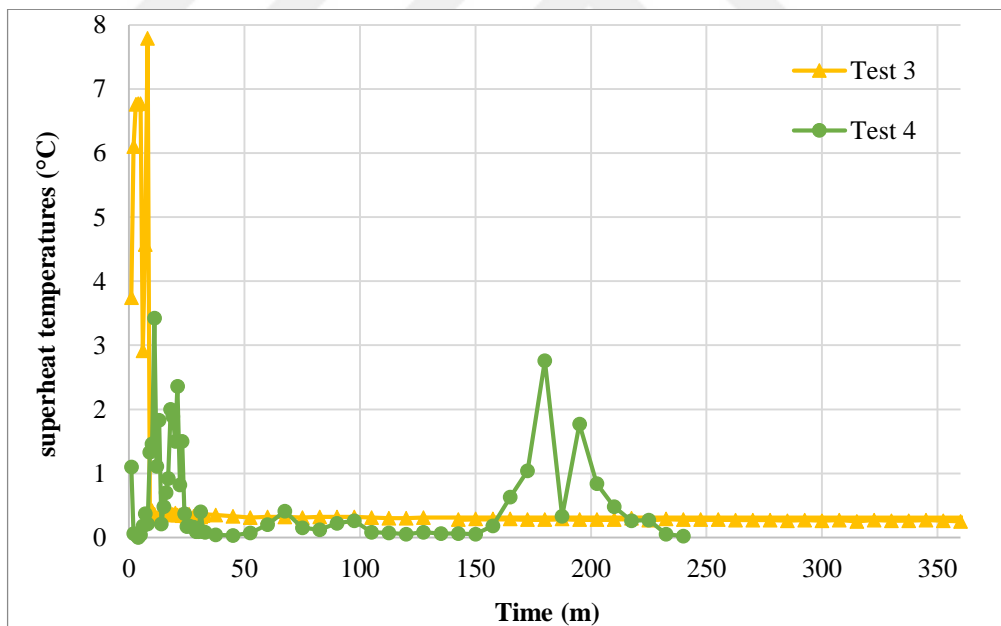


Figure 5.48: The changing of superheat temperature versus minutes during test operation.

Another important point is the starting time of defrost. This situation is very important, in order to adjust optimum defrost interval. Huang (2008) stated that a refrigerator should defrost when half of a single flow channel area is blocked by frost and also if the exceed this point, the heat transfer rate decreases rapidly. In scope of

this study, the blockage ratios are close to 50% for both rooms as shown at Table 5.8. Therefore, the information given by related study is convenient with this study.

Table 5.8: The comparison of measured parameters among two test.

	Fin thickness	Tube thickness	Blockage Ratio
Conditioning Room	1.5605	1.5912	52.39% (15 min. later)
Calorimetric Room	1.9298	1.91397	62.85%5 (25 min. later)

If considered the practical usage of defrost operations, it is encountered that it is waited growing away from desired air inlet temperature. When taken into account these tests, if it has been waited the breaking of air inlet temperature, it would be run in detrimental area for fans, which has entitled as stall and surge situations. Therefore, the fans are going to get out of order before its original life time but this period depends on fan's mechanical capability.

6. CONCLUSION

In this experimental study, the effects of air flow maldistribution on evaporator at both dry and frost condition was investigated in detail. The major findings and conclusions of this research may be summarized as follows:

- For dry condition:

FrtCoils software and experimental results have verified that although it has been ensured a little improvement at outlet of refrigerant circuits by more uniform air flow, no significant change at heat transfer rate was observed.

Hence, the AMD up to about 19% does not have significant impact on the heat transfer rate.

The heat transfer rate outcomes taken with FrtCoils and experiments are quite close because of the fact that the AMD identified doesn't affect the thermal characteristic of internal flow.

- For frosting condition:

It has been dealt with firstly a new approach about detrimental impacts of frost on fan structure if the air pressure drop surpasses design value and speculated that the maximum air pressure drop value could be superior time for starting of defrost operation because the product at this time has as much as %50 blockage as mentioned literature. If this detection is verified with further studies, it would be developed a new defrost control method running according to air pressure drop measurement.

It is detected that as the air pressure drop of centrifugal fan is more stable during test operation, air pressure drop of the axial fan breaks quicker. even if the air flow rate belonging to axial fan decreases more seriously than centrifugal fan, the decrement of heat transfer rate is lower. This situation could be based on that the effect of air flow rate under frosting test is negligible.

It is detected that the axial fan will increase the pressure head steadily but with a stall in the middle region which will decrease the air volume faster, thereby, it was obtained more uniform frost pattern at windward of unit cooler, which could ensure lower decrement of heat transfer.

As the AMD determined isn't significant impact on heat transfer rates of dry conditions, it is speculated for frosting test that cause of difference of heat transfer rate between calorimetric and conditioning room test could be effect of AMD on mass transfer phenomenon.

The effect of air velocity on initial frost growth hasn't been detected due to the fact the frost formation has occurred at stabilization period of the test operation.



7. RECOMMENDATIONS

Further studies should be taken into account following recommendations;

In order to identify the effect of AMD on evaporator exactly under both dry and frost condition, refrigerant side maldistribution has to be prevented by using flow balance valve or expansion valve for each circuits separately. However, according to our experience, it should not be designed an evaporator having only one circuit without distributor, because it is quite difficult to ensure steady superheat temperature due to the fact that the product exposes directly the negative effect of the suction of compressor

Not only AMD, but also the type of blockage should be taken into account, which may occur at practical application, especially automotive cooling system.

The air measurements should be performed via PIV device, in order to be taken more accurate data. Besides, it should be studied to develop new air flow simulation methods such as CFD tools because classical measurements are very expensive and difficult.

Investigation of AMD in larger equipment such as dry coolers and air cooled condensers in terms of the correlation between air side maldistribution and heat transfer performance should be studied.

Further studies have to investigate the effect of refrost condition for impact of AMD because the retain water on heat exchanger has detrimental impacts on change of heat transfer rate of evaporator seriously and type of surface retention according to AMD can be different effect on this situation.

It should be investigated defrost performance of evaporators according to type of AMD as like refrost condition.

The initial frost growth should be investigated in a test setup, ensured rather sensitive air temperature and relative humidity. Besides, the frost growth period should be determined and followed the time period according to AMD and air velocity.

AMD measurement isn't determined only air inlet temperature but also it has to be considered air inlet humidity and temperature.

REFERENCES

- Aganda A. A., Coney J. E. R., Sheppard C. G. W., (2000), "Airflow maldistribution and the performance of a packaged air conditioning unit evaporator", *Applied Thermal Engineering*, 20(6), 515-528.
- Bayrak E., Konukman A. E. Ş., (2016), "Investigation of the effect of air flow maldistribution on evaporator thermal performance", *Proceedings of the TTMD XII. International HVAC+R Technology Symposium*, 167-174, Istanbul, Turkey, March 31-2 April.
- Bayrak E., Şahin N., (2015), "Kanatlı Borulu Evaporatörlerde Devre Tasarımının Kapasiteye Olan Etkisinin Deneysel Olarak İncelenmesi", 12. Ulusal Tesisat Mühendisliği Kongresi, İzmir, Türkiye, 8-11 Nisan.
- Bell S., (1999), "A Beginner's Guide to Uncertainty of Measurement, Measurement Good Practice Guide", No:11(2), Thermal and Length Metrology National Physical Laboratory, Middlesex, United Kingdom.
- Chen N., Xu L., Feng H. D., Yang C. G., (2005), "Performance investigation of a finned tube evaporator under the oblique frontal air velocity distribution", *Applied Thermal Engineering*, 25, 113–125.
- Chena H., Thomas L., Besant R. W., (2013), "Fan supplied heat exchanger fin performance under frosting conditions", *International Journal of Refrigeration*, 26, 140-149.
- Choi J. M., Payne W. V., Domanski P. A., (2003), "Effects of Non-Uniform Refrigerant and Air Flow Distributions on Finned- Tube Evaporator Performance", *International Congress of Refrigeration*, Washington, D.C., USA, 17-22 August.
- Cui J., Li W. Z., Liu Y., Zhao Y. S., (2011), "A new model for predicting performance of fin-and-tube heat exchanger under frost condition", *International Journal of Heat and Fluid Flow*, 32, 249–260.
- Da Silva D. L., (2012), "Frost Formation on Fan-Supplied Tube-Fin Evaporators: A Visual and Numerical Analysis", *International Refrigeration and Air Conditioning Conference*, Paper 1164, Purdue University, Indiana, USA, 16-19 July.
- Datta S. P., Das P. K., Mukhopadhyay S., (2014), "Obstructed airflow through the condenser of an automotive air conditioner effects on the condenser and the overall performance of the system", *Applied Thermal Engineering*, 70, 925-934.
- Domanski P. A., Yashar D., Kaufman K. A., Michalski R. S., (2004), "Optimized design of finned-tube evaporators using learnable evolution methods", *International Journal HVAC&R Research*, 10(2), 201-212.

Domanski P. A., Choi J. M., Payne W. V., (2007), “Longitudinal Heat Conduction In Finned-Tube Evaporators”, International Congress of Refrigeration, Beijing, China, 21-16 August.

Domanski P. A., Yashar D., (2007), “Optimization of Finned-Tube Condensers Using an Intelligent System”, International Journal of Refrigeration, 30(4), 482-488.

Ehsan M., Lorenzo C., Daniel F., “Experimental Investigation of Frost Growth on Microchannel Heat Exchangers”, (2010), International Refrigeration and Air Conditioning Conference, paper 1114, Purdue University, Indiana, USA, 12-15 July.

EUROVENT, (2010), “Eurovent Rating Standard for Direct Expansion Forced Convection Unit Air Cooler for Refrigeration”, Eurovent Certification Company, Paris, France.

Groll E. A., Braun J. E., Bach C. K., (2011), Optimizing refrigerant distribution in Evaporators, Final project report prepared for California Energy Commission, Purdue University, Indiana, USA.

Haijie Q., Weizhong L., Bo D., Zhihai Z., Weiyong Z., (2014), “Experimental study of the characteristic of frosting on low-temperature air cooler”, Experimental Thermal and Fluid Science, 55, 106–114.

Hongtao Q., Singh V., Aute V., Radermacher R., (2010), “Optimization of Fin Density for Air Cooled Heat Exchanger”, International Refrigeration and Air Conditioning Conference, Paper 1089, Purdue University, Indiana, USA, 12-15 July.

Huang J. M., Hsieh W. C., Ke X. J., Wang C. C., (2008), “The effects of frost thickness on the heat transfer of finned tube heat exchanger subject to the combined influence of fan types”, Applied Thermal Engineering 28, 728–737.

Janssen D. D., (2014), “Experimental Strategies for Frost Analysis”, Master Thesis, University of Minnesota, USA.

Jiaying G., Tiewu G., Xiuling Y., Dong H., (2008), “Effects of air flow maldistribution on refrigeration system dynamics of an air source heat pump chiller under frosting conditions”, Energy Conversion and Management, 49, 1645–1651.

Kim J., Braun J. E., Groll E. A., (2008), “Analysis of Refrigerant Flow Distribution in Evaporators” International Refrigeration and Air Conditioning Conference, Paper 966, Purdue University, Indiana, USA, 14-17 July.

Kim M. H., Bullard C. W., (2002), “Air-side thermal hydraulic performance of multi louvered fin aluminum heat exchangers”, International Journal of Refrigeration, 25(3), 390-400.

Kim D., Kim C., Lee K. S., (2015), “Frosting model for predicting macroscopic and local frost behaviors on a cold plate”, International Journal of Heat and Mass Transfer, 58, 135–142.

Lee J., Domanski P. A., (1997), "Impact of air and refrigerant maldistributions on the performance of finned-tube evaporators with R-22 and R-407C", Building Environment Division National Institute of Standards of Technology Final Report, U.S. Department of Commerce, Gaithersburg, Maryland, USA.

Lee T. S., Wu W. C., Chuah Y. K., (2010), "An improvement of airflow and heat transfer performance of multi-coil condensers by different coil configurations", International Journal of Refrigeration, 33 (7), 1370-1376.

Lee K. S., Kim W. S., Lee T. H., (1997), "A one-dimensional model for frost formation on a cold flat surface", International Journal of Heat and Mass Transfer, 40(18), 4359-4365.

Mohs W. F., (2013), "Heat and mass transfer during the melting process of a porous frost layer on a vertical surface", Phd Thesis, University of Minnesota, USA.

Padhmanabhan S. K., Daniel F., Cremaschi L., Ehsan M., (2011), "Modeling non-uniform frost growth on a fin-and-tube heat exchanger", International Journal of Refrigeration, 34, 2018-2030.

Schmidt E. O., Kristensen M. S., (2014), "Optimisation of Defrost Strategy for an Air-to-Water Heat Pump - Dynamic Modelling and Experimental Study of Frost Formation on Cross-Flow Heat Exchanger Surface", Aalborg University Master Thesis, Denmark.

Tashiro Y., Hamada M., "Experimental Evaluation of the Frost Formation", (2014), International Refrigeration and Air Conditioning Conference. Paper 1395, Purdue University, Indiana, USA, 14-17 July.

Yaici W., Ghorab M., Entchev E., (2014), "3D CFD analysis of the effect of inlet air flow maldistribution on the fluid flow and heat transfer performances of plate-fin and-tube laminar heat exchangers", International Journal of Heat and Mass Transfer, 74, 490–500.

Yan W. M., Li H. Y., Wu Y. J., Lin J. Y., Chang W. R., (2003), "Performance of finned tube heat exchangers operating under frosting conditions", International Journal of Heat and Mass Transfer, 46, 871–877.

Yashar D., Domanski P. A., Cho H. H., (2011), "An experimental and computational study of approach air distribution for a finned-tube heat exchanger", HVAC&R Research, 7(1), 76-85.

Yashar D. A., Lee S., Domanski P. A., (2015), "Rooftop air-conditioning unit performance improvement using refrigerant circuitry optimization", International Journal of Refrigeration, 83, 81-87.

Ye H. Y., Park J. S., Lee K. S., (2014), "Frost retardation on fin-tube heat exchangers using mass transfer characteristics with respect to air velocity", International Journal of Heat and Mass Transfer, 79, 689–693.

Ye H. Y., Lee K. S., (2013), “Performance prediction of a fin-and-tube heat exchanger considering air-flow reduction due to the frost accumulation”, *International Journal of Heat and Mass Transfer*, 67, 225–233.



BIOGRAPHY

Ergin Bayrak was born in 1989 in Karaman. After he had graduated from Edirne Anatolian High School in 2007, took the Bachelor's Degree from Yıldız Technical University Department of Mechanical Engineering in 2012. He started graduate school at Gebze Technical University, Graduate School of Natural and Applied Sciences Department of Mechanical Engineering. He has still been working at Friterm Thermal Devices A.S Research and Development Department as Laboratory Test Engineer. He has still continued researches about specific problems in finned tube heat exchanger. Also, he has two international and one national conference paper within scope of this area.



APPENDICES

Appendix A: Experimental Uncertainty Analysis

The measurement uncertainties coming from instruments directly affect the test result and overlooking of this process may result in incorrect assessing of test data and in correct outcomes. Hence, performing the uncertainty analysis is very important and necessary for process. In this context, it was calculated the uncertainty values as mentioned in detail at following section and the uncertainty value of heat transfer total capacity in the present investigation were calculated according to Stephanie Bell's study 'A Beginner Guide to Uncertainty of Measurement'.

The accuracy values taken from manufacturers is tabulated as showed at Table A.1 and reading uncertainties for each instruments, which is used UT550, is added and final uncertainties is calculated as follow;

Table A.1. Measurement uncertainties.

Measurement	Instrument	Location	Range	Accuracy
Temperature	Chino PT100	the refrigerant outlet temperature	-60-150°C	±0.1°C
Temperature	Chino PT100	the temperature before expansion valve	-30-70°C	±0.1°C
Temperature	T Type Thermocouple	outlet of circuits	-200-350°C	±0.3°C
Pressure	Danfoss PTX7517	evaporation pressure	0-4 MPa	±0.25%
Pressure	Danfoss PTX7517	condensation pressure	0-6 MPa	±0.25%
Refrigerant flow rate	Krohne MFM1081K-12	the refrigerant preparation system	0-720 kg/h	±0.6%
Power Meter (DPM1)	Yokogawa WT210	fan electrical consumption	--	±0.1%
Power Meter (DPM2)	Yokogawa WT230	total electrical consumption	--	±0.1%
Step controller	Yokogawa UT550	reading value of ref. flow rate	--	±0.1%
Step controller	Yokogawa UT550	reading value of ref. pressure	--	±0.1%
Step controller	Yokogawa UT550	reading value of temperature	--	±0.3°C
Static pressure difference (air)	Yokogawa EJA110A	the inlet and outlet of product	0-800 Pa	±0.075%
Static pressure difference (nozzle)	Yokogawa EJA120A	the inlet and outlet of nozzles	-50-450 Pa	±0.15%
Static pressure difference (refrigerant)	Rosemount 1151DP51	the inlet and outlet of product	0-600 kPa	±0.25%

First of all, it has to be considered the accuracy of devices throughout from device ensuring related measurement to the other device ensuring reading of related measurement. It can be shown examples below;

For PT100 temperature sensors;

$$w_T = \sqrt{(w_{PT100})^2 + (w_{UT550})^2} \quad (A1.1)$$

For pressure transmitters;

$$w_P = \sqrt{(w_{transmitter})^2 + (w_{UT550})^2} \quad (A1.2)$$

For flow meter;

$$w_{m_f} = \sqrt{(w_{flow\ meter})^2 + (w_{UT550})^2} \quad (A1.3)$$

- The uncertainty of refrigerant side heat transfer rate

The uncertainty of refrigerant side heat transfer rate is determined by considering entire measurements in order to reach this heat transfer rate and related calculations are as follows:

$$Q_r = m_r \cdot (H_2 - H_1) \quad (A1.4)$$

where

$$H_2 = U_2 + P_2 \cdot \vartheta_2 \quad H_1 = U_1 + P_1 \cdot \vartheta_1 \quad (A1.5)$$

$$H_2 = cv_2 \cdot dT_2 + P_2 \cdot \vartheta_2 \quad H_1 = cv_1 \cdot dT_1 + P_1 \cdot \vartheta_1 \quad (\text{A1.6})$$

where

For both H_2 and H_1 which refer outlet and inlet enthalpies respectively, the terms of c_v and ϑ were taken from NIST REFPROP Version 9.0 program. However, the terms, m_R was measured by flowmeter MFM1081K-12 whose accuracy is 0.6%, P_2 and P_1 refer evaporation pressure and condensation pressure of fluid, whose accuracies are 0.25%, T_1 and T_2 refer inlet and outlet refrigerant temperature respectively whose accuracies are 0.1°C. As aforementioned and calculated, reading uncertainties for flow meter, temperature sensors and pressure sensors is added and recalculated. Within the following sections, the uncertainty of enthalpy differences is going to be calculated and determined the uncertainty of refrigerant side heat transfer rate. Finally, we are going to deduct uncertainty of total laboratory heat transfer rate depending on obtained results.

- Fundamental uncertainty equations:

$$W_R = \left[\left(\frac{\delta R}{\delta x_1} w_1 \right)^2 + \left(\frac{\delta R}{\delta x_2} w_2 \right)^2 + \left(\frac{\delta R}{\delta x_3} w_3 \right)^2 + \dots + \left(\frac{\delta R}{\delta x_n} w_n \right)^2 \right]^{1/2} \quad (\text{A1.7})$$

or

$$\frac{W_R}{R} = \left[\left(\frac{w_{x_1}}{x_1} \right)^2 + \left(\frac{w_{x_2}}{x_2} \right)^2 + \dots + \left(\frac{w_{x_n}}{x_n} \right)^2 \right]^{1/2} \quad (\text{A1.8})$$

where W_R and w_1 is total accuracy ratio and accuracy ratio related to independent value, R is the measured parameter, x_1, x_2, \dots, x_n are variable parameters which affect the measurements.

- Uncertainty Analysis:

$$W_{H_2} = \left[\left(\frac{\delta H_2}{\delta T_2} w_{T_2} \right)^2 + \left(\frac{\delta H_2}{\delta P_2} w_{P_2} \right)^2 \right]^{1/2} \quad (\text{A1.9})$$

$$\frac{W_{H_2}}{H_2} = \sqrt{\frac{(w_{T_2} \cdot cv_2)^2 + (w_{P_2} \cdot \vartheta_2)^2}{H_2^2}} \quad (\text{A1.10})$$

$$W_{H_1} = \left[\left(\frac{\delta H_1}{\delta T_1} w_{T_1} \right)^2 + \left(\frac{\delta H_1}{\delta P_1} w_{P_1} \right)^2 \right]^{1/2} \quad (\text{A1.11})$$

$$\frac{W_{H_1}}{H_1} = \sqrt{\frac{(w_{T_1} \cdot cv_1)^2 + (w_{P_1} \cdot \vartheta_1)^2}{H_1^2}} \quad (\text{A1.12})$$

For uncertainty of refrigerant side heat transfer rate is formed as follows:

$$W_{Q_r} = \left[\left(\frac{\delta Q_r}{m_r} w_{m_r} \right)^2 + \left(\frac{\delta Q_r}{H_2} w_{H_2} \right)^2 + \left(\frac{\delta Q_r}{H_1} w_{H_1} \right)^2 \right]^{1/2} \quad (\text{A1.13})$$

$$W_{Q_r} = [((H_2 - H_1) \cdot w_{m_r})^2 + (m_r \cdot w_{H_2})^2 + (-m_r \cdot w_{H_1})^2]^{1/2} \quad (\text{A1.14})$$

The total uncertainty ratio for refrigerant side heat transfer rate is written as follows:

$$\frac{W_{Q_r}}{Q_r} = \sqrt{\frac{(H_2 - H_1)^2 \cdot w_{m_r}^2}{m_r^2 \cdot (H_2 - H_1)^2} + \frac{m_r^2 \cdot w_{H_2}^2}{m_r^2 \cdot (H_2 - H_1)^2} + \frac{m_r^2 \cdot w_{H_1}^2}{m_r^2 \cdot (H_2 - H_1)^2}} \quad (\text{A1.15})$$

$$\frac{W_{Q_r}}{Q_r} = \sqrt{\frac{w_{m_r}^2}{m_r^2} + \frac{w_{H_2}^2}{(H_2 - H_1)^2} + \frac{w_{H_1}^2}{(H_2 - H_1)^2}} \quad (\text{A1.16})$$

As a result, if the terms of m_r and $(H_2 - H_1)$ are written according to test condition, it can be obtained the total refrigerant side heat transfer rate uncertainty easily.

- The uncertainty of air side heat transfer rate:

The value of air side heat transfer capacity is transmitted to computer by reading with $P_{powermeter1}$ and $P_{powermeter2}$, which is refer the electric power of tested product and entire electrical power consumption ensuring against tested product respectively.

The total air side heat transfer rate;

$$Q_a = P_{powermeter1} + P_{powermeter2} \quad (A1.17)$$

The uncertainty for air side heat transfer rate is formulated as following;

$$W_{Q_a} = \left[\left(\frac{\delta Q_a}{\delta P_{powermeter1}} w_{powermeter1} \right)^2 + \left(\frac{\delta Q_a}{\delta P_{powermeter2}} w_{powermeter2} \right)^2 \right]^{1/2} \quad (A1.18)$$

$$W_{Q_a} = \left[(w_{powermeter1})^2 + (w_{powermeter2})^2 \right]^{1/2} \quad (A1.19)$$

Total uncertainty ratio for air side heat transfer rate is written as follows:

$$\frac{W_{Q_a}}{Q_a} = \left[\frac{(w_{powermeter1})^2 + (w_{powermeter2})^2}{Q_a^2} \right]^{1/2} \quad (A1.20)$$

As a result, it is obtained the uncertainty formulation of related heat transfer rate. It should be noted that $w_{powermeter2}$ includes the power values of P_{AHUfan} , $P_{heaters}$, $P_{coil fan}$, $P_{panel board}$, $P_{heat leakage}$. Besides, the heat leakage value (the temperature difference between calorimetric and conditioning room) couldn't take

into account because this value is negligible for the close value to SC1 and SC2 test condition, which are determined by Eurovent.

- The uncertainty of total heat transfer rate:

The total heat transfer rate is written as follows:

$$Q_t = \frac{Q_a}{2} + \frac{Q_r}{2} \quad (A1.21)$$

the uncertainty for total heat transfer rate is formulated as following;

$$W_{Q_t} = \left[\left(\frac{\delta Q_T}{\delta Q_a} w_{Q_a} \right)^2 + \left(\frac{\delta Q_T}{\delta Q_r} w_{Q_r} \right)^2 \right]^{1/2} \quad (A1.22)$$

total uncertainty ratio is found as below:

$$\frac{W_{Q_T}}{Q_T} = \sqrt{\frac{\left(\frac{\delta Q_T}{\delta Q_a} w_{Q_a} \right)^2 + \left(\frac{\delta Q_T}{\delta Q_r} w_{Q_r} \right)^2}{Q_T^2}} \quad (A1.23)$$

Note: The uncertainty calculations belonging to heat transfer rate has been calculated according to refrigerant side because of the fact that the uncertainty value of air side is higher than refrigerant side for entire measurements.

- The uncertainty of air velocity:

The air flow rate measurements were carried out by means of 3 mm hot bulb anemometer. Accordingly, it has been taken into account the uncertainty value for each measured velocity and determined the uncertainty ratio for test operations carried out both calorimetric and conditioning room.

$$w_{hotbulb} = \pm(V_{measured} \cdot (0.05) + 0.2) \quad (A1.24)$$

$$V_{avg} = \frac{V_1 + V_2 + \dots + V_n}{n} \quad (A1.25)$$

$$\frac{W_{V_{avg}}}{V_{avg}} = \sqrt{\frac{\left(\frac{\delta V_{avg}}{V_1} w_{V_1}\right)^2 + \left(\frac{\delta V_{avg}}{V_2} w_{V_2}\right)^2 + \dots + \left(\frac{\delta V_{avg}}{V_n} w_{V_n}\right)^2}{V_{avg}^2}} \quad (A1.26)$$

- The uncertainty of AMD:

As mentioned at previous sections, AMD is defined as the ratio of standard deviation to mean velocity. The uncertainty value of AMD is calculated as referenced the AMD formula, design velocity, which is 3.94 m/s and each measured velocity. This phenomenon is found for both calorimetric and conditioning room test operations.

- The AMD value of calorimetric room:

$$\sigma = \sqrt{\frac{1}{n-1} \sum_{i=1}^n \left[\frac{v_i - \bar{v}}{\bar{v}} \right]^2} \quad (A1.27)$$

$$\bar{v} = 3.94 \text{ m/s}$$

so;

$$\sigma = \sqrt{\frac{1}{271} \sum_{i=1}^{272} \left[\frac{v_i - 3.94}{3.94} \right]^2} \quad (A1.28)$$

$$\sigma = \sqrt{\frac{1}{4206.89} \sum_{i=1}^{272} (v_i - 3.94)^2} \quad (A1.29)$$

$$\sigma = 21.6\%$$

$$w_\sigma = \sqrt{\frac{1}{4206.89} \cdot \left[\left(\frac{\delta\sigma}{v_1} w_{v_1} \right)^2 + \left(\frac{\delta\sigma}{v_2} w_{v_2} \right)^2 + \dots + \left(\frac{\delta\sigma}{v_n} w_{v_n} \right)^2 \right]} \quad (\text{A1.30})$$

$$\frac{\delta\sigma}{v_i} = \left(\frac{1}{2} \left(\frac{1}{4206.89} \cdot \sum_{i=1}^{272} (v_i - 3.94)^2 \right)^{-1/2} \cdot \sum \left(\frac{2v_i - 7.88}{4206.89} \right) \right) \quad (\text{A1.31})$$

$$w_\sigma = 0.004$$

$$\sigma = 21.6\%$$

The Uncertainty of AMD (Air Maldistribution Degree): $\frac{w_\sigma}{\sigma} = 1.87\%$

- The AMD value of conditioning room:

$$\sigma = \sqrt{\frac{1}{n-1} \sum_{i=1}^n \left[\frac{v_i - \bar{v}}{\bar{v}} \right]^2} \quad (\text{A1.32})$$

$$\bar{v} = 3.94 \text{ m/s}$$

so;

$$\sigma = \sqrt{\frac{1}{287} \sum_{i=1}^{272} \left[\frac{v_i - 3.94}{3.94} \right]^2} \quad (\text{A1.33})$$

$$\sigma = \sqrt{\frac{1}{4455.27} \sum_{i=1}^{272} (v_i - 3.94)^2} \quad (\text{A1.34})$$

$$\sigma = 21\%$$

$$w_\sigma = \sqrt{\frac{1}{4455.27} \cdot \left[\left(\frac{\delta\sigma}{v_1} w_{v_1} \right)^2 + \left(\frac{\delta\sigma}{v_2} w_{v_2} \right)^2 + \dots + \left(\frac{\delta\sigma}{v_n} w_{v_n} \right)^2 \right]} \quad (\text{A1.35})$$

$$\frac{\delta\sigma}{v_i} = \left(\frac{1}{2} \left(\frac{1}{4455.27} \cdot \sum_{i=1}^{272} (v_i - 3.94)^2 \right)^{-1/2} \cdot \sum \left(\frac{2v_i - 7.88}{4455.27} \right) \right) \quad (\text{A1.36})$$

$$w_\sigma = 0.003$$

$$\sigma = 15.7\%$$

The Uncertainty of AMD (Air Maldistribution Degree): $\frac{w_\sigma}{\sigma} = 1.60\%$

- The uncertainty of static air pressure drop:

The pressure drop occurring between windward and backward of heat exchanger was measured by probes mounted each side of product and the change of air pressure drop was read via EJA110A differential pressure transmitter. The uncertainty of air pressure drop is determined according to the following equation.

$$w_{air\ pressure\ drop} = \sqrt{(w_{differential\ pressure\ transmitter})^2 + (w_{UT550})^2} \quad (\text{A1.37})$$

The accuracy of EJA110A transmitter is given as 0.075%.

$$w_{differential\ pressure\ transmitter} = 0.075\%$$

The UT550 step controller accuracy is calculated according to its accuracy specifications for 1-5V standard signal. Normally, the transmitter has 4 to 20 mA DC output. This signal is converted to 1-5V voltage signal by placing a resistor.

From UT550's specifications for 1-5V standard signal, the accuracy is:

$$w_{UT550} = 0.1\%$$

As a result, the uncertainty of air pressure drop is found as following:

$$w_{ref.pressure\ drop} = \sqrt{(0.075\%)^2 + (0.1\%)^2} = 0.12\% \quad (A1.38)$$

- The uncertainty of refrigerant pressure drop:

At this stage, it is used Rosemount 1151 differential pressure transmitter in order to determine refrigerant pressure drop in heat exchanger. The output coming from this device is transmitted to data logger. So, it is needed to calculate total uncertainty value for this measurement. In scope of this study, it was taken into account maximum total uncertainty.

$$w_{ref.pressure\ drop} = \sqrt{(w_{differential\ pressure\ transmitter})^2 + (w_{datalogger})^2} \quad (A1.39)$$

$$w_{max.differential\ pressure\ transmitter} = 0.25\%$$

The maximum data logger accuracy is calculated according to Agilent 34970A accuracy specifications for DC current because differential pressure transmitter differential pressure transmitter has 4 to 20 mA DC output.

From related specifications, the 1-year accuracy of data logger is:

$$(0.05\% \text{ of range}) + (0.02\% \text{ of reading})$$

$$(0.05\% \cdot 20 \text{ mA}) + (0.02\% \cdot 20 \text{ mA}) = 0.014 \text{ mA}$$

Total maximum accuracy for data logger: $0.014 \text{ mA} / 20 \text{ mA} = 0.07\%$

As a result, the uncertainty of air pressure drop is found as following:

$$w_{ref.pressure\ drop} = \sqrt{(0.25\%)^2 + (0.07\%)^2} = 0.259\% \quad (A1.40)$$

- The uncertainty of frost thickness:

The uncertainty of frost thickness measurement result from two reasons. One of them is the error from reading the pixel values, the another is reference meter measurement error. In scope of this study, both the meter and the fin pitch was admitted as reference length and maximum error of these measurement is 0.2 mm and also as the image resolution in scope of this study is 4224×2376 , the maximum error of reading is about 1 pixel, thereby, corresponding frost thickness is about 0.06 mm. Thus, the overall uncertainty for fin and tube frost thicknesses are about 0.208 mm as specified at following equations.

$$\begin{aligned} w_{frost\ thickness} &= \sqrt{(w_{reading\ error})^2 + (w_{reference\ meter})^2} \quad (A1.41) \\ &= \sqrt{(0.06)^2 + (0.2)^2} \\ &= \mp 0.208 \text{ mm} \end{aligned}$$

- The uncertainty of blockage ratio:

As mentioned previous sections, the blockage ratio resulting from frost formation is defined as following;

$$BR = 1 - \frac{space\ area_{after\ frost}}{space\ area_{non-frost}} \quad (A1.42)$$

where

$$space\ area_{non-frost} = (X_t - D_o). (FP - FT) \quad (A1.43)$$

$$space\ area_{after\ frost} = (X_t - D_o - 2\delta_t). (FP - FT - 2\delta_f) \quad (A1.44)$$

If the BR is rearranged as following;

$$BR = 1 - \frac{(X_t - D_o - 2\delta_t). (FP - FT - 2\delta_f)}{(X_t - D_o). (FP - FT)} \quad (A1.45)$$

$$BR = 1 - \frac{(22.5 - 2\delta_t). (6.85 - 2\delta_f)}{154.25} \quad (A1.46)$$

$$BR = \frac{154.125 - [(22.5 - 2\delta_t). (6.85 - 2\delta_f)]}{154.125} \quad (A1.47)$$

it is obtained;

$$BR = 0.291\delta_f + 0.088\delta_t - 0.025\delta_t\delta_f \quad (A1.48)$$

If implied the uncertainty equations;

$$W_{BR} = \left[\left(\frac{\delta BR}{\delta \delta_f} w_{\delta_f} \right)^2 + \left(\frac{\delta BR}{\delta \delta_t} w_{\delta_t} \right)^2 \right]^{1/2} \quad (A1.49)$$

$$W_{BR} = \left[\left((0.0291 - 0.025\delta_f). 0.208 \right)^2 + \left((0.088 - 0.025\delta_f). 0.208 \right)^2 \right]^{1/2} \quad (A1.50)$$

The fin and tube frost thickness were found as 1.5605 and 1.5912 for conditioning room and 1.9298 and 1.91397 for calorimetric room, respectively. If these values are putted in equation A.50, it will be obtained the uncertainty values of BR for each room.

for conditioning room;

$$W_{BR} \cong \mp 5.39\%$$

for calorimetric room;

$$W_{BR} \cong \mp 5.22$$

Appendix B: The Matlab Codes for Image Processing

Matlab image processing codes ensuring the transform from captured image to white (frost) and black images (space) was specified as shown below.

```
frost = imread('related image.jpg');  
frost = rgb2gray(frost); %convert to greyscale  
BW = im2bw(frost, graythresh(frost)) %convert to black and white images  
imtool(BW)
```